2014

The Journal of Kenya Chemical Society
Volume 8: Issue 1

Kenya Chemical Society
Department of Chemistry
P.O. Box 30197 - 00100 Nairobi
Email: kenchemsoc@gmail.com
www.kenchemsoc.org

Contents

From the Editor

The editorial desk is pleased to welcome you to JKCS volume 8: Issue 1 an issue dedicated to the late Professor Naftali T. Muriithi who passed away in March 2014. At the time of his passing he was the editor in chief The KCS and an Associate Professor of Inorganic Chemistry at Kenyatta University where he mentored and taught many students as lecturer and supervisor since 1972. He was among others the founders of KCS and steered it to greater heights through his personal sacrifice and significant contributions both physically and financially. The entire KCS and editorial team in solidarity with all members call upon all Chemists to emulate and steer the growth of KCS to prosperity and legacy Professor Muriithi desired. We would push to have KCS registered and recognized as a professional body in Kenya.

In this issue you we present multidisciplinary research cutting across chemistry disciplines ranging from inorganic to physical to analytical to organic among other emerging areas like nanotechnology and computational chemistry. These include: iron-ore beneficiation of clay by Prof. Muriithi (posthumous); Diffusivity of sulphate ions in portland cement; photoremediation using Titania; Micellar properties of surfactants; wastewater treatment technique; Molecular Modeling of Ethyl Benzene among others.

Thank you for reading and your contributions.

The Acting Editor, KCS
Dr. Dickson Andala

BENEFICIATION OF IRON-BEARING KAOLINITIC CLAYS FROM MUKURWE-INI BY MINERAL ACIDS LEACHING

[1]Dr.Dickson Andala, [2] Mr. Wachira David Maina[*], [2]Prof. Naftali Muriithi
1. Department of Chemistry, Multimedia University of Kenya, **2** .Department of Chemistry, Kenyatta University, KENYA
[*]Correspondence Author email: mainawachira14@yahoo.com

ABSTRACT
Clay has many applications; however, its utility depends on its level of purity. Given that iron is the fourth most abundant element on the earth's crust, it is not possible to find pure clay from anywhere free from iron. The presence of iron in clays has a profound effect on their physico-chemical properties. This study aimed at determining the level of iron present in Mukurwe-ini clay followed by reduction if on the higher side so as to obtain high-grade clay using suitable acid treatment. Studies were carried out on representative samples, which were taken from iron bearing clays from Mukurwe-ini, Nyeri County. Characterization of the clay was done in its natural form, and after acid treatment, to determine its mineralogical and chemical composition. Natural clay was refluxed with sulphuric, and hydrochloric, acids of different concentrations at 100º and 200ºC for 2 hours followed by thorough washing in distilled water to remove the acid matrix. Atomic absorption spectroscopy, X-ray fluorescence spectroscopy, and X-ray diffraction analysis techniques were used to determine the physico-chemical characteristics of natural and acid leached clays. The results indicate that SiO_2, Al_2O_3, and Fe_2O_3 are the major components of Mukurwe-ini clay, MgO, CaO, K_2O, TiO_2, MnO, and Na_2O are present in trace amounts. XRD characterization shows that Mukurwe-ini clays consist primarily of quartz, kaolinite, albite, and microcline minerals. Iron content was drastically reduced from 2.8% to less than 1% in the acid washed samples.XRD mineralogical analysis of acid-activated clays showed reduced levels of the minerals albite, microcline and kaolinite in comparison to raw clays a clear indication of solubility in the acids. Kaolinite was found to be more soluble in sulphuric acid than hydrochloric acid.

Key terms: *Clay minerals, kaolinite, Feldspar and, acid treatment*

1.0 INTRODUCTION

Iron is the fourth-most abundant element in Earth's crust (6% of mass); next to oxygen, silicon, and aluminium, and therefore, its ubiquitous presence in clays should be no surprise [1]. It is important to understand the nature and the chemical forms in which iron exists in the clays. Primary iron minerals such as goethite and hematite (hydrated oxides) are the main source of iron in clays. These oxides are strongly adsorbed on the surface of clay particles where iron acts as a compensating cation pillar between the silicates layers [1]. In this role, iron affects the cation-exchange capacity of the clay minerals and consequently their physico-chemical properties. The iron is also present in the crystal structure of clay minerals because of isomorphic substitution of cations in the tetrahedral and octahedral sites of the clay minerals. It is present as part of minerals such as Olivine ($[Mg,Fe]_2SiO_4$), Amesite $(Mg,Fe)_4Al_4Si_2O_{10}(OH)_8$ and Feldspars ($K[Al,Fe]Si_3O_8$) among many others [2]. It also occurs in the form of carbonates, sulphides, sulphates, phyllosilicates, agricultural soil, hydromorphic and lateritic soils [1]. The presence of iron has a major effect in determining the physico- chemical properties of phyllosilicates, largely because of its redox activity [1]. Swelling clays can cause build- up of pressure in many infrastructures resulting in destructive disruptions of highways, building foundations, airport runways, and railway lines [3]. Research by other workers suggests that the extent of this swelling can be controlled by altering the oxidation state of iron in the clay from +3 to +2 [3].

Presence of iron gives an undesirable colour to clay minerals and clay products when they are fired [4]. Confinement of iron in structural form and in low concentration is more often than not tolerable. Raw materials with iron oxides concentration of 0.5-3.0% reduce whiteness of clay minerals, giving them a brown-yellow colouration and therefore limiting their use in high-grade ceramics applications [5]. In colloidal form, physical methods are in most cases adequate in the reduction of hematite and goethite by magnetic separation; however, removal of structural iron presents a difficult challenge [3]. Most chemical methods use leaching agents such as mineral or organic acids. Studies available in literature indicate that acid treatment, besides leaching cations from octahedral and tetrahedral sheets, dissolves impurities such as calcite and opens the edges of the platelets and consequently their surface area and pore diameters increase [6]. The use of chlorination in extractive metallurgy is gaining popularity in removing the impurities mainly of iron and titanium from clay minerals especially kaolin. This method has given excellent results [4].

Chemical treatment of clays will however alter their natural properties. Treatment of clay with acids, for instance will adversely affect its plasticity. This property is of utmost importance in ceramic making and structural engineering. It is a well-established fact that at high acid-clay ratios, the layered crystal structure of most clay minerals is destroyed and a non-crystalline silica phase is created [7]. Acid treatment for instance, normally proceeds by removing cations adsorbed on the surfaces, those in the interlamella layer, and then the structural cations. The dissolution of cations in clay minerals is a function of concentration of the acid, composition of the clay minerals, temperature, acid-clay ratio, and time of treatment. Acid treatment of clay minerals results in increase of surface area of the clay particles due to destruction of the clay mineral structure and its eventual conversion to free form of SiO_2 [4, 8]. Removal and reduction of iron impurities is therefore of great importance for the usability of clays in many applications, particularly in ceramic, paper and catalysis industries where purity requirement are specifically high. When iron is confined in structural form, low concentrations are often tolerable. In order to make high quality ceramic products, clay with low iron content, preferably less than 1% is

desirable [9]. Kenya spends a lot of money importing quality clays. In the year 2008, Kenya imported 963.3 metric tons of kaolinite clays valued at US $400,000 [10]. In the month of March and April 2013 alone, Kenya imported roasted clays from India amounting to 5840 metric tons [11]. Ironically this is happening in a country where a large chunk of her populace live in abject poverty, but endowed with millions of tonnage of clays, which however cannot be used in industries that require high quality clays for their products in spite of having literally millions of tonnage of clays locally which are unsuitable for making high quality ceramic products because of intolerable high levels of iron.

Beneficiation of local clay raw materials is of paramount importance, hence the need to understudy different methods of improving and upgrading these materials. Special attention must be paid to extraction and refining technology of indigenous clay raw materials, which has a potential for substantial socio-economic development. Iron impurities in clay can be reduced using physical and chemical methods. Most chemical methods use leaching agents such as mineral or organic acids. Studies available in literature indicate that acid treatment, besides leaching cations from octahedral and tetrahedral sheets, dissolves impurities such as calcite and replaces the exchangeable cations with hydrogen ions. The treatment also opens the edges of the platelets and consequently their surface area and pore diameters increase[6]. The use of chlorination in extractive metallurgy is gaining popularity in removing the impurities mainly of iron and titanium from clay minerals especially kaolin. This method has given excellent results [4]. The current study attempts to find out whether, the level of iron content can be minimized by suitable acid treatment; most effective conditions of iron-removal based on the chemical composition of clays from Mukurwe-ini sub-County.

2 METHODOLOGIES

2.1 Sampling Method

Clay samples used in this work came from Rutune Location which is to the southeast of Mukurwe-ini sub-County, Nyeri County (Latitude 00º34´00´´S, Longitude 37º03´00´´E). The samples were collected from three mines located in Kariara sub-location (land area of approximately 8.7Km^2) [12] by random sampling. The mines were approximately 500m apart along the same dene where the clay deposits were located. For each mine, three samples were collected at three depths namely 0.45m, 0.9m, and 1.5m. The samples were packed in plastic containers and coded (Table 1)

Table 1: Sampling and Coding of Samples

Mine	Sample code	Depth of sample collection (m)
A	Muk A1	0.45
	Muk A2	0.90
	Muk A3	1.50
B	Muk B1	0.45
	Muk B2	0.90
	Muk B3	1.50
C	Muk C1	0.45
	Muk C2	0.90
	Muk C3	1.50

2.2 Instrumentation

Atomic absorption and X–ray spectroscopy techniques were used for elemental analysis of the raw and treated clays. Nature of minerals present in raw and treated clays was determined using X-ray diffraction. Calibrations of AAS and XRFS instruments were done using standard SY-2, MRG-1, and MRG-1 rock samples procured through Department of Mines and Geology, Ministry of Mining of Kenya.

2.3 Preparation of Standard Solutions

Samples were prepared for AAS analysis using the method described by Haruna *et al* [13], and Karoki [9].

2 4 X-Ray Fluorescence Spectroscopy Analysis

About 10g of dried clay sample was ground to particle size 200µm using a laboratory pulveriser. 5g of starch were added and a uniform mixture of two obtained by shaking and swirling in a plastic container. The mixture was made into pellets using a Herzog pellet maker. The pellets so prepared were analysed using an X-ray fluorescence Spectrometer model, PANalytical MiniPal2, Philips for the various oxide compositions. Results were in terms of oxides percentages.

2.5 X-ray diffraction analysis

The raw and acid treated samples were subjected to qualitative and quantitative phase analysis, for phase identification and quantification. This was done using a Bruker D2 Phaser.

2. 6 Treatment of Clays with Acids

Each clay sample was prepared by air-drying and grinding to a particle size of 200µm. About 20g of prepared sample was weighed into a 250-ml Pyrex conical flask and 100ml of 12M HCl was added. The resulting slurry was heated at 100ºC in a fume chamber using an electrically heated hot plate for 2 hours. Ice-cold distilled water was carefully added to the resulting slurry, which was then filtered using Whatman filter paper No 541 to separate acid matrix from the clay. This filtration was done under gravity. The clay was washed thoroughly with distilled water until neutral point was obtained with a pH indicator. The residue was then dried in an oven at 105ºC for 2 hours, cooled and crushed. The treatment process was repeated with 10M, 8M, 6M, 4M, and 2M HCl. Treatment was repeated at 200 ºC. The chemical and mineralogical composition was determined using AAS, and XRFS [14]. These treatments were repeated with sulphuric acid

3 RESULTS AND DISCUSSION

3.1 Analysis of Raw Clays

The results of elemental analysis show that Mukurwe-ini clays contain silica and alumina as major quantities; however, MgO, CaO, Na_20, K_2O, and TiO_2 are present in trace amounts. Iron is also present in the range 1.4-4.2 % (Table 2). This clay therefore, cannot be used in the manufacture of high-grade ceramic products such as white porcelain, glossy paper, and other products requiring clay with less than 1 % iron content [9]. Furthermore, the SiO_2:Al_2O_3 ratio greater than one is suggestive of a clay suitable not for bleaching but for zeolite development[15].

Table 2: AAS Elemental Analysis of Raw Clay Samples

SAMPLE	SiO_2	Al_2O_3	CaO	MgO	Na_2O	K_2O	TiO_2	MnO	Fe_2O_3	LOI	TOT
Muk A1	56.75±0.33	23.04±1.17	0.10±0.01	0.33±0.01	0.27±0.02	1.20±0.06	1.96±0.62	0.01	1.40±0.12	11.45	96.51
Muk A2	58.04±0.89	22.50±0.34	0.08±0.02	0.35±0.01	0.26±0.04	1.18±0.01	1.78±0.46	0.01	1.43±0.17	11.47	97.1
Muk A3	82.75±0.94	5.62±0.33	0.08±0.02	0.24±0.06	0.08±0.03	0.40±0.01	0.26±0.08	0.01	1.86±0.30	6.88	98.18
Muk B1	46.36±0.32	28.38±0.07	0.08±0.03	0.34±0.08	0.11±0.02	0.44±0.02	1.14±0.31	0.01	2.52±0.12	20.61	99.99
Muk B2	48.31±0.20	27.98±0.28	0.08±0.02	0.34±0.07	0.13±0.02	0.62±0.03	1.12±0.44	0.01	1.77±0.37	20.26	100.62
Muk B3	54.43±0.58	25.72±0.03	0.10±0.02	0.33±0.06	0.28±0.03	0.97±0.08	1.88±0.17	0.01	1.70±0.12	15.15	100.57
Muk C1	62.83±1.24	18.72±0.24	0.10±0.01	0.31±0.09	0.31±0.03	0.79±0.03	1.75±0.39	0.01	1.73±0.17	14.13	100.67
Muk C2	49.75±0.43	24.79±0.35	0.09±0.01	0.29±0.06	0.34±0.07	0.86±0.08	1.24±0.67	0.01	4.23±0.32	18.17	99.77
Muk C3	77.49±0.59	9.93±0.24	0.10±0.01	0.26±0.08	0.24±0.03	0.96±0.26	0.82±0.26	0.01	0.96±0.09	8.61	99.38

3.2 Result of Mineralogical Analysis

Quantification of the minerals in the clay by XRD spectroscopy showed that it consists of quartz (57.90%), albite (5.30%), microcline (16.10%), and kaolinite (20.80%) (Figure 1). The raw clay exhibits well-defined peaks at 2θ values at 12º, 25º, and 38º, which are typical reflections of the clay mineral kaolinite [16] and which correspond to d values of 7.17Å and 3.58Å, characteristic of the mineral kaolinite [17]. Quartz, albite, and microcline are all non-clay minerals hence kaolinite is the only clay mineral present and its presence imparts the property of plasticity in the clay, hence its usability in high-grade ceramics products.

3.3 Analysis of Acid Washed Clays

3.3.1 AAS and XRFS Analysis

It was noted that the chemical composition of the clays changed substantially. As the concentration of the acid increased, there was marked increase in dissolution of cations and hence a reduction in Al_2O_3, MgO, CaO, Na_2O, Fe_2O_3, and TiO_2; however K_2O was retained in the acid matrix (Table 3).

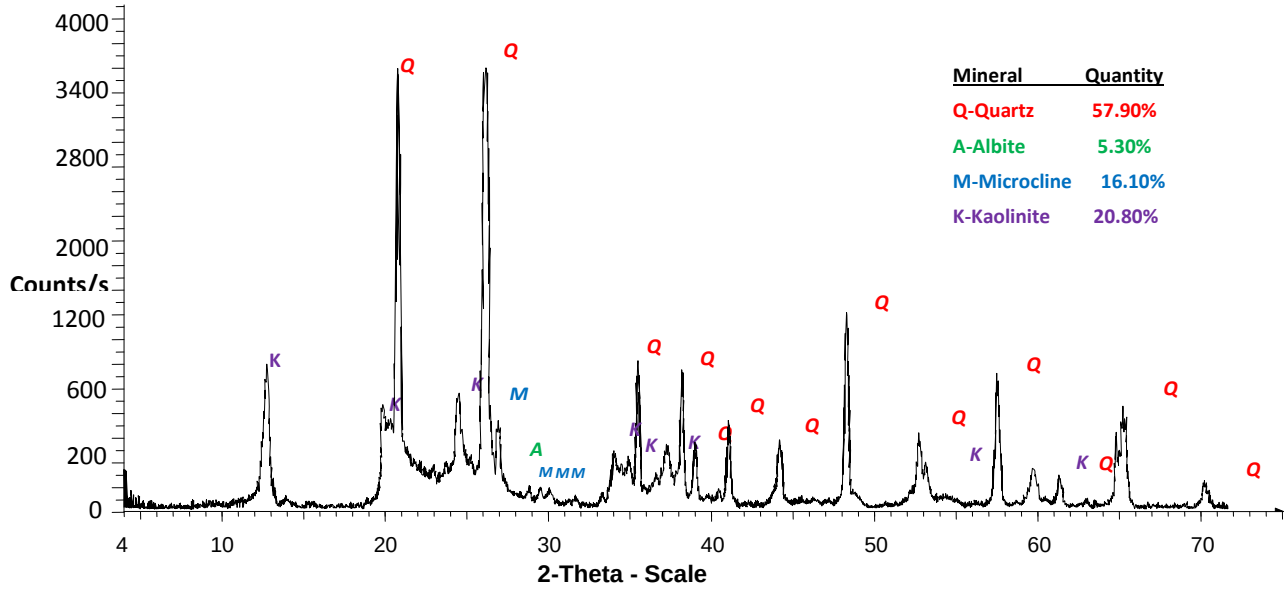

Figure 1: XRD Spectrum of Raw Clay

Table 3: Summary of Treatment of samples with HCl at 100°C

Concentration	SiO_2 Mean±SE	Al_2O_3 Mean±SE	CaO Mean±SE	MgO Mean±SE	Na_2O Mean±SE	K_2O Mean±SE	TiO_2 Mean±SE	MnO Mean±SE	Fe_2O_3 Mean±SE
Raw sample	59.64±2.37^{a}	20.73±1.48^{c}	0.09±0.00^{e}	0.31±0.01^{e}	0.22±0.02	0.82±0.06	1.34±0.13	0.01±0.00^{a}	1.95±0.18^{c}
12M	66.15±1.87^{bc}	13.26±1.12^{ab}	0.08±0.00^{d}	0.24±0.01^{d}	0.26±0.03	2.82±1.89	3.46±2.64	0.00±0.00	0.39±0.03^{a}
10M	72.96±2.13^{c}	13.14±1.16^{ab}	0.07±0.00^{cd}	0.22±0.01^{c}	0.26±0.02	0.92±0.08	0.77±0.07	0.00±0.00^{a}	0.41±0.04^{a}
8M	69.32±2.00^{bc}	11.56±1.08^{a}	0.07±0.00^{cd}	0.21±0.01^{c}	0.24±0.02	0.67±0.07	0.71±0.07	0.00±0.00^{a}	0.54±0.05^{a}
6M	63.26±1.91^{ab}	19.14±1.38^{c}	0.07±0.00^{cd}	0.18±0.01^{b}	0.24±0.02	1.03±0.06	1.20±0.14	0.010±0.00^{a}	0.88±0.08^{b}
4M	62.48±2.20a^{b}	18.25±1.57^{c}	0.05±0.00^{a}	0.14±0.01^{a}	0.23±0.02	1.02±0.06	0.85±0.09	0.00±0.00^{a}	0.88±0.08^{b}
2M	64.07±2.28^{ab}	16.67±1.37^{bc}	0.06±0.00^{b}	0.31±0.01^{e}	0.18±0.01	0.67±0.05	0.99±0.12	0.013±0.00^{b}	0.96±0.07^{b}
p-value	<0.001	<0.001	<0.001	<0.001	0.052	0.355	0.476	<0.001	<0.001

Mean values within the same column followed by superscripts do not differ significantly (one-way ANOVA, SNK-test=0.05).

Acid attack caused fast exchange of hydrated exchangeable cations with H^+, which then attacked the structural OH^- groups[18]. Potassium cations may have reacted with amorphous silica in the matrix to produce potassium feldspar, which is resistant to acid attack [19]. Hydrochloric acid gave better iron dissolution levels than sulphuric acid because of ease of filtration of its slurry, and solubility of salts in its matrix [20](Figure 2). It was noted however that the clay minerals were more soluble in sulphuric acid than hydrochloric acid as indicated by high Si/Al ratio for sulphuric acid (Table 2). From this analysis, it was noted that hydrochloric acid had the least levels of de-alumination compared to the other acid. Increasing Si/Al ratio (Table 2) implies leaching of Al^{3+} from octahedral layer due to acid attack; at higher acid concentrations (above 8M), there was significant reduction of alumina due to severe leaching of clay structure leading to de-alumination of the clay.

Table 5: Summary of Results of Acid Treatment and Comparative Effectiveness of the Acids (Sample Muk-B2) at a 100°c

Acid	Concentration	% SiO_2	% Al_2O_3	Si/Al ratio	% Fe_2O_3	%Fe_2O_3 removed
Raw clay	Nil	48.31	27.98	1.73	1.77	
HCl	2M	55.87	22.66	2.47	1.43	19.21
	4M	51.70	25.17	2.05	1.26	28.81
	6M	54.98	23.39	2.38	1.06	40.11
	8M	60.85	15.32	3.97	0.71	59.89
	10M	58.15	18.95	3.07	0.48	72.08
	12M	57.97	18.20	3.19	0.38	78.53
H_2SO_4	2M	49.57	23.08	2.15	1.47	16.95
	4M	54.33	18.17	2.99	1.26	28.81
	6M	63.10	18.02	3.50	1.09	38.42
	8M	67.04	13.58	4.90	0.82	53.67
	10M	67.52	11.13	6.07	0.58	67.23
	12M	74.58	7.28	10.24	0.43	75.71

A keen analysis of the summary given in Table 2 reveals rapid reduction of aluminium and iron for acid concentrations between 4 and 8M.

These are the most suitable conditions for acid treatment of the clays at a working temperature of 100 ºC. Loss of ignition of the clays increased after acid treatment. This was due to increase in amorphous silica that made water adsorption higher [15]

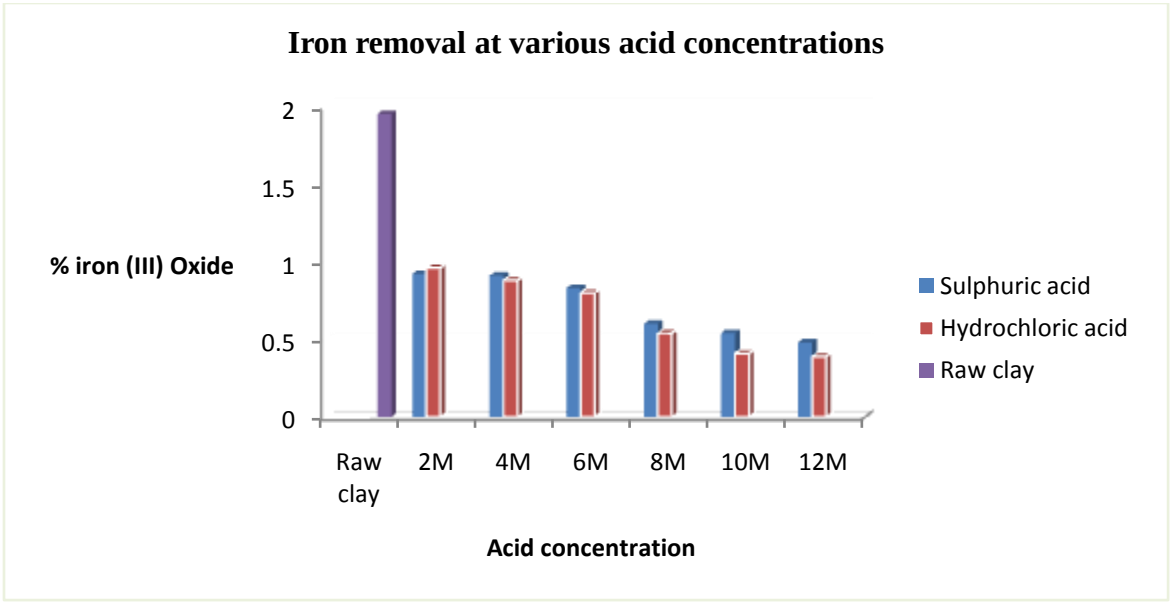

.

Figure 2: Effect of acid concentration on iron removal at 100ºC

Rapid reduction of alumina and iron occurs at higher temperatures even at low acid concentration (Figure 3).Acid concentration of between 2-4M the most appropriate acid strengths at 200ºC for dissolution of iron in the clays. Figure 3 provides a snapshot of comparison of sulphuric acid treatment at 100ºC and 200ºC in iron dissolution.

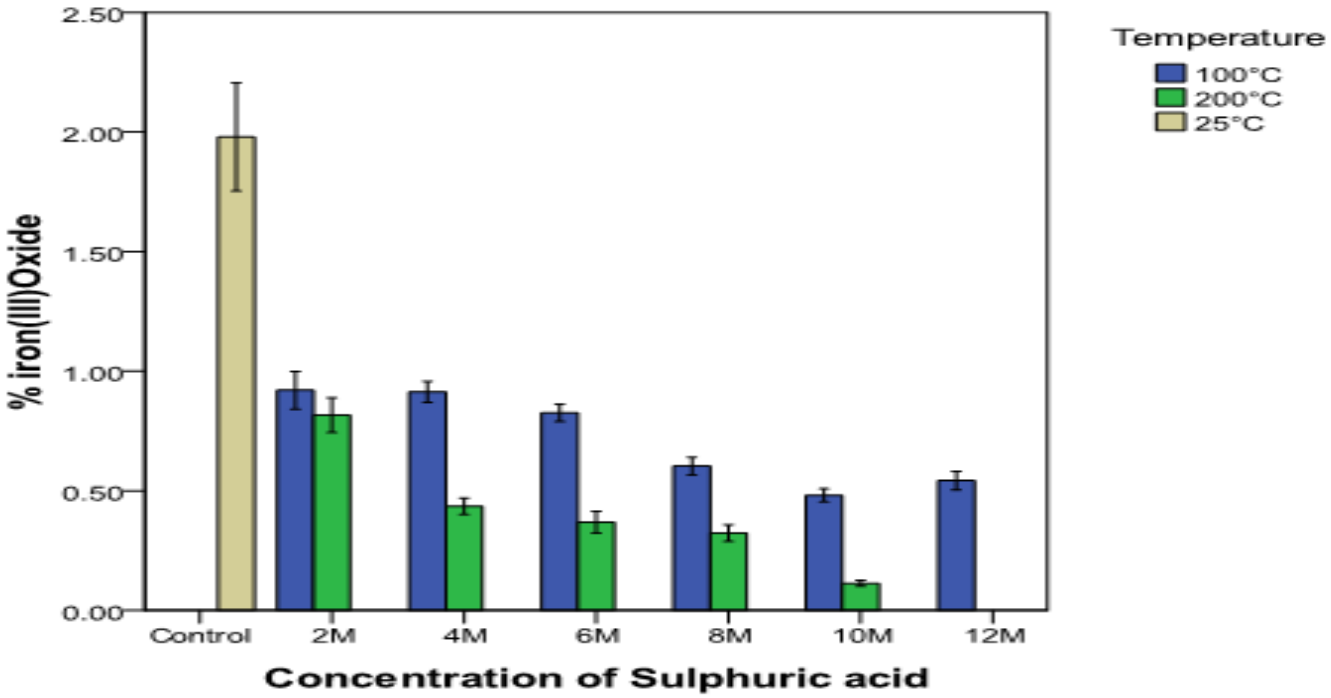

Figure 3: Comparison of Iron removal by Sulphuric acid at 100ºC and 200ºC

3.3.2 XRD Analysis of Acid Washed Clay

Analysis of the XRD diffractogram indicates dissolution of the minerals kaolinite and albite in the acid; however quartz and microcline are largely unaffected by the acid treatment (Figure 4). The acid-washed clay was composed of quartz (61.40%), microcline (22.30%), and kaolinite (5.40%), hence the disappearance of peaks for albite mineral, the reduction and the significant widening of the intensity of kaolinite peaks. This was caused by dissolution of these minerals in the acid, which interfered with ordered structure and natural properties of the clay. The retention of the reduced peak however shows that the structure was only partially affected. Potassium was retained in the acid matrix in form of the mineral microcline ($KAlSi_3O_8$) which is resistant to acid attack.

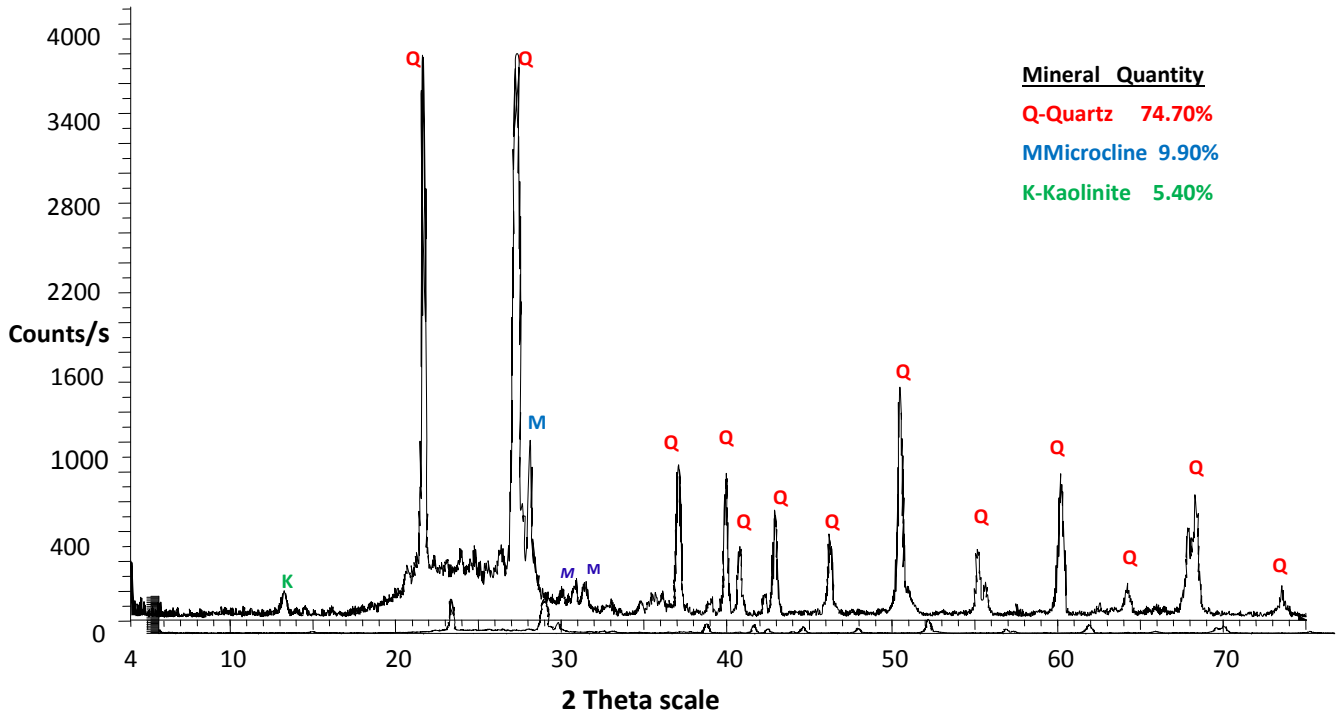

Figure 4: XRD Spectra of acid washed clay

4. CONCLUSION

This study has established that the major minerals in Mukurwe-ini clay include quartz (57.69%), kaolinite (20.80%), albite (5.30%), and microcline (16.10%), implying that kaolinite is the only clay mineral present in this clay. From the XRD analysis of the clay, sodium and potassium were retained in the clay as the minerals albite ($NaAlSi_3O_8$) and microcline ($KAlSi_3O_8$) respectively, commonly called the feldspars. Presence of kaolinite mineral in the clay makes it suitable for use in ceramics. This study has also shown that the quality of the clay is noticeably improved by acid treatment by reducing its iron content to less than 1%, which is ideal for making high-grade ceramics and specialized application in paper industry, catalysis, filler material, white cement and many others where high clay purity is required. The most suitable conditions for iron dissolution, according to this study were acid concentration of 2-4M at 200ºC or 4-6M at 100ºC.

REFERENCES

1. Stucki, W. (2006). Properties of iron in clays. In Lagaly, G., Theng, K., Bergaya. F, (Ed.) Handbook of Clay Science. Development in Clay Science (Vol.1) AMSTERDAM, Elsevier Ltd. Page 424
2. Anthoni.J. F. (2000). Classification of common rocks. Retrieved from *www.seafriend.org.nz/environ/soil/rocktbl1.htm.*Retrieved 13th June 2012
3. Stucki, W., Golden, C., and Charles, R. (1984). Effects of reduction and re-oxidation of structural iron on the surface charge dissolution of Smectites. *Clay and Clay minerals, 32*(5), 350-356
4. Ruiz, M. & Gonzalez, J. (2006). Bleaching Kaolin and clays by chlorination of iron and Titanium. *Applied clay Science 33*(2006), 219-299

5. Calderon, D., Martinez, M., Mendez, O. and Rodriguez, J. (2005). Iron leaching of Mexican clay of Industrial interest by Oxalic Acid. *Advances in technology of materials and materials processing, 7* [2] *(2005)161-166.*
6. Valenzuela-Diaz, F. R., & Souza-Santos, P. (2011). Studies on the acid activation of Brazilian smectitic clays. *Química Nova 24* (3), 345 -353
7. Jones, W. & Kooli, F. (1996). Characterizations and catalytic properties of Saponite. Clay modified by acid activation. *Clay and Clay minerals.32* (1997), 633-647
8. Kang, S. & Giselle, S. (2001). Characterization of Montimorillonite surfaces after modification by Organosilane. *Clay and Clay minerals 49*(2) 119-225
9. Karoki, K. (2009). *Analysis and treatment of clays from Mwea to assess their value as a source of Aluminium and Ceramic products.* (Master of Science Un-Published), Kenyatta, Nairobi, Kenya. Pages 3 - 31
10. Muriithi, N. T., Karoki K. B. & Gachanja A. N. (2012). Chemical and mineral analyses of Mwea clays. Full Length Research Paper. *International Journal of Physical Sciences Vol. 7*(44), pp. 5865-5869
11. www.infodriveindia.com
12. Jaetzold, R., Schmidt, H., Hornetz, B. & Shisanya, C. (2006). "Ministry of Agriculture FARM MANAGEMENT HANDBOOK OF KENYA.VOL. II. Natural Conditions and Farm Management Information (Second Edition).PART B CENTRAL KENYA. Subpart B2. Central Province.'' Ministry of Agriculture, Kenya, in Cooperation with the German Agency for Technical Cooperation (GTZ) pages 343 - 425
13. Haruna, K., Onoja, P. & Chiroma, M., (2007).Characterization of Mayo-Belwa clays. *Leonardo Electronic Journal of Practices and Technologies 6* (11)123-130
14. Onukwuli, D., & Ajemba, R. (2012). Evaluation of the Effects of acid activation on adsorptive properties of Clay from Ukpor in bleaching Palm oil. *International Journal of Multidisciplinary Sciences, 3*(5), 46-52
15. Usman, M.A., Ekwueme, K.I., Alaje, T.O., Mohammed, A.O. (2012). Research article, Characterization, acid activation, and bleaching performance of Ibeshe clay, Lagos,Nigeria.*International Scholarly Research Network volume 2012,Article ID 658508,5 pages.* Doi:10.5402/2012/658508. Accepted 11 January, 2012
16. Panda, A.K., Mishra, B.G., Mishra, D.K. & Singh, R.K. (2010). Effect of sulphuric acid treatment on the physic-chemical characteristics of kaolin clay. *Colloid and surfaces A: Physiochemical and Engineering Aspects 363*(2010) 98-104.
17. Harris, W & White, N, (2007), Methods of soil analysis. Part 5. Mineralogical methods. SSSA Book Series No.5, Soil Society of America, Madison, USA, Chapter 4
18. Martin,P.,Madejova,I.,Slavka,A.,Peter,U.,& Peter,K. (2012). Stability of kaolin sand from the Vysny Petrovec deposits (South Slovakia) in acid environment. *Geologica Carpathica, 63 (*6) 503-512
19. Motlagh, K.M., Youzbashi, A.A. & Rigi, A.Z. (2011). Effect of acid activation on structural and bleaching properties of a Bentonite, *Iranian Journal of materials science and Engineering, vol 9*(4), 50 – 56
20. Al-Zahrani, A. & Abdul-Majid, M. (2009). Extraction of alumina from local clays by hydrochloric acid process. *Journal of Engineering Science 20*(2), 29-41

DIFFUSIVITY OF SULPHATE ION IN SELECTED ORDINARY PORTLAND AND PORTLAND POZZOLANA CEMENTS MORTAR

[1]Mutitu, D. K., [1]Karanja, J. K. and [2]Wachira, J. M.
[1]Department of Chemistry, Kenyatta University, P. O. Box 43844 – 00100 Nairobi, KENYA
[2]School of Pure and Applied Sciences, Embu University College, P. O. Box 6 – 60100, Embu, KENYA

ABSTRACT
Cement is subject to degradation by aggressive media. This study investigated sulphate diffusivity in mortar made from selected Kenyan cements which included three brands of Ordinary Portland Cements (OPC) and three brands of Portland Pozzolana Cements (PPC) sampled within Kenyan markets. The test cements were used to make mortar prisms at different water/cement ratios. Compressive strength was determined at the 7^{th} and 28^{th} day of curing. The mortars were subjected to laboratory prepared 3.5 % by mass of sodium sulphate solution under accelerated ion migration test method for a period of thirty six hours using a 12V DC power source. The compressive strength before subjecting to aggressive media was found to increase with curing duration as well as on decreasing w/c. Compressive strength at all w/c ratios was found to increase after the aggressive media ingress, however, prolonged exposure or exposure to high levels of sulphate is known to be deleterious to cement/concrete. After subjecting the mortar cubes to SO_4^{2-} media, they were sliced and the cores from the slices analyzed for SO_4^{2-} content. From these results, apparent diffusion coefficient, $D_{app,}$ was approximated from solutions to Fick's 2^{nd} law using the error function. PPC at all w/c ratios showed lower D_{app} than OPC. SO_4^{2-} ingress for both cement types across all cement categories, increased with the increase in w/c ratio. Chemical analysis results showed that the Kenyan Cement meet the minimum chemical and phase requirements.

Key Words: Diffusivity, Aggressive media, water/cement ratio, Compressive strength, Ingress.

1.0 INTRODUCTION

An environment of between 20 to 50 °C and humidity of about 35 – 50 percent with the presence of aggressive ions make concrete/mortar structures vulnerable to deterioration and as a result shorten their service life span (Atkinson & Hearne, 1990). Chloride and sulphate ions are common in many water masses, making them readily available to cement matrix either during cement paste making or to constructed cement structures (Tibbetts, 1968).

Hydrated OPC has a resultant high $Ca(OH)_2$, about 20 percent by weight, that makes it susceptible to the aggressive ions (Cabrera & Plowman, 1988). Blending OPC with pozzolanic materials makes it less permeable, thus reducing the ingress of aggressive media (Cabrera & Plowman, 1988; Marangu, Muthengia, & wa-Thiong'o, 2014; Muthengia, Muthakia, & Thiong'o, 2012; Mutitu, Karanja, & Wachira, 2014). The pozzolana reacts with the resultant $Ca(OH)_2$ producing more cementitious material. This increases the compressive strength of resultant mortar/concrete, although after a longer period compared to OPC. The pozzolana thus improves on cement quality and reduces the $Ca(OH)_2$ content, the most susceptible component.

Unavailability of sewerage drainage systems leads to use of septic tanks or simply pits, allowing waste water run-offs, as well as unauthorized/unsupervised construction procedures (NEMA, 2012). This exposes the constructed cement structures to aggressive media. When sulphate ions ingress cement mortar or concrete, it has beneficial effect of enhancing cement hydration which increases the cement strength but the ions ingress also causes changes which include extensive cracking, expansion, alteration of paste composition with calcium aluminate monosulphate hydrate phase converting to ettringite and in later stages gypsum formation (Jelenic, Panovic, Halle, & Gacesa, 2010). These products lead to loss of bond between the cement paste and aggregate and eventually to loss of concrete/mortar strength (Jelenic *et al*., 2010).

The aim of this study was to investigate the diffusivity of sulphate ions and their effect on compressive strength development of selected Kenyan OPC and PPC mortars. Test cements were selected Kenyan OPC and PPC. The test cements were labelled with respect to company source and cement category; the letters A, B and C represented companies while O and P represented OPC and PPC respectively. AO for example, represents OPC from company A and AP represents PPC from company A.

2.0 EXPERIMENTAL PROCEDURE

OPC and PPC cements were sampled from companies' appointed distributors in Kenyan major towns. Cements from three major cement making companies were used. 10 kg cement was bought from the appointed distributors in the three towns respectively. The sand as obtained from the sampling site was washed by spraying with tap water and sun-dried for three days to a constant weight as per ASTM C 0117 (2004). The dried sand was graded to meet the standard sand aggregates grade in accordance to ASTM C 1077 (2011).

Mortar preparation and curing was done in accordance to KS EAS 18:2008. Mortars of w/c ratio 0.55, 0.60 and 0.70 were prepared for both OPC and PPC. Mortars were labelled for identification as BO 05, BP 05, BO 06, BP 06, BO 07 and BP 07. The letter B in the label represent company B, O represents OPC, P represents PPC and 05 represent w/c ratio of 0.55. Similar labelling was used for cements from companies A and C. In each cement category, 18

prisms were prepared. Compressive strength for the mortars was determined at the 7^{th} and 28^{th} day of curing.

About 100.00 g of cement sample for each category was separately ground to pass through a 76 µm mesh sieve. The ground sample was used for the analysis of cement oxides using x-ray fluorescence in the usual manner. The cement oxides analysed included Na_2O, K_2O, CaO, MgO, SiO_2, TiO_2, Al_2O_3, Fe_2O_3 and MnO_2. Loss on Ignition was done in accordance to ASTM C 1157 (2004).

Diffusing test was done in accordance to ASTM C 1556 (2004). The cement mortar cured for 28 days was reduced to 100 mm length. An electrochemical cell was set-up in accordance to [6]. The mortar specimen was placed between two cells and covered with a fabric material. The set-up is shown in plate 2.1.

Plate 2.1: Accelerated Ion Migration Test Cell Set Up

The anodic compartment was filled with 500 ml of water. An equal volume of 3.5 % Na_2SO_4 was placed in the cathodic compartment. Stainless steel electrodes were placed separately in the compartments. The electrodes were connected to a 12 ± 0.1 V direct current (DC) power source. The diffusion period started when the solutions in both the anodic and cathodic compartments were placed and the electrodes connected in circuit. The top of the container was then covered with a polyethylene paper and the entire set up maintained at 22 ± 1 °C for thirty six hours. During the experimental period, the solutions were stirred periodically using a glass rod. For every cement category 6 mortar prisms were subjected to Sulphate ingress.

For each category of cement, three mortar cubes were subjected to compressive strength analysis while three mortar cubes for each ingress ion were sliced into 10 mm slices along the length using a water-lubricated cutting machine. A rotary hammer drill was used to drill through a circular portion of 25 mm from the centre of each mortar slice. The mortar obtained was ground

to pass through a 76 µm mesh sieve. The ground samples were then subjected to SO_4^{2-} analysis. Triplicate analyses were done for each category of cement.

SO_4^{2-} analysis was done in accordance to ASTM C1580 (2007). Analysis for SO_4^{2-} in standard solution and sample was analysed using turbidimetric method in the usual manner. Calibration curves were used to determine the SO_4^{2-} ion concentration in test solutions.

The results were presented in sulphate concentration versus depth of cover. The sulphate diffusion coefficients, $D_{mig,}$ were derived from the solution to the second Fick's law of diffusion. The error fitting curves given as equation 2.1 using the method of least squares (Andrande & Sanjuan, 1999; Machard, Gerald, & Delagrave, 1998) was used.

$$\frac{C_{(x,t)}}{C_s} = 1 - \text{erf}\left(\frac{x}{2\sqrt{D_{mig}t}}\right) \quad \text{.....2.1}$$

where erf (y) is the error function, t is the duration of exposure of the concrete sample, x is the distance from the exposed surface penetrated by the ion, $C_{(x,t)}$ is the ion concentration (w/w) at the distance x, C_s is the ion concentration at the exposed surface (w/w) and $D_{mig,}$ is the Migration diffusion coefficient.

Since the sulphate ion ingress was accelerated by a potential difference, then apparent diffusion coefficient, D_{app}, was obtained from equation 2.2 (Andrande & Sanjuan, 1999; Cabrera & Plowman, 1988).

$$D_{app} = \frac{RT}{z_i F} D_{mig} \frac{Int^2}{\Delta Ø} \quad \text{.....2.2}$$

where R is the Gas constant, F is the Faraday constant, T is the temperature of the electrolyte in K, z_i is the valency of the ion i, $\Delta Ø$ is the Effective Applied Voltage in V, t is the duration of the test/exposure in seconds and D_{app} is the Apparent Diffusion coefficient.

3.0 RESULTS AND DISCUSSION

3.1 Chemical Analysis Results

The results for the chemical analysis of oxides in percent by mass (except for Cl^-) for various categories of cements are given in table 3.1.

Table 3.1: Chemical Analysis Results (% w/w Oxides and LOI against Cement Category)

Constituent	Cement Category					
	BO	**BP**	**AO**	**AP**	**CO**	**CP**
Al_2O_3	3.417±0.150	6.337±0.035	3.980±0.010	5.880±0.010	4.323±0.021	6.730±0.020
SiO_2	19.397±0.035	38.640±0.036	22.740±0.104	35.320±0.036	19.863±0.015	32.680±0.030
SO_3	5.725±0.000	1.661±0.000	5.460±0.000	3.133±0.000	4.336±0.000	3.622±0.000
Na_2O	0.300±0.000	0.910±0.010	0.410±0.000	0.883±0.006	0.280±0.000	1.057±0.006
K_2O	0.463±0.006	1.727±0.087	0.667±0.006	1.007±0.006	0.710±0.000	1.433±0.006
CaO	65.867±0.058	39.933±0.252	63.100±0.436	42.333±0.306	54.400±0.361	44.033±0.252
MgO	0.990±0.020	0.787±0.015	2.113±0.025	1.887±0.015	0.933±0.006	1.160±0.020
Fe_2O_3	3.353±0.006	5.093±0.015	3.407±0.012	4.320±0.036	2.923±0.015	4.537±0.025
MnO	0.100±0.000	0.207±0.006	0.173±0.006	0.187±0.006	0.300±0.000	0.300±0.000
LOI	3.710±0.009	3.710±0.009	1.520±0.001	3.910±0.003	1.280±0.002	3.060±0.003

All test cements were within the range prescribed by Kenya Standards requirement (KS EAS 18, 2008). The various chemical constituent constitute the hydration products upon reaction with water which offer the strength of concrete or mortar. All sampled cements are suitable for the purpose they are designed for. PPC exhibited higher Al_2O_3, SiO_2 and Fe_2O_3 contents than OPC. The packing of pozzolana grains between cement hydration products decreases permeability of concrete/mortar (Cheng, Huang, Wu, & Chen, 2005; Hossain & Lachemi, 2004). Pozzolanic reaction leads to more CSH and CAH compounds which possess cementitious properties (Cheng *et al*., 2005; Hossain & Lachemi, 2004).

The results for the phase composition in per cent by mass for various categories of cements are given in table 3.2.

Table 3.2 Phase Composition of Test Cements

	Phase % (w/w) ± S.D.			
Sample	**C_3S**	**C_2S**	**C_3A**	**C_4AF**
BO	52.360±0.138	27.593±0.113	4.178±0.077	10.205±0.019
BP	21.676±1.046	54.304±0.893	4.569±0.690	12.456±0.046
AO	52.391±1.055	25.686±0.524	4.785±0.045	10.367±0.035
AP	20.555±2.152	57.100±1.723	4.711±0.052	11.929±0.061
CO	37.227±1.204	28.871±0.087	6.512±0.034	8.895±0.046
CP	9.600±1.154	54.926±0.956	5.876±0.095	11.980±0.077

The table shows the main cement phases from Bogue's calculations (Bogue, 1955). The various cements have the major cement phases within the Kenya Bureau of standards acceptable range as per KS EAS 18: 2008. Typical OPC should have tricalcium silicate (C_3S), dicalcium silicate (C_2S), tetracalcium aluminium ferrite (C_4AF) and tricalcium aluminate (C_3A) within the range of 20 – 57 percent, 20 - 52 percent, 7 - 16 percent and 4.5 - 12 percent respectively (Blanks & Kennedy, 1955). PPC exhibited lower C_3S than OPC while the converse is true for C_2S. Perhaps, the latter could be attributed to the silica content in pozzolana which is not accounted for in the Bogue's calculations. The test cement CO had extremely low C_3S content. Perhaps this could be attributed to the raw meal content.

All the test cements exhibited C_3A within the acceptable range. The C_3A phase is a point of attack to sulphates. Decreasing the C_3A content in cement reduces the heat of hydration of cement involved (Ghorab, Kishar, & Elfetouh, 2008). This is important in large construction works where an enormous amount of concrete is required. The reduction of C_3A may increase the diffusivity of chloride ions since the phase acts as a chloride sink forming the Friedel's salt (Magdalena, Babara, Gwenn, & Fredrik, 2010)

3.3 Compressive Strength at the 7Th and 28Th day

Compressive strength results for various categories of cements at varied w/c ratio are represented in Figure 3.1.

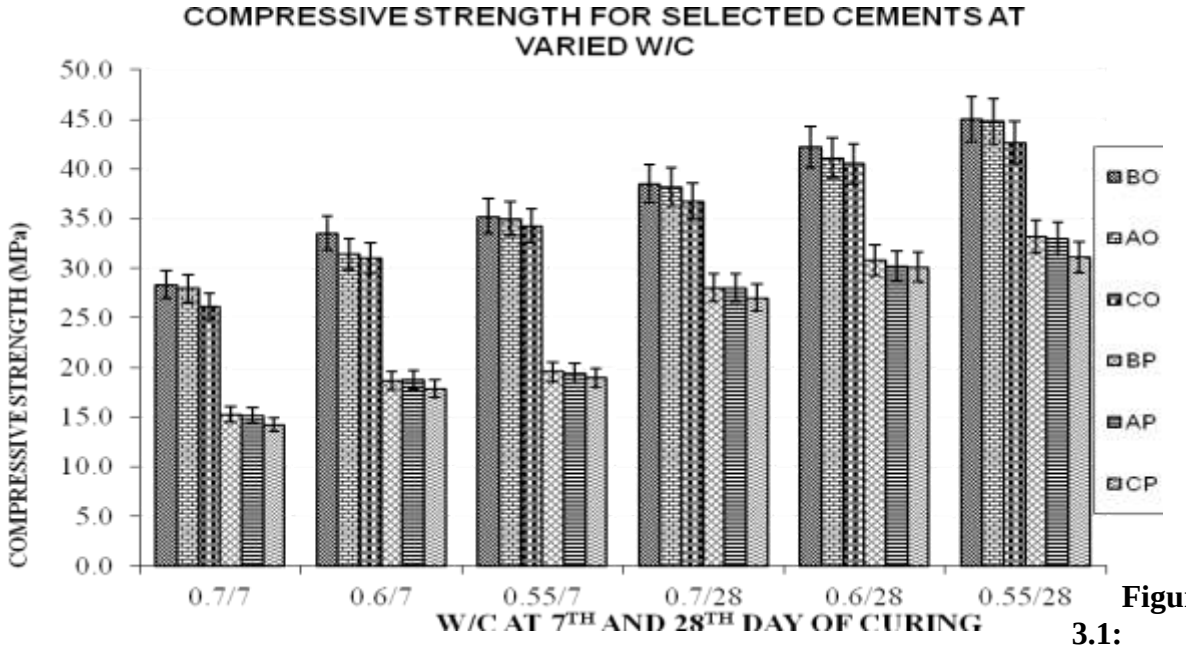

Figure 3.1: Compressive strength for selected cements at varied w/c ratio

Key: 0.7/7 represents test cement at w/c ratio 0.7 at 7th day of curing, 0.7/28 Represents test cement at w/c ratio 0.7 at 28th day of curing, 0.6/7 represents test cement at w/c ratio 0.6 at 7th day of curing, 0.6/28 represents test cement at w/c ratio 0.6 at 28th day of curing, 0.55/7 represents test cement at w/c ratio 0.55 at 7th day of curing while 0.55/28 Represents test cement at w/c ratio 0.55 at 28th day of curing.

The compressive strength was observed to increase with curing age for all cement categories. Kenyan standard, KS EAS 168-1 (2008) requires that PPC have a minimum strength of 15 MPa at the 7th day of curing while at the 28th day be at 32 MPa. OPC should have a minimum of 25 MPa at the 7th day while at the 28th day it should have a minimum of 42.5 MPa. All cement samples had met the standard requirement.

Generally, OPC attains higher strength at early age compared to PPC (Jeffrey, Mondal, & Mideley, 2012). This has been attributed to the slow strength development of the incorporated pozzolana in PPC (Jeffrey *et al*., 2012; Jelenic *et al*., 2010). OPC had a higher C_3S content than PPC. C_3S contributes to early strength development (Way & Shayan, 2009).

In all cement categories, it was observed that the higher the w/c ratio, the lower the compressive strength. The compressive strength for all mixes decreased with increasing w/c ratio. This is as would be expected (Jeffrey *et al*., 2012; Jelenic *et al*., 2010). The more the free water content of the fresh mortar the greater would be the volume of pores left in the hardened mortar and therefore the less the gel/space ratio. W/c ratio is therefore a measure of the void volume relative to the solid volume in hardened cement paste, and its strength goes up as the void volume goes down. So, the lower the w/c ratio, the lower is the void volume/solid volume, and the stronger

the hardened cement paste. The higher hydration rate of OPC may have substantially reduced its porosity compared to the PPC. The beneficial effect of pozzolana blend may have been overridden by the porosity due to high w/c ratio (Andrande & Sanjuan, 1999; Cabrera & Plowman, 1988).

3.4 Compressive strength Results for Test Cements after Subjecting to Sulphate Solutions

The percent gain in compressive strength for the various categories of cements at varied w/c ration after being subjected to SO_4^{2-} are given in figure 3.2

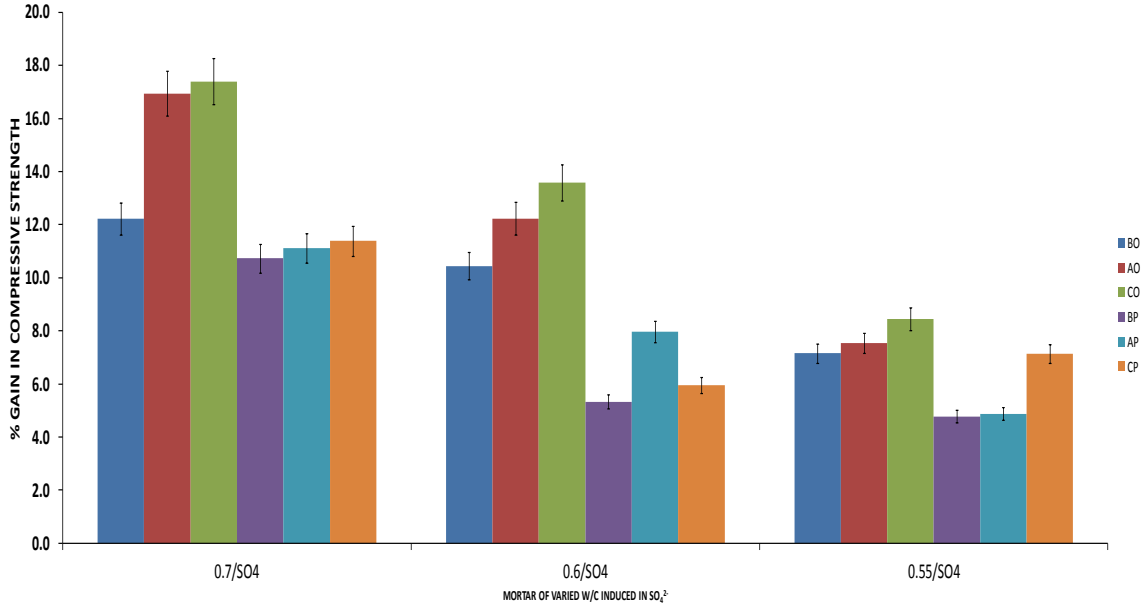

Figure 3.2 Percent gain in compressive strength for selected cements at varied w/c ratio in sulphate solutions

Key: $0.7/SO_4$ represents test cement at w/c ratio 0.7 ingress by SO_4^{2-}, $0.6/SO_4$ represents test cement at w/c ratio 0.6 ingress by SO_4^{2-}, $0.55/ SO_4$ represents test cement at w/c ratio 0.55 ingress by SO_4

There was observed increase in compressive strength gain in all cases. This is because SO_4^{2-} is known to initiate residual cement hydration. The strength gain was higher the higher the w/c ratio. Perhaps this could be attributed to space availability of space for residual cement hydration.

3.5 Sulphate Profiling

Results for sulphate ingress into selected mortars at varied w/c ratio and depth of cover are presented in figure 3.3 and 3.5 for OPC and 3.4 and 3.6 for PPC.

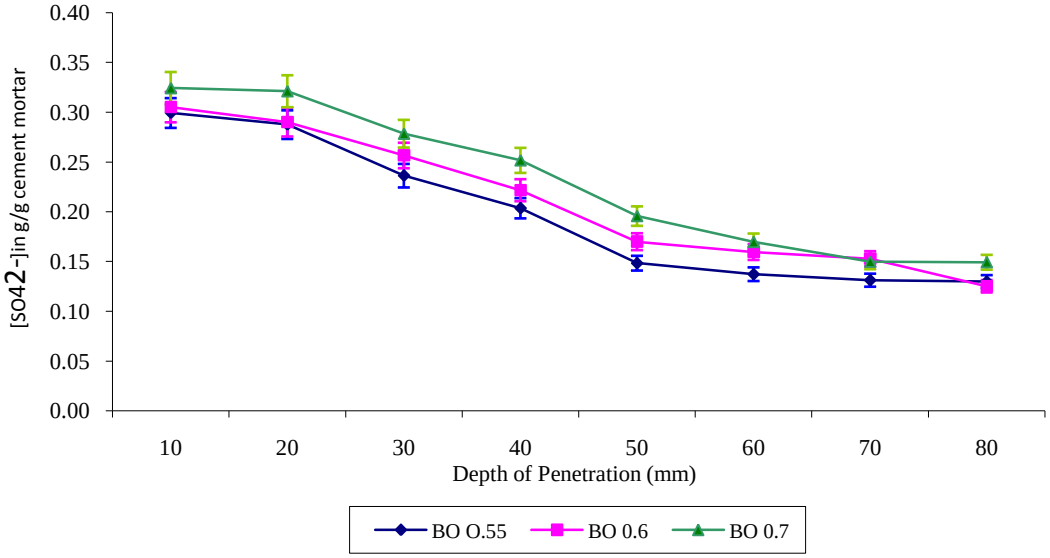

Figure 3.3: Sulphate profile for OPC against depth of cover

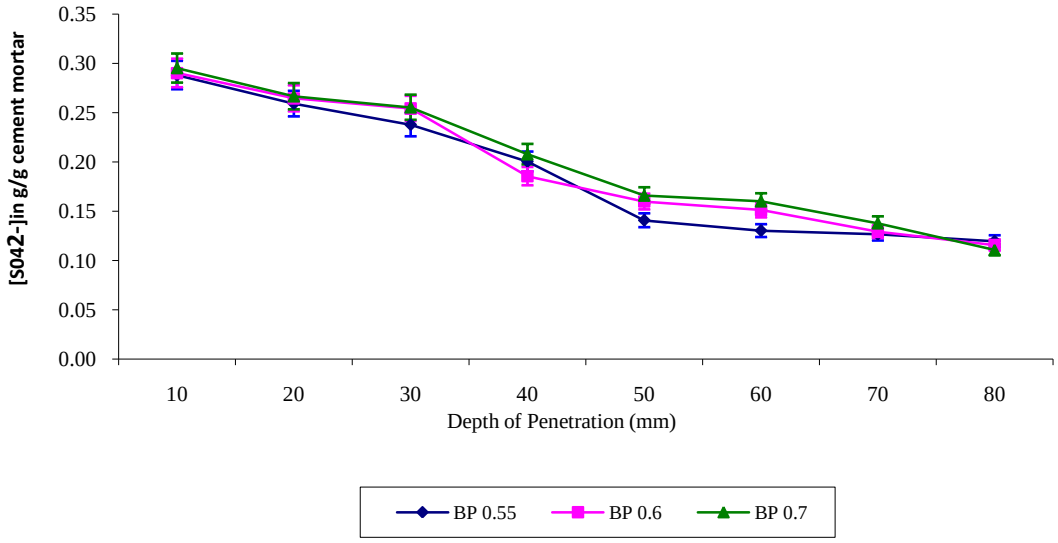

Figure 3.4: Sulphate profile for PPC against depth of cover.

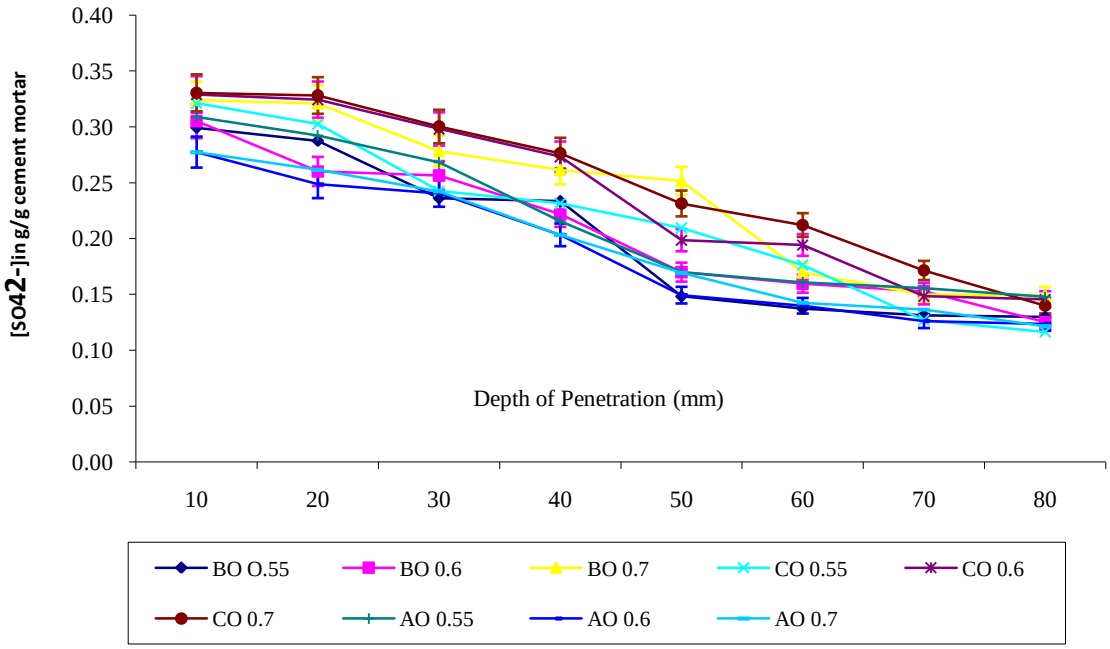

Figure 3.5: Sulphate Profile for OPC against Depth of Cover.

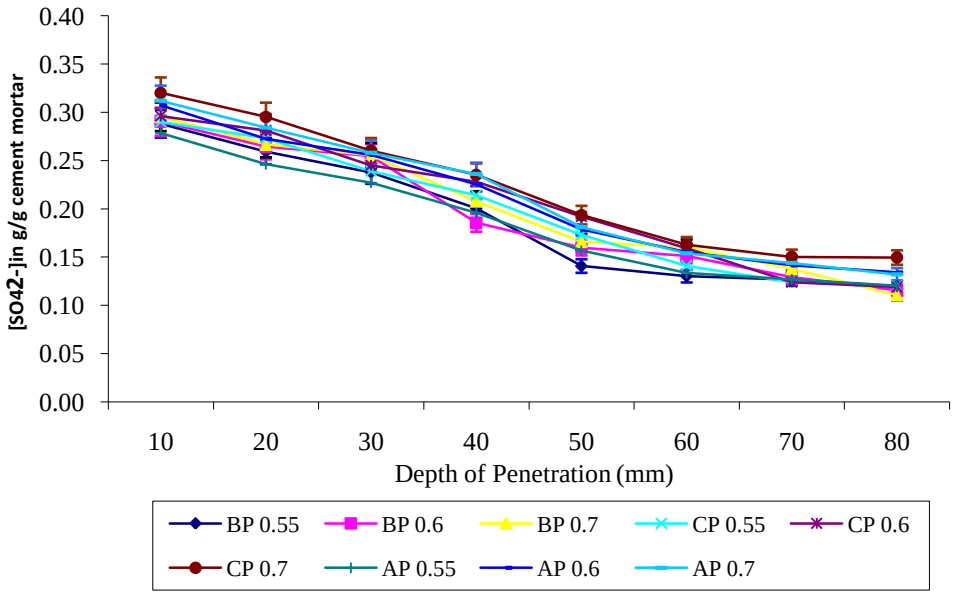

Figure 3.6: Sulphate Profile for PPC against Depth of Cover.

In all cases, w/c ratio affected the ingress of the SO_4^{2-}. The higher the w/c ratio, the higher the ingress of the SO_4^{2-}. This may be attributed to porosity and permeability of the resultant mortar or concrete. Expansive products are expected to be formed when mortar is subjected to sulphates (Jeffrey *et al*., 2012; Jelenic *et al*., 2010), and hence seal voids due to high w/c ratio. This may not have taken place. Perhaps micro cracks, due to the expansive products (Jelenic *et al*., 2010; Machard *et al*., 1998) may have predominated and hence aided in ingress of the sulphates.

The type of cement was predominant over the effect of w/c ratio in view of the extent of sulphate ingress in all depths of cover. OPC exhibited higher sulphate ingress than PPC at all depths of cover. OPC had higher $Ca(OH)_2$ content than PPC. The high content of $Ca(OH)_2$ in OPC reacts with SO_4^{2-} forming gypsum and ettringite. These two products initially cause expansion which occurs as voids in the mortar (Atkinson & Hearne, 1990). This in turn increases the permeability of SO_4^{2-} in OPC than PPC (Andrande & Sanjuan, 1999; Atkinson & Hearne, 1990). Pozzolana grains provide packaging which reduces SO_4^{2-} permeability (Jeffrey *et al*., 2012). OPC generally had higher C_3A phase than the PPC. C_3A phase reduce cement durability on reacting with SO_4^{2-}. This is attributed to the formation of an insoluble layer of $3CaO{\cdot}Al_2O_3{\cdot}3CaSO_4{\cdot}32H_2O$ over the surface of the aluminate crystals, passivating them (Jeffrey *et al*., 2012). This reaction is expansive and can disrupt mature concrete/mortar (Jeffrey *et al*., 2012). The addition of pozzolana to Portland cement contributes sufficient aluminium to suppress formation of ettringite and hence the sulphate diffusivity drops.

3.6 Sulphate Apparent Diffusivity Coefficients

Table 3.3 gives the D_{app} with corresponding sulphate surface concentration (C_s) and r^2 values of the error fitting curves.

Table 3.3: D_{mig}, D_{app} and r^2 – Values for Different Cement Mortars at Different w/c ratio in Na_2SO_4

Cement type	w/c	$D_{mig.}$ (x $10^{-8}m^2/s$)	D_{app} (x $10^{-11}m^2/s$)	r^2 - Value	C_s (%)
BO	0.7	2.9422	7.3123	0.9318	3.8536
	0.6	2.7685	6.8807	0.9688	3.4033
	0.55	2.5689	6.3845	0.9257	3.4634
AO	0.7	3.1871	7.9211	0.9783	3.0529
	0.6	2.8793	7.1561	0.9551	3.1100
	0.55	2.7836	6.9181	0.9434	3.5005
CO	0.7	3.9204	9.7434	0.9664	3.8025
	0.6	2.8961	7.1978	0.9495	3.9173
	0.55	2.8456	7.0722	0.9774	3.6098
BP	0.7	2.5744	6.3983	0.9803	3.2958
	0.6	2.5432	6.3208	0.9628	3.2911
	0.55	2.2637	5.6260	0.9533	3.3162
AP	0.7	2.6075	6.4806	0.9802	3.4938
	0.6	2.5499	6.3372	0.9812	3.4682
	0.55	2.5065	6.2295	0.9776	3.1506
CP	0.7	2.8951	7.1951	0.9783	3.5898
	0.6	2.6327	6.5432	0.9832	3.4157
	0.55	2.4500	6.0891	0.9834	3.3693

PPC cement mortars exhibited lower apparent diffusion coefficients (D_{app}) than OPC across all w/c ratios. As observed earlier from figures 3.7 and 3.8, PPC exhibited lower sulphate ingress than OPC. Similar observations were reported by other authors (Atkinson & Hearne, 1990; Diamond, 1996). They attributed this to lower permeability due to pozzolanic reaction and packaging of pozzolana grains.

It was observed, as expected, that the higher the w/c ratio the higher the D_{app}. Again as observed from figures 3.7 and 3.8 (in appendix) there was more sulphate ingress in mortars with higher w/c ratio than with lower w/c ratios. This resulted in higher D_{app}. (Andrande & Sanjuan, 1999; Tibbetts, 1968). This could be attributed to increased permeability due to high porosity. The D_{app} values in the range of 10^{-11} imply that the test cement mortars on sulphate ingress/attack caused little expansive products.

4.0 CONCLUSIONS

Despite the observed sulphate ingress, the values of D_{app} in the range observed are within the expected range. This implies that the cement would perform within the expected duration

without failure or with minimal repair. However, care should be exercised while using the cements where sulphates and /or other aggressive ions are known or expected to be present.

4.1.1 Recommendations

Despite the performance of the test cements in the test media, it would be desirable to subject the cement in real life scenario where the aggressive ions are found for a long period. More work is also necessary to establish suitable cement that is locally made, and can withstand such aggressive media for an appreciable period. Further work should be done to establish how sulphate ions diffusivity to cement constructed structures could be minimised

References

Andrande, C., & Sanjuan, M. A. (1999). Experimental Procedure for Calculation of Chloride Diffusion Coefficients in Concrete from Migration Tests. *Advances in Cement Research, 6*, 127 - 134.

Atkinson, A., & Hearne, J. A. (1990). *Mechanistic Model for the Durability of Concrete Barriers Exposed to Sulphate Bearing Ground Waters.* Paper presented at the Materials Research Society Symposium Proceedings.

Blanks, R. F., & Kennedy, H. L. (1955). *The Technology of Cement and Concrete*. New York: John Wiley and Sons, INC.

Bogue, R. H. (1955). *The Chemistry of Portland Cement* (2nd ed.): Reihold Publishing Corporation.

Cabrera, J. G., & Plowman, C. (1988). The Mechanism and Rate of Attack of Sodium Sulphate Solution on Cement and Cement/PFA Pastes. *Advances in Cement Research, 1*(3), 171 - 179.

Cheng, A., Huang, R., Wu, J., & Chen, C. (2005). Influence of GGBS on Durability and Corrosion Behaviour of Reinforced Concrete. *Materials Chemistry and Physics, 93*, 404.

Diamond, S. (1996). Delayed Ettringite Formation - Processes and Problems. *Cement and Concrete Composites, 18*, 205 - 215.

Ghorab, H. Y., Kishar, E. A., & Elfetouh, S. H. A. (2008). Studies on the Stability of Calciumsulfoaluminate Hydrates Part II: Effect of Alite, Lime and Monocarboaluminate Hydrate. *Cement and Concrete Research, 41*, 1208 - 1223.

Hossain, K. M. A., & Lachemi, M. (2004). Corrosion Resistance and Chloride Diffusivity of Volcanic Ash Blended Cement Mortar. *Cement and Concrete Research, 34*, 695 - 702.

Jeffrey, J. W., Mondal, P., & Mideley, C. M. (2012). Mechanisms of Cement Hydration. *Cement and Concrete Research, 41*, 1208 - 1223.

Jelenic, A. I., Panovic, A., Halle, R., & Gacesa, T. (2010). Effect of Gypsum on the Hydration and Strength of Commercial Portland Cements Containing Alkali Sulfates. *Cement and Concrete Research, 7*, 239 - 246.

Machard, J., Gerald, B., & Delagrave, A. (1998). Ion Transport Mechanism in Cement Based Materials *Materials SCience of Concrete, 5*, 307 - 400.

Magdalena, B., Babara, L., Gwenn, S., & Fredrik, P. G. (2010). Impact of Chloride on the Mineralogy of Hydrated Portland Cement Systems. *Cement and Concrete Research, 40*(7), 1009 - 1022.

Marangu, J. M., Muthengia, J. W., & wa-Thiong'o, J. K. (2014). Performance of Potential Pozzolanic Cement in Chloride Media. *IOSR Journal of Applied Chemistry, 7*(2), 36 - 44.

Muthengia, J. W., Muthakia, G. K., & Thiong'o, J. K. (2012). Cementing Material from Rice Husk - Broken Bricks - Spent Bleaching Earth - Dried Calcium Carbide Residue *Mediterranean Journal of Chemistry, 2*(2), 401 - 407.

Mutitu, D. K., Karanja, J. K., & Wachira, J. M. (2014). Diffusivity of Chloride Ion in Mortar Cubes Made Using Ordinary Portland and Portland Pozzolana Cements. *IOSR Journal of Applied Chemistry*, *7*(2), 67 - 73.

NEMA. (2012). The State of Sewerage Systems in Urban Centres in Kenya by 2012 (pp. 3 - 25).

Tibbetts, D. C. (1968). Performance of Concrete in Sea Water: Some Examples from Halifax. *Performance of Concrete*, *Canadian Building Series*(2), 159 - 180.

Way, S. J., & Shayan, A. (2009). Early Hydration of Portland Cement in Water and Sodium Hydroxide Solutions: Composition of Solutions and Nature of Solid Phases. *Cement and Concrete Research, 19*, 759 - 769.

Effects of Calcination Temperature on Titanium dioxide Photocatalyst Morphology

Patrick K Tum[1], Fredrick D.O. Oduor[1]

[1] University of Nairobi, Department of Chemistry, P.O Box 30197-00100, Nairobi, Kenya

Abstract

Organic compounds can be degraded photo catalytically using titanium dioxide (TiO_2). In this study, the effect of calcination temperature on the morphology of TiO_2 catalyst prepared from an aqueous suspension of 'anatase paste' of concentration 10g/l. TiO_2 photocatalysts were prepared and characterized by Scanning Electron Microscope (SEM), X-ray Diffraction (XRD), and Brunauer Emmett Teller (BET) surface area determination techniques to determine its morphological properties which include crystalline size, particle size and specific surface areas vis-à-vis temperature. For TiO_2 produced from 'anatase paste', an increase in calcination temperature from 300°C to 900°C resulted in an increase in particle size and decrease in surface area. Higher calcination temperature favoured formation of larger particles. Data obtained from XRD measurements show that particle crystal size calculated using Scherer's formula increased with an increase in calcination temperature.

Keywords: morphology, calcination, photocatalyst, anatase, paste, scherer.
*Corresponding author. Email: patricktum@uonbi.ac.ke

INTRODUCTION

Titanium Dioxide as a photocatalyst

Titanium dioxide as a semi-conductor has been successfully used as a photo catalyst for the oxidative degradation of organic compounds including pesticides and dyes. The anatase form is the most practical for photo catalytic environmental applications such as water purification, wastewater treatment and water disinfections (Rebernik *et al.,* 2006). It is biologically and chemically inert, stable with respect to photo-corrosion and chemical corrosion and inexpensive (Morawski *et al.,* 2003). Its disadvantage is however, too high band gap energy (about 3.2eV) that enables titanium dioxide to absorb only UV light with wavelength lower than 388 nm thus reducing the solar harvesting efficiency down to 5% (Hasnat *et al.,* 2005).

Effects of calcination temperatures of TiO_2

The photocatalytic activity of TiO_2 for the degradation of organic compounds increases with the anatase content of the catalyst and also with the crystalline size of TiO_2 per unit surface area of the catalyst. Annealing above 700°C results in a dramatic decrease in the photocatalytic activity of TiO_2. The decrease in photoactivity was found to be correlated with decrease in surface area of the TiO_2 particles (Halman, 1995). Calcination temperatures above 700°C caused considerable sintering of the particles and thus decreased the surface area (Černigoj *et al.,* 2006). At calcination temperatures below 600°C, the predominant crystal form is anatase that is transformed to rutile at higher temperatures of calcination (Černigoj *et al.,* 2006).

Use of glass to immobilize TiO_2 leads to suggestions that the diffusion of sodium ions from the substrate during thermal treatment could stimulate the recrystalization of the anatase to rutile phase (Černigoj *et al.,* 2006). Anatase TiO_2 is thermodynamically metastable and can be easily transformed into the stable rutile phase when heated to temperatures between 500°C-

600°C (He and Lin 2007). In this study, it was found that with increased calcination temperatures of up to 900°C, no rutile phase was present in the catalyst structure. Nevertheless the anatase phase has a higher crystallinity and is preferred for photocatalysis since higher crystallinity means fewer defects to allow recombination of photogenerated electrons and holes. It is practically important to develop methods that lead to a stabilization of anatase TiO_2 at higher temperatures so that the phase transformation in the later thermal treatment can be avoided (Černigoj, *et al* 2006).

In addition to the crystalline transformation obtained by high-temperature calcinations, crystalline growth and serious sintering are observed with increasing temperature of calcinations, leading to the drastic decrease in surface area. However, powders with large surface areas are usually associated with low crystallinity and large number of crystalline defects. A balance between surface area and crystallinity must be found in order to obtain the highest photoactivity.

RESULTS AND METHODOLOGY

Chemicals

TiO_2 anatase paste was synthesized via the sol gel method from tetrabutyl titanate $Ti(OC_4H_9)]_4$ purchased from Degussa using the sol-gel method following procedures reported by (Yuan and Zhang, 1998).

Preparation of TiO_2 particulate layers

TiO_2 particulate layers were prepared by deposition from an aqueous suspension of anatase paste of concentration 10g/l on microscopic glass slides of dimensions (7.5cm × 2.5cm).
The aqueous catalyst suspension was pre-treated before deposition using an ultra-sound decibel to break down agglomerates present and make the suspension uniform.
Using a 5ml syringe a volume of 3.75 ml of the catalyst suspension was immobilized before allowing drying at room temperature. The catalysts were then dried in the oven at 25°C for duration of 2 hours.

The amount of catalyst immobilized was calculated to be 0.5 mg/cm^2. The final geometrical area covered by TiO_2 catalyst was trimmed down to occupy (2.5cm × 3.5cm) of the microscopic glass representing a geometrical area of 8.75 cm^2. The TiO_2 particulates were thereafter annealed at temperatures of 300°C and 900°C for various time durations. Figure 1 below shows particulate films of TiO_2 prepared from 'anatase paste'

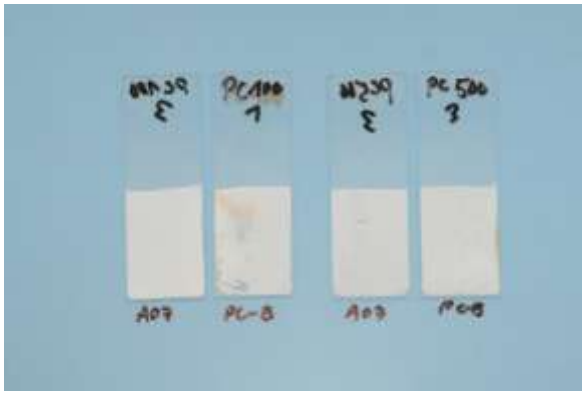

Figure 1: TiO_2 particulate films prepared from 'anatase paste' covering a geometrical area of 8.75cm^2.

Figure 2: below shows the Calciner that was used to anneal the TiO_2 particulate layers at temperatures of 300°C and 900°C for various durations.

Figure 2: Calciner used to anneal TiO_2 particulate layers (ICT, Prague).

Characterizing TiO_2 surface morphology

Particle size (XRD)

Particle size determination is an important parameter to determine photocatalytic efficiency, since the predominant way of electron/hole recombination may differ depending on the particle size (Ma *et al.,* 1998).

This method determines the crystal size of particles using X-rays and based on elastic scattering of X-rays from particles. Crystal size was calculated using the Scherer equation and expressed in nm.

$$l = k\lambda / \beta \cos\theta$$

Where λ is the wavelength of rays, k is a constant taken to be 0, 9 (assuming no crystal distortions in the lattice), β is the full width at half maximum of the radians corrected for the instrumental broadening and θ is the diffraction angle in degrees (Černigoj *et al.*, 2007).
The equipment used was a SEIFERT XRD 3000 at ICT, Prague following a procedure described by (Černigoj *et al.,* 2007).

Particle size (SEM)

The technique uses a type of electron microscope that makes images of solid particles by scanning them with a beam of electrons. This involves sample atoms interacting with electrons and emitting information about surface topography to form an image. From SEM images produced, crystal size can be estimated. The equipment used was HITACHI S 4700 available at ICT, Prague. The procedure followed has been suggested by (Černigoj *et al.,* 2007).

Surface area (BET)

The technique measures the surface area of particles from the physical adsorption of nitrogen gas on its surface. The theory also assumes that only a mono-layer of gas is adsorbed on the surface. The next step involves calculating the total number of molecules of gas adsorbed on the catalyst surface. Surface area was determined by multiplying the number of gas molecules adsorbed by the cross-sectional area of adsorbate molecule yielding the specific surface area

expressed in m^2/g. The equipment used was an ASAP 2020 available at ICT, Prague to determine the surface area of the catalyst using procedures described by (Cernigoj et al., 2007).

TiO_2 surface morphology

The table below summarizes TiO_2 surface morphology by determining particle size [nm], crystalline size[nm] and surface area [m^2/g]. An analysis of how the percentage of amorphous phase in TiO_2 changes with increasing calcination temperatures is also shown.

Table 1: Morphological Characteristics of TiO_2 photocatalyst prepared from "anatase paste" at various calcinations temperatures and time durations.

Calcination temperatures	Particles size	Crystalline size	Surface area	Amorphous phase
°C/min	nm (SEM)	nm(XRD)	m^2/g BET	% (XRD)
Initial powder	-	-	76	26
300/30 min	not visible	8	81	-
400/30 min	Less than 50 nm	10	80	-
600/30 min	Less than 50 nm	38	54.5	-
700/30 min	50 nm	54	28	8
700/8 hrs	-	-	17	-
800/30 min	100 nm	83	18	-
800/4 hrs	-	-	13	-
800/8 hrs	-	-	12	-
900/ 30min	150-200 nm	146	4	5
950/30 min	-	-	2.5	0

From the results obtained by SEM, XRD and BET analysis: The amount of amorphous phase present in calcined TiO_2 photocatalyst decreases with an increase in calcination temperature.
The results also indicate that an increase in calcination temperature results in reduction of specific surface area [m^2/g] of TiO_2. In addition longer calcination periods also lead to a further decrease in surface area. At calcination temperature of 700°C, specific surface area reduced from 28 m^2/g for calcination duration of 30 minutes to 17 m^2/g for calcination duration of 8 hours. At calcination temperature of 800°C, specific surface area reduced from 18 m^2/g for calcination duration of 30 minutes to 12m^2/g for calcination duration of 8 hours.

Crystalline size measurement calculated by the Scherer's formula indicate an increase in crystalline size with increasing calcination temperatures. This phenomenon is caused by sintering of TiO_2 crystals which is more pronounced at higher calcination temperatures. At calcination temperature of 900°C and calcination duration of 30 minutes the crystalline size determined by XRD was 146 nm. However particle size determined from SEM images show that particle size is about 150-200 nm for calcination duration of 30 min.

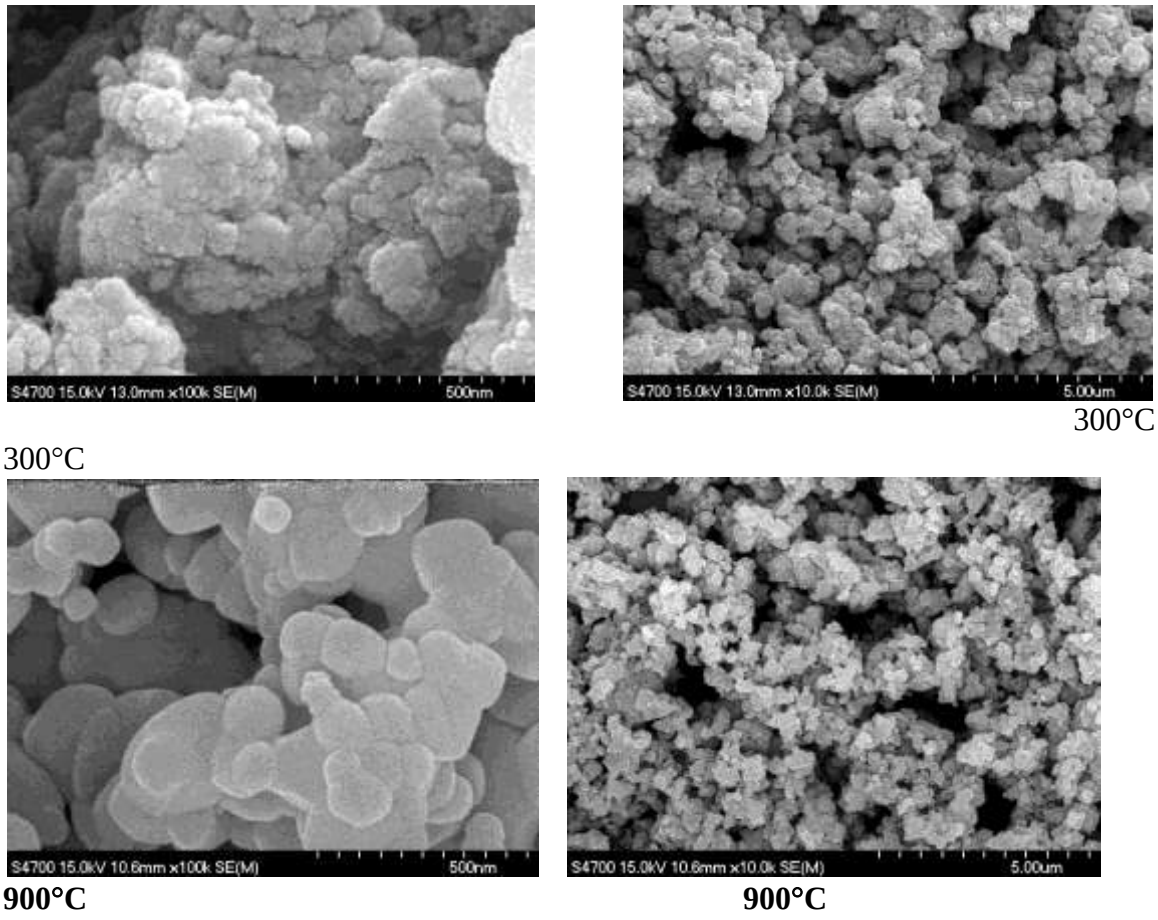

Figure 3 SEM Images showing the morphology of TiO_2 particulate layers prepared from 'anatase paste' annealed at 300°C and 900°C respectively.

The images in figure 3 represent particle size distribution and morphology of TiO_2 particulate layers annealed at temperatures of 300°C and 900°C. The images are reflect at a scale of 500 nm /5μm. The images also show that TiO_2 particles annealed at 900°C are visibly larger compared to particles calcined at 300°C. Comparing particle size from SEM images with the calculated particle size from (XRD), the values are very similar. The particles observed in Fig. 3 are mainly individual crystals.

Figure 4: below shows TiO_2 particulate layers annealed at 700°C for 30 min and 8 hrs respectively and. characterized using Tunneling Electron Microscope (TEM) technique.

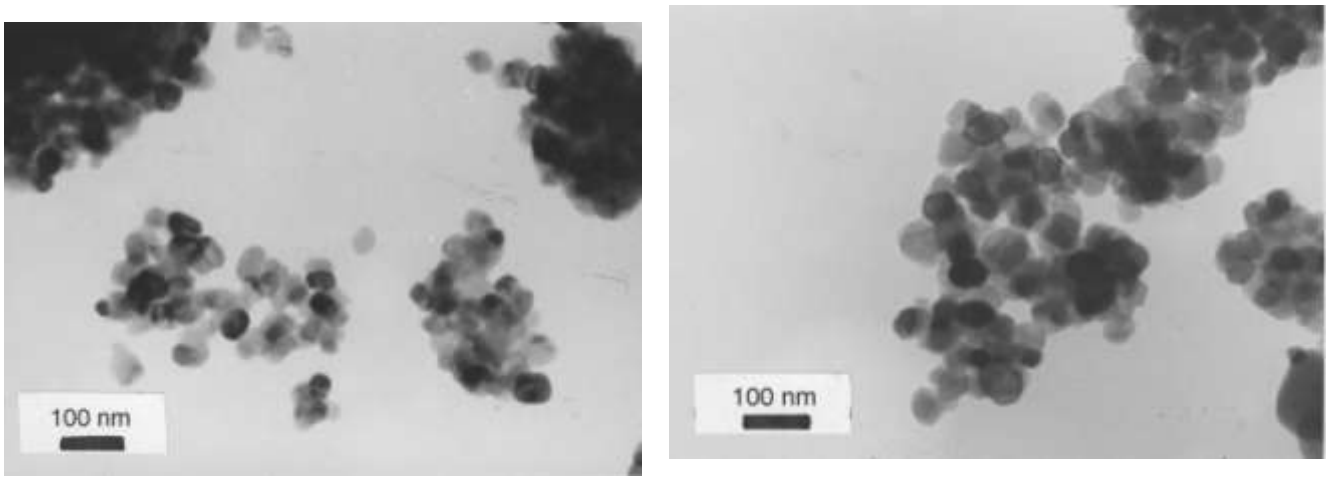

700°C, 30 mins **700°C, 8 hrs**

Figure 4*:* Tunneling Electron Microscope (TEM) images showing morphology of TiO_2 prepared from 'anatase paste' and annealed at 700°C for 30 min and 8 hrs respectively. From figure: 4 crystals calcined at 700°C for 8 hours appear to have undergone a change in crystal morphology. The crystals appear larger compared to crystals calcined for 30 minutes at the same temperature. This is most likely due to sintering of particles and hence forming larger crystals.

Figure 5: below represents a change in TiO_2 structure from anatase to rutile phases with increased calcination temperatures.

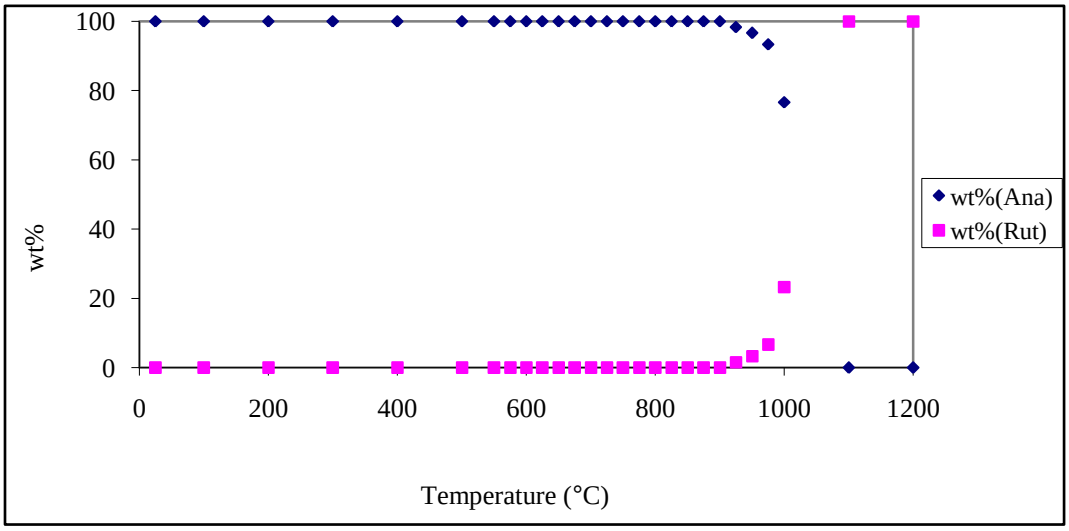

At temperature above 900°C, the rutile phase in the TiO_2 structure increases and the anatase phase decreases. Fig.5: Effects of calcination temperature on TiO_2 structure No rutile phase exists in the TiO_2 photocatalyst structure at temperatures below 900°C. At temperatures above 900°C, the rutile phase begins to emerge. At temperatures between 1100°C-1200°C, the rutile

phase in TiO_2 rises to 100%. However, these values are estimates of how much anatase and rutile phases exist in the powder material.

CONCLUSIONS

It was concluded that TiO_2 particle sizes increase with increasing calcination temperature. The observed particle sizes obtained using the SEM technique compare with the calculated values. The observations of this investigation clearly demonstrate that with increasing calcination temperature, the proportion of anatase phase in TiO_2 photocatalyst structure decreases. At 900°C the rutile phase begins to emerge and at 1100°C, the proportion is almost 100%.

ACKNOWLEDMENTS

The authors thank Prof. Josef Krysa of the Institute of Chemical Technology, Prague, Czech Republic for the advice, support and use of his lab at the Department of Inorganic Technology.

REFERENCES

Černigoj, U.L., Štangar, U., Trebše, P. (2007) Evaluation novel Carberry type photoreactor for the degradation of organic pollutants in water. *Journal of Photochemistry and Photobiology A: Chemistry* **188**,169-176.

Černigoj, U.L., Štangar, U., Trebše, P., Opara, K.U., Gross, S. (2006) Photocatalytically active TiO_2 thin films produced by surfactant-assisted sol-gel processing. *Thin Solid Films*, **495**, 327-332.

Hasnat, M.A., Siddiquey, I.A., Nuruddin, A. (2005) Comparative photocatalytic studies of degradation of a cationic and an anionic dye. *Dyes and Pigments* **66**,185-188.
Halman, M. **(1995)** Photodegradation of Water Pollutants. CRC Press, 28-30.

He, D. and Lin, F.(2007) Electrochemical aspects of photocatalysis application to detoxification and disinfection scenarios. *Materials Letters* **61**, 3385-3387.

Ma, H.M., Lu, Z., Zhang, M.S. (1998) Environmental applications of semiconductor photocatalysis *Journal of Applied Physics. A* **66,** 264 – 271.

Morawski, A.W., Zielinska, B., Grzechulska, J. (2003) Photocatalytic decomposition of textile dyes on TiO_2-Tytanpol A11 and TiO_2-Degussa P25. *Journal of Photochemistry and Photobiology A: Chemistry* **157**, 65–70.

Rebernik, R.P., Černigoj, U.L., Štangar, U., Trebše, P. (2006). Comparison of different Characteristics of TiO_2 films and their photocatalytic properties. *Acta Chimica Slovenica* **53**, 29-35.

Yuan, Z.H. and Zhang, L.D.(1998) TiO_2 mediated photocatalytic degradation of orange II with the presence of Mn^{2+} in solution. *Nanostruct. Mater*. **10**,11-27.

THERMODYNAMICS OF MICELLIZATION OF AMPHIPHILIC NON-IONIC TRI-BLOCK COPOLYMER AND ANIONIC SURFACTANT SODIUM DEDOCYLSULPHATE IN AQUEOUS SOLUTIONS

[1]Benard Kiplangat Rop*, [2]Lazarus Kipichii Tanui and [2]Pius Keronei Kipkemboi

1. Department of Chemistry, University of Nairobi, P. O. Box 30197-00100, Nairobi, Kenya
2. Department of Chemistry and Biochemistry, University of Eldoret, P.O. Box 1125-30100, Eldoret, Kenya

*Corresponding author: (E-mail: kiplangatrop@gmail.com)

ABSTRACT

Physico-chemical properties of aqueous solutions of non-ionic tri-block copolymer $(PEO)_{19}(PPO)_{43}(PEO)_{19}$(Pluronic P84) and anionic sodium dedocylsulphate (SDS) surfactants have been studied. Additives such as salts, co-solvents, polymers have marked effect on micellization, clouding and solubilisation behaviour of surfactant solutions. Studying effects of various additives on the critical micelle concentration (CMC) and other micellar properties of individual surfactant components and their mixtures can be useful for optimizing their properties for various applications. The CMCs for SDS in pure water and in aqueous mixed solutions were determined with electrical conductivity whereas those for amphiphilic block copolymer were obtained using UV-Visible spectroscopy. The micellar behaviour of anionic SDS surfactant in aqueous media has been investigated over the temperature range 298.15 - 313.15 K. Thermodynamic parameters of micellization evaluated from CMC data are also reported. Other thermodynamic and solution properties of aqueous mixtures of block copolymer P84 were investigated with cloud point and viscometric techniques. Analysis of conductometric data indicates that inorganic salts lower CMC values of aqueous SDS. The CMC also shows a decrease in presence of poly(ethylene glycol) (PEG) and no dependence on change in concentrations of P84. The intrinsic viscosity values of P84 (1 wt. %) in presence of inorganic salts were significantly lowered. The values of free energy of activation of flow indicates the existance of spherical micelles being dependent on the nature and concentration of the additive. The copolymer also exhibited cloud point depression in presence of inorganic salts, whereas PEG did not significantly affect both the intrinsic viscosity and cloud point.

KEY WORDS: *Surfactants, physico-chemical properties, critical micelle concentration, micellization, aqueous mixtures*

INTRODUCTION

The study of physico-chemical properties of various forms of organized assemblies composed of surfactants is currently an actively pursued area in several laboratories [1]. Surfactants can be low molecular weight synthetic surfactants, natural lipids and large molecules such as block copolymers [2]. They are commonly classified according to polarity of their head groups as; anionics, cationics, non-ionics and zwitterions [3]. Extensive structural, kinetic and thermodynamic studies have been performed in surfactant-water systems. The usual approach of surfactant is that of studying its property as a function of concentration [4]. At specific amphiphilic concentration, the critical micelle concentration (CMC), they form aggregates called micelles. Almost all physico-chemical properties versus concentration plots for a given surfactant-solvent system show an abrupt change in slope in that narrow concentration range, CMC [5]. The CMC is single most important characteristic of a surfactant, useful in the consideration of practical use of surfactants. Micelles are thermodynamically stable aggregates, and their size, shape and charge may be modulated by other components and/or by varying surfactant concentration, temperature and pressure [6]. Surfactant self-assembly leads to a range of different

structures: spherical, cylindrical micelles, lamellar phase, reversed micelle and bicontinuous structure [7]. Micellar growth can be controlled in different ways, such as addition of electrolytes, non-electrolytes, weakly surface active solubilizates or variation of temperature [8].

Amphiphilic tri-block copolymers consisting of a relatively hydrophobic poly(propylene oxide) and two hydrophilic poly(ethylene oxide) end blocks (PEO-PPO-PEO) are commercially available as Pluronics. These block copolymers have been subject to a wide variety of recent publications. Despite their long time use, many aspects of their solution behaviour remains unclear, stimulating a large number of studies reported in literature [2, 8]. Their unique chemical structure offers a model system to study systematic variations in the hydrophobic–hydrophilic character that affect micellar solution properties [9, 10]. Investigation in mixtures of surfactants, surfactants and polymers, in aqueous solutions are of interest so as to gain fundamental understanding with regard to their technological applications [3, 10]. Recently, as pluronic tri-block copolymers are applied to more complex environments such as biological systems in drug and gene delivery, researchers are turning their attention to more complex systems of pluronics and other components such as inorganic salts, organic additives and surfactants of other types [11-14].

Surfactant mixtures commonly used in many practical applications usually form mixed micellar aggregates that frequently exhibit characteristic properties that are remarkably different and offer superior performance than those of individual components. Synergistic behaviours of mixed surfactant systems can be exploited to reduce the total amount of surfactant used in particular application resulting in reduction of cost and environmental impact [9, 13, 16]. Surfactants may bind co-operatively with water soluble polymers to form complexes and these interactions are largely confined to anionic surfactants. Among all mixed polymer-surfactant systems, sodium alkyl sulphates, especially sodium dedocylsulphate ($C_{12}SO_4Na$), are the most used anionic surfactants. In aqueous solutions, they form micelles and may also interact with water soluble polymers such as poly(ethylene glycol) [6]. In order to have closer look on the mechanism of their action, knowledge on aqueous solution properties are necessary. Pluronics BASF code named; F127, L64, P123, 25R4 have been used in polymer–surfactant studies [12-15] due to their interactions ionic surfactants. However, to the best of our knowledge, there is scarce information regarding physico-chemical properties Pluronic P84 and anionic surfactant (SDS) in aqueous solutions.

Surfactants are important in practical applications as detergents, emulsifiers, cosmetics, dispersants or vehicles in pharmaceutical formulations, defoaming and floatation agents, and more recently in electronics and computer industries [9]. Detergents accounts for the bulk of all surfactant usage, anionics being the most widely used. Modern surfactant formulation contains many different additives to increase the performance or assist in manufacturing process. Detergent additives include: builders (silicates, phosphates, carbonates, zeolites, sodium carboxymethylene cellulose), hytrotropes (toluene, xylene and cumensulfonates, alkyl diphenoxide disulfonates) and optical brighteners (fluorescent dyes). Surfactants used particularly in the household and industrial sector are discharged into sewers. The main determinant of formulation philosophy over the last decade has been greater awareness of the environmental responsibilities, and thus the market pull for “greener” products has been overriding force for surfactant development. Biodegradable surfactants and alternatives for phosphates are being sought for environmental reasons, eutrophication of lakes and streams. Additionally, there exist a challenge of finding ways to minimize the cost of manufacture for existing surfactants and development of detergents performing well at lower wash temperature.

This paper deals with an experimental study of physico-chemical properties of Pluronic P84 and SDS in aqueous solution in presence of electrolyte and non-electrolyte additives. Additives such as salts, co-solvents

and polymers have marked effect on micellization, clouding and solubilisation behaviour of surfactant solutions. They modify the surfactant-solvent interactions consequently changing the CMC, size of micelles and phase behaviour in the surfactant solutions. The effect of additives on the CMC and other micellar properties of the individual surface active components in mixture and the interaction between them afford an understanding on the role of each, and make possible the selection in a rational and systematic manner of components for optimal properties**.**

EXPERIMENTAL

Materials

The pluronic P84 obtained as a gift from BASF was used without further purification. The nominal molecular weight is 4,200 g mol^{-1} (40 wt. % PEO, content) with the following composition $(PEO)_{19}(PPO)_{43}(PEO)_{19}$. Anionic surfactant, sodium dedocylsulphate $C_{12}H_{25}OSO_3Na$ (purity >95%), was obtained from Aldrich Chemical Company. Poly(ethylene glycol) was from Merck with nominal molecular weight of 20,000. Inorganic salts (NaCl, Na_2SO_4, $AlCl_3$), Iodine and KI used were all Analar-grade.

All solutions were prepared by diluting known weights of concentrated stock solutions using demineralized and distilled water with conductivity of less than 2 μS at 298.15 K. The concentrations aqueous solutions used in the experiments ranged from 0.1-10 wt. % P84; 0.05-100 mM SDS; 0.025-2.0 M Inorganic salts (NaCl, Na_2SO_4, $AlCl_3$), and 0.1-2 wt. % PEG.

Determination of CMC

*Conductivity measurements:*The measurements were carried out in a digital conductivity meter (Philips PW 9526) using a dipping-type conductivity cell (PW 9510/60) with platinized electrodes and cell constant of 0.740 cm^{-1}, calibrated with aqueous KCl solution. Each portion of varied concentrations of aqueous SDS solutions with fixed concentrations of additives in a thermostated water bath was allowed 20 minutes of equilibrium attainment before each measurement.

Spectral changes of iodine-iodide mixture: All CMC measurements were performed at 293.15 K. For iodine/iodide mixture, a stock solution containing respectively 6.4×10^{-4} and 2.0×10^{-3}mol L^{-1} was prepared. A 1 mL aliquot of this solution was diluted to 5 mL with polymer solution. The absorbances were measured using UV-Visible spectrophotometer (Shimadzu PharmaSpec, Model UV–1700). The CMC determinations were made using maximum of absorbance at 291 nm.

Viscosity measurements

The kinematic viscosities were measured with Cannon-Ubbelohde type capillary viscometer (No.100 B989), with viscometer constant of 0.01413 mm^2/s^2. All polymer solutions were left at least 24 hours to equilibrate at 298.15 K to avoid aging effects. Prior to measurement, the samples were left in the viscometer mounted vertically in thermostated water bath at 298.15 K, for at least 20 minutes to attain thermal equilibrium in the investigated region. The flasks and the viscometer were kept properly stoppered and sealed during equilibration. The viscometer was cleaned with distilled water and dried every time before each measurement. The flow time for constant volume of solution through the capillary was measured with digital stopwatch. The same procedure was repeated at 303.15, 308.15 and 313.15 K. Measurement for each sample was carried out in triplicates, progressively with increasing surfactant concentration and the mean taken. All measurements were performed in a circulating water thermostat whose temperature was controlled to ±0.005 K.

Determination of cloud point

The copolymer solutions were allowed to equilibrate at low temperature overnight prior to measurements. 5 mL aliquot were filled with 10 mL glass vials from the diluted stock ranging from 0.5–10 wt. %. The vials were covered with rubber stoppers, sealed with aluminum caps, and immersed partially in the bath fluid. Around the temperature of interest, the bath temperature was raised in 0.2 K increments, each followed by 3–5 minutes equilibration period. At the end of equilibration period, the vials were lifted out of the bath fluid momentarily and inspected visually for cloudiness. The samples were then allowed to slowly cool under stirring condition and the temperature for the disappearance of turbidity also noted. The cloud point (CP) was the average of temperature at which clouding appeared and disappeared. The reproducibility of the measurements was found to be within ±0.2 K.

RESULTS AND DISCUSSION

The Critical Micelle Concentrations

Conductivity measurements are commonly used in the study of ionic micellar solutions. For nearly all ionic surfactants in aqueous solutions, there is a substantial change in slope at the onset of aggregation. The specific conductivity values versus surfactant concentration for SDS systems studied are presented in Figures 1-3. The plot of the system investigated as presented in Figure 1 is typical of anionic or cationic surfactant in aqueous solution. In order to gain thermodynamic insight into the binary aqueous solutions of SDS in pure water, the conductivity was measured as a function of surfactant concentration at various temperatures of 298.15, 308.15 and 313.15 K. Figure 1 depicts the behaviour of conductivity for SDS/H_2O binary system at various temperatures from which CMC values were determined.

At each temperature with increase in surfactant concentration, the specific conductivity varies linearly with distinct break points, the CMC. The conductivity shows gradual increase with increase in temperature, indicating that temperature influences the CMC of surfactant solution. This may be attributed to increase in the thermal energies of the molecular entities [17]. At 298.15 K, well defined break point appears at approximate concentration of 8.2 mM of the surfactant indicating the CMC. The value of CMC is very close to that found for the same system by surface tension measurements, CMC = 8.0 mM [18]. The slight differences observed could be attributed to the different methodology used.

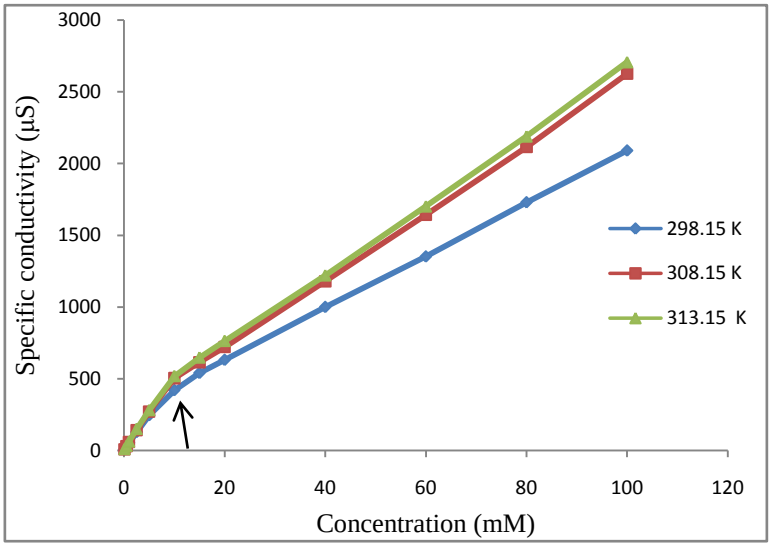

Figure 1: The variations of specific conductivities and concentration of SDS with temperature

It is also observed that increase in conductivity above the CMC is smaller than that below the CMC (Figure 1). The change in electrical conductance of ionic surfactant solutions at the CMC is due to different degree of surfactant ionization below (surfactant monomers behave as strong electrolytes) and above (micelles are partially ionized) the CMC. Below the CMC, no micelles are formed; then the specific conductivity of aqueous SDS solution, is made up of independent contributions of anions and cations [22]. Above the CMC, the specific conductivity has smaller slope because of two reasons; the confinement of fraction of counter-ions to the micellar surface results in an effective loss of ionic charges, and the micelles can contribute to charge transport to lesser extent than the free ions owing to their lower mobility [22].

The dependence of CMC upon the temperature was used to evaluate thermodynamic parameters of micellization for surfactant systems. The counter-ion degree of binding, β, and hence standard free energy of micellization, ΔG°_m, was calculated from the CMC values using Rosen Equation [5, 16].

For ionic surfactant;

$$\Delta G_m^{\circ} = (1+\beta)\, RT \ln X_{CMC} \text{ ---------- (1)}$$

whereas, for non-ionic surfactant;

$$\Delta G_m^{\circ} = RT \ln X_{CMC} \text{ ---------- (2)}$$

where, X_{CMC} = CMC expressed as mole fraction units.

The enthalpy change (ΔH°_m) of micellization was evaluated from the equation;

$$\ln \text{CMC} = \left(\frac{\Delta H^{\circ}_m}{RT} \right) + c \text{ ---------- (3)}$$

The calculated values of entropy change (ΔS^{o}_m) of micellization were obtained from the equation;

$$\Delta S^{\circ}_m = \left(\frac{\Delta H^{\circ}_m - \Delta G^{\circ}_m}{T} \right) \text{ ---------- (4)}$$

The values of CMC and thermodynamic parameters (ΔG^{o}_m, ΔH^{o}_m, ΔS^{o}_m) of micellization for aqueous SDS (298.15 K) in presence of inorganic salt additives are presented in Table 1. Aqueous SDS appears to give lower values of CMC, with Na_2SO_4 appearing to lower the CMC (8.2-0.5 mM) much more than NaCl (8.2-1.8 mM) in the same concentration range studied. SDS aggregates at increasingly lower concentrations as salt concentration is increased, consistent with the idea that micelles form in order to minimize the exposure of non-polar acyl chains to the ionic solutions [19].The presence of salt ions near the polar heads of surfactant molecules decreases the repulsion force between the head groups. They neutralize the charge at the micelle surface thereby decreasing the thickness of the micellar atmosphere around the surfactant ion heads. The electrostatic repulsion between them thus enables surfactant molecules to approach each other more closely and form larger aggregates. Therefore, micellar charge shielding in salt environment is the reason for significant lowering of CMC [5, 20]. The SDS systems also exhibits increase in counter-ion degree of binding (β) with increasing salt concentration. The effect is more pronounced for aqueous Na_2SO_4 + SDS as compared to NaCl + SDS system.

Table 1: Values of CMC, counter-ion degree of binding (β), free energy (ΔG^{o}_{m}), enthalpy (ΔH^{o}_{m}) and entropy change (ΔS^{o}_{m}) of micellization for SDS in presence Na_2SO_4 and NaCl at 298.15 K

ADDITIVE	CMC (mM)	β	$-\Delta G^{\circ}_{m}$ (kJ mol^{-1})	$-\Delta H^{\circ}_{m}$ (kJ mol^{-1})	ΔS°_{m} (J mol^{-1} K^{-1})
$[Na_2SO_4]$M					
0	8.2	0.70	37.15	2.08	118
0.025	2.0	0.73	43.85	5.50	129
0.050	1.5	0.94	50.56	6.21	149
0.075	0.5	0.96	55.23	8.93	155
[NaCl]M					
0	8.2	0.70	37.15	2.08	118
0.025	2.5	0.74	43.14	4.94	128
0.050	2.0	0.81	45.88	5.38	136
0.075	1.8	0.80	46.10	5.76	135

The specific conductivity versus concentration curves for SDS systems containing PEG and P84 are presented in Figures 2 and 3 respectively. The values of CMC and thermodynamic parameters in presence of PEG and P84 are presented in Table 2. The values determined show decreased CMC values from 8.2-4.7 mM as amount of PEG additive was increased while no change was observed as P84 concentration was increased. The ethoxylated chains of the PEG coil around the charged head groups of the anionic surfactant, screening the electrostatic repulsions and thereby favouring micelle formation resulting in low CMC. The CMC being low compared to that of pure SDS in aqueos solution, is explained by penetration of the polymer into ionic micelles and thereby reduce charge interaction. For SDS + P84 mixed surfactant system, no change in CMC is observed on the account of the formation of mixed ionic/non-ionic micelles. At CMC, surfactant molecules undergo co-operative self-association to form large surfactant aggregates [21]. In this process both ideal and non-ideal mixing contributions may occur. Since the hydrophobic effect which drives the overall process is not specific to surfactant "head" group, the formation of randomly mixed surfactant aggregates will tend to be favored. This can be viewed as leading to the "ideal" component of mixing in the aggregate.

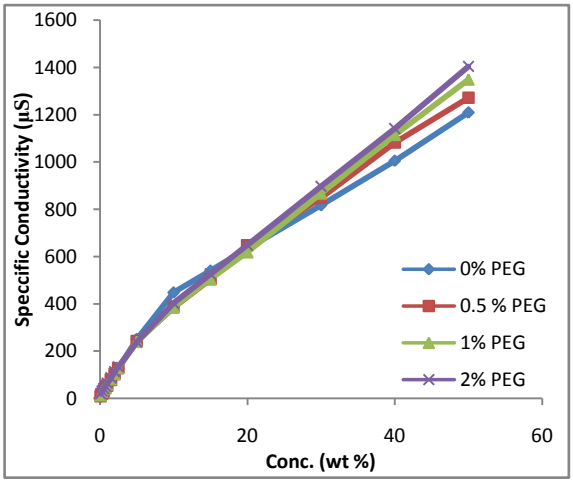

Figure 2: Specific conductivity versus concentration of sodium dedocylsulphate in presence of PEG at 298 K

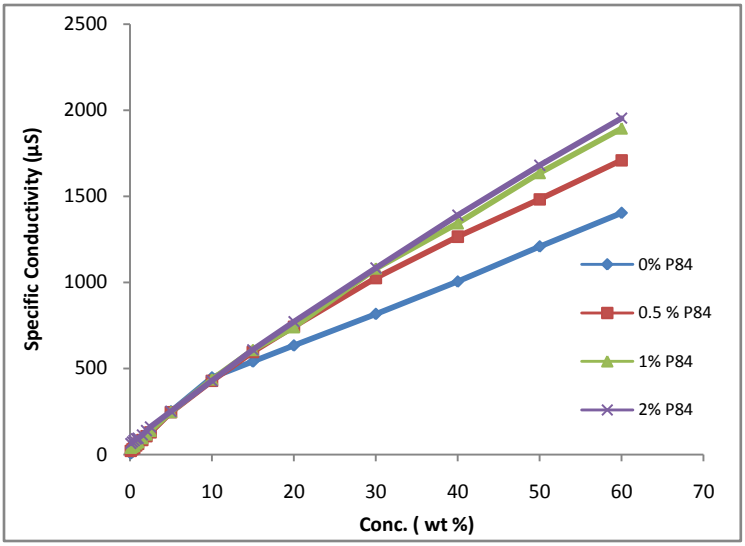

Figure 3: Specific conductivity versus concentration of sodium dedocylsulphate in the presence of P84 at298 K

Table 2: Values of CMC, counter-ion degree of binding (β), free energy (ΔG^{o}_{m}), enthalpy (ΔH^{o}_{m}) and entropy change (ΔS^{o}_{m}) of micellization for SDS in presence of PEG and P84 at 298.15 K

ADDITIVE	CMC (mM)	β	$-\Delta G^{o}_{m}$ (kJ mol^{-1})	$-\Delta H^{o}_{m}$ (kJ mol^{-1})	ΔS^{o}_{m} (J mol^{-1} K^{-1})
[PEG] wt. %					
0	8.2	0.70	37.15	2.08	118
0.5	5.0	0.53	35.31	3.24	108
1.0	4.8	0.48	34.30	3.33	104
2.0	4.7	0.46	31.84	3.38	95
[P84] wt. %					
0	8.2	0.70	37.15	2.08	118
0.5	8.2	0.44	31.47	2.00	99
1.0	8.2	0.32	28.84	2.00	90
2.0	8.2	0.17	25.57	2.00	79

The variations for ΔH^{o}_{m} and ΔS^{o}_{m} were quite sensitive to temperature and concentration of additives. The values of ΔH^{o}_{m} were found to range from -2.0 to -8.93 kJ mol^{-1}, being exothermic in the entire systems studied (Tables 1 and 2). The ΔH^{o}_{m} values for aqueous SDS systems containing inorganic salts and PEG were found to be more exothermic (see Tables 1 and 2) with increasing concentration of the additive, being more pronounced in SDS+Na_2SO_4, whereas in SDS+P84 (mixed surfactant system) shows no change. The exothermicity may be attributed to surfactant-additive interaction which results in the stability of the system [**23**], and therefore the formation of micelles was very much favoured in presence of inorganic salt additives. The values of ΔS^{o}_{m} also increased with increasing concentration of inorganic salts, but were observed to decrease for the systems containing PEG and P84.

However, in all the systems ΔS^{o}_{m} remained positive within ranging from 95 to 118 J mol^{-1} K^{-1}, an indication that micellization was entropy dominated. According to literature [23] the positive values of ΔS^{o}_{m} are attributed to the disruption of water structure. At the same time, water-water bonds are broken resulting in an increase in ΔS^{o}_{m}. This can be explained in two aspects: firstly, iceberg formation of water molecules surrounding the solute (surfactant) molecules would increase the system "order", then the micellization process; by removing the surfactant molecules from the aqueous medium to the micelle, would actually increase the entropy of the system

simply due to the rupture of the iceberg. Secondly, the degree of rotational freedom of hydrophobic chain of the surfactant molecules in the interior of the micelle is much larger than in aqueous medium; in other words, the configurational entropy of the hydrophobic chain of the surfactant molecules is increased when surfactant molecules are removed from aqueous medium to micelle [5, 24].

Spectrophotometric method (Figure 4) was used to determine the CMC value of non-ionic surfactant pluronic polymer P84. This determination was based on the shift that the UV-Visible absorption spectrum of the iodine/iodide mixture experience in micellar medium. The method is based on changes caused by this polymer on the absorption spectra of a solution containing a mixture of iodine and iodide. It has already been applied to analytical determination of similar copolymers and to study temperature-driven aggregation of some of these polymers [**26**]. Below the CMC, the absorption spectra are similar to that of aqueous I_2/I^- mixtures. As polymer concentration passes the CMC the peaks at 300 and 250 nm, ascribed to species of I_3^-, start decreasing to almost disappearing. It is assumed that the equilibrium of tri-iodide formation is displaced towards iodine and iodide as the micelles are formed, as a consequence of large solubilization of more hydrophobic iodine by micelle hydrophobic sites. Therefore, polymer self assembly leads to an abrupt absorbance decrease, thus allowing the determination of CMC. As observed in Figure 4, at 293.15 K, the maximum absorbance value is 1.27 (0.5 wt. % P84), which decreased sharply and linearly to a minimum value of 0.05 (2.2 wt. % P84) where it breaks. This was then followed by gradual and also linear increase in absorbance values from 0.05 to 1.1 with increased concentration of P84 up to 6 wt. %.

However, no sharp CMC or CMT (critical micellization temperature) have been observed for block copolymers. In practice, a certain CMC range with some notable uncertainty is usually detected. A large difference is often noted between the CMC values determined by different methods because the sensitivity of the techniques to the quantity of molecularly dispersed copolymers (unimers) present in solution may vary. For common surfactants, a considerable amount of CMC data has been collected whereas, for block copolymers only scarce CMC data have been available in the literature so far [27]. Further, the values reported in the literature differ substantially; the lack of sufficient temperature control, in conjunction with batch-to-batch variations, may be responsible for the observed variations.

The absorbance measurements (Figure 4) showed a break at approximately 2.2 wt. % (≡ 5.23 mM) P84 as the value of CMC, which is lower than that of SDS (8.2 mM). This is because aggregation is mainly due to hydrophobic interaction among the hydrocarbon chains for non-ionic surfactants. This is more feasible because the hydrophobic groups are easily separated from the aqueous environment, whereas for ionic surfactants, high concentrations are necessary to overcome the electrostatic repulsions between the ionic head groups during aggregation [9].

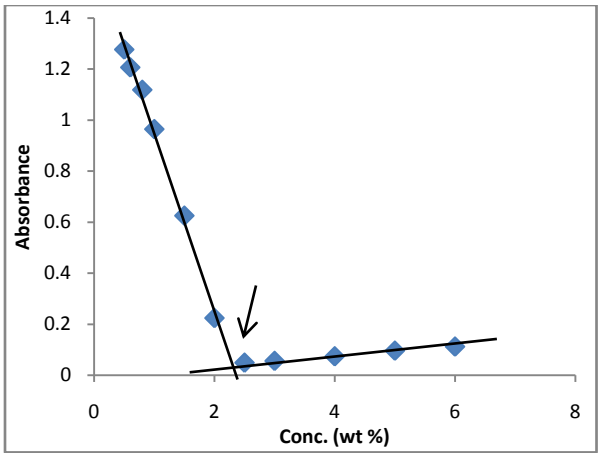

Figure 4: Spectral changes of I_2/I^{-1} mixture with increasing concentration of P84 (wt. %) at 293.15 K

The value of $\Delta G°_m$ involved in micellization process was found to be -22.58 ±1.1 kJ mol^{-1}. For various Pluronic PEO-PPO-PEO copolymers, the reported values of $\Delta G °_m$, $\Delta H°_m$ and $\Delta S°_m$, range from -24.5 to -28.8 kJ $mo1^{-1}$, 169 to 339 kJ $mo1^{-1}$, and 0.64 to 1.24 kJ mol^{-1} K^{-1}, respectively [27].The free energy, $\Delta G°_m$, is high and negative indicating spontaneous formation of thermodynamically stable micelles [**22**].

Viscosities of Aqueouos Mixtures of Pluronic P84 Bock Copolymer Solutions

Parameter of great importance for polymer characteriation is the intrinsic viscosity, $|\eta|$, which depends on the concentration and size of the dissolved macromolecules, as well as the solvent quality and temperature [**28**].Viscosity measurements are based on flow liquid/solution through a capillary tube. The variation in the viscosity of the solution gives information on the phenomenon of the micellar association [29]. It has been used in polymer analysis and in the field of polymer-surfactant interactions. The viscosities of solutions were calculated with respect to the viscosity values of water.

Relative viscosity, $\eta_r = {}^{\eta}/_{\eta_\circ} = t/t_\circ$ ---------- (5)

where: $\eta_{o,}$ viscosity of pure solvent; η, viscosity of solution; $t_{o,}$ efflux time of solvent; t, efflux time of solution

Specific Viscosity, $\eta_{sp} = {}^{(\eta - \eta_\circ)}/_{\eta_\circ} = \eta_r - 1$ ---------- (6)

Intrinsic viscosity, $|\eta| = \left({}^{\eta_{sp}}/_{C}\right)|_{c\to 0}$

$$\equiv \left[{}^{(\eta_r - 1)}/_{C}\right]_{c\to 0} \quad \text{---------- (7)}$$

The intrinsic viscosity generally decreased with an increase in temperature from 298.15 to 313.15 K in all the systems studied. The decrease in $|\eta|$ values were from; 18.8 to 8.6 cm^3/g for P84, 11.8 to 4.0 cm^3/g for P84+Na_2SO_4, 26.6 to 2.7 cm^3/g for P84+NaCl, 19 to 8.4 cm^3/g for P84+$AlCl_3$, and 169 to 48 cm^3/g for P84+PEG, as depicted in Figures 5-9. This is an indication of pronounced micellar dehydration. That, the viscosity of a liquid decreases with a rise in temperature is well known [23]. An increase in random movements of solute surfactant molecules also occurs in an increasing temperature because of an increasing kinetic energy. The micelles become compact with an increase in temperature owing to the dehydration of the oxyethylene chains.

The relationship between the intrinsic viscosity and concentration of P84 at various temperatures is presented in Figure 5. The intrinsic viscosity was found to decrease with increase in temperatures, with maximum of 18.8 cm^3/g at 298.15 K and minimum of 8.6 cm^3/g at 313.15 K, indicating pronounced micellar dehydration. Perusal of Figure 5 shows that, intrinsic viscosity falls to a minimum at ≈2 wt. % P84 (CMC) surfactant solution and then suddenly rises in the same pattern. In the pre-micellar region (<2 wt. %), the properties change almost linearly and give information on the solvent-monomer and monomer-monomer interactions. Just above the CMC (>2 wt. %), the properties were found to change strongly with surfactant concentration owing to the transfer of the surfactant from water to the micelles. At high surfactant concentration, the properties tend to a constant value and the deviations reflect micelle-micelle and monomer-micelle interactions [4].The intrinsic viscosity, $|\eta|$, has been taken by some researchers [23] to be equal to $(\eta_r - 1)/c$ without the condition of the limiting concentration and hence, $|\eta|$ was calculated without taking zero concentration limit into account. It has been observed in some cases that, below definite concentration, the curve of (η_{sp}/c) which equals to $(\eta_r - 1)/c$ plotted against concentration shows an upward or downward turn [28]. This was attributed to adsorption of polymer chains on the glass walls of the viscometer, expansion of the individual coils and conformational changes.

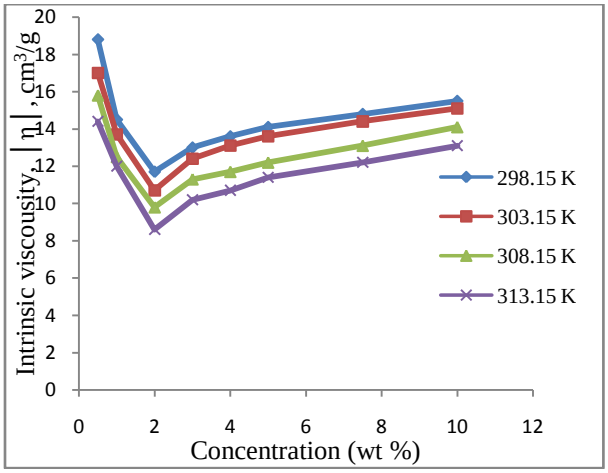

Figure 5: Intrinsic viscosity versus concentration of P84 (wt. %)

Figures 6-9 show intrinsic viscosity of P84 (1 wt. %) as a function of concentration of additives. The intrinsic viscosity was found to decrease with increase temperature and concentration of the additive. In the presence of Na_2SO_4, NaCl and PEG, there was a sharp decrease in a similar trend, upon which it tends to a constant value (Figures 6, 7 and 9) while P84+$AlCl_3$ system showed a minimum taking a U-shape (Figure 8). It is observed that, the intrinsic viscosity values in presence of electrolytes are lower than in PEG. The low intrinsic viscosity with increasing concentration of the salt additives in turn leads to high viscosity due to the larger effective size of the copolymer micelles in solution. Addition of salts cause dehydration of ethylene oxide units from dehydrated PEO shell from the side of PPO core leading to an increase in the core radius of the spherical micelles [**30**]. The U-Shape displayed in presence of $AlCl_3$ is attributed to the complexation of polyoxyethylene chains of the copolymer.

Temperature affects sphere-to-rod transition thereby decreasing the viscosities of micellar solutions, as the temperature is increased, due to break up of cylindrical micelles responsible for high viscosities observed. Such decrease in micellar size with temperature at high concentrations of electrolytes has been reported [31]. Transition from rod-to-spherical micelles by effect of temperature occurs at 298.15, 303.15, 308.15 and 313.15

K. At temperatures higher than 313.15 K, the system would contain almost only spherical micelles (with relative viscosities similar to water) while temperatures lower than 298.15 K solubility problems could arise.

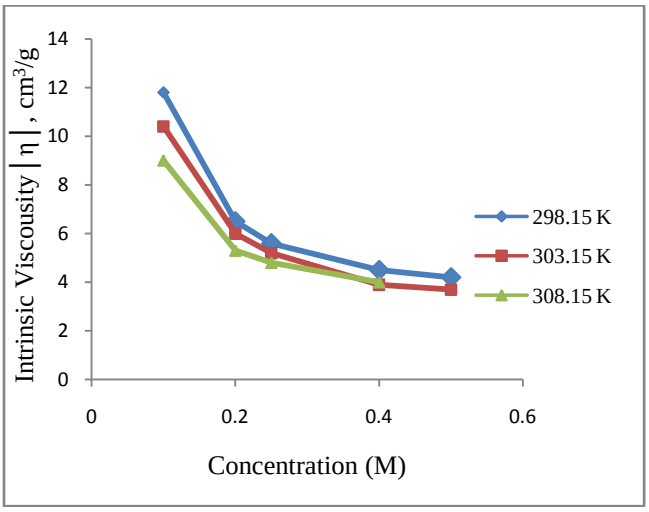

Figure 6: Intrinsic viscosity of P84 (1 wt. %) versus concentration of Na_2SO_4

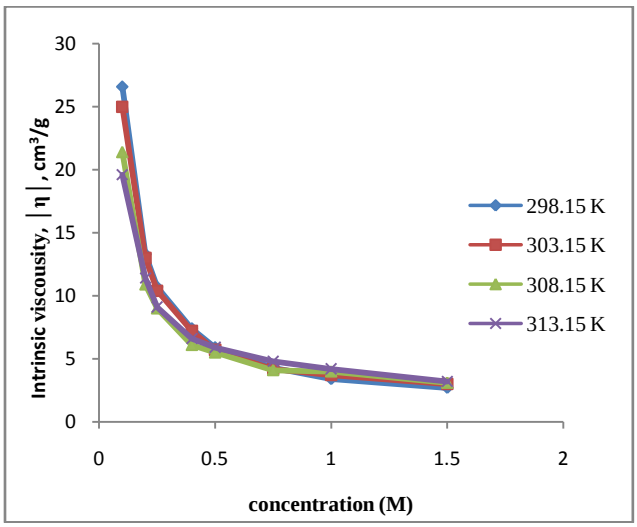

Figure 7: Intrinsic viscosity of P84 (1 wt. %) versus concentration of NaCl

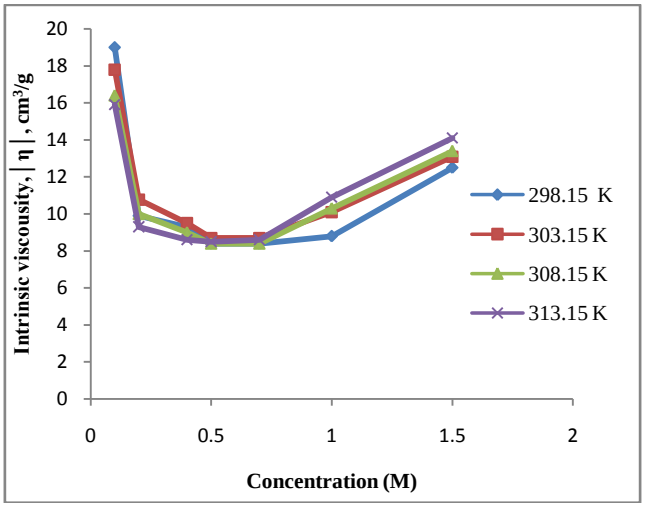

Figure 8: Intrinsic viscosity of P84 (1 wt. %) versus concentration of $AlCl_3$

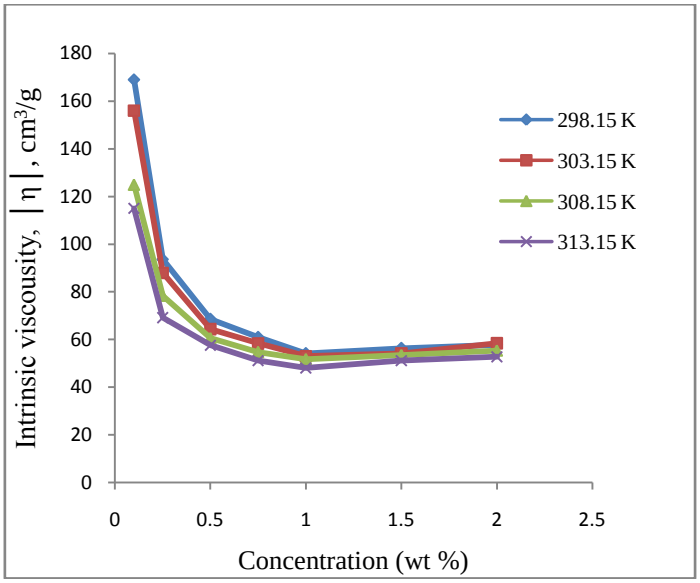

Figure 9: Intrinsic viscosity of P84 (1 wt. %) versus concentration of PEG

Thermodynamic activation parameters (ΔG*, Δ H*, ΔS*) of the viscuos flow for Pluronic P84 (1 wt. %) in presence of additives are presented in Table 3. From Eyring theory of viscosities, the activation free energies (ΔG*) were determined from the relative viscosities (Eqn. 5) using equation (8).

$$ln(\eta/\eta_\circ) = ln\,A \times exp(\Delta G^*/RT) \quad \text{---------- (8)}$$

where; A, is a constant and ΔG*, is the activation free energy term.

The linearity of the ln $(\eta/\eta_\circ)$ vs $(1/T)$ plot yields the slope $(\Delta G^*/R)$, where the activation free energy of the viscous flow was evaluated.

Form the dependence of ΔG* with temperature and using the well-known equation **[31],**

$$\frac{\delta(\Delta G^*/T)}{\delta(1/T)} = \Delta H^* \text{----------} \quad (9)$$

The activation enthalpy (ΔH*) for the viscous flow was then calculated and thus obtained values of ΔG* and ΔH*, allowed the calculation of the entropic contribution to the activation free energy.

The results in Table 3 shows the values of ΔG* decreasing with increased concentration of inorganic salts and changes from positive to negative. In presence PEG, it is also found to decrease, but not sensitive to change in concentration and remained positive in the range studied. Positive values of ΔG* in the systems indicate a nonspontaneous flow [23] and vice versa. The Eyring picture of shear between two layers of liquids involves the successive passage of individual particles from one equilibrium position to another. Such transfer would determine the energy required to create a hole to push back other particles. The ΔG* values reflect the free energy necessary to create a hole or, perhaps more important to produce an "activated micellar structure" capable of being rapidly transformed into a smaller cylindrical and finally into a spherical micelle [31]. The low values of ΔG* in absence and presence of additive is an indication of the existance of spherical micelles in all the systems studied. Table 3 also shows the ΔG* or ΔH* values are also dependent on the nature and concentration of the additive. The ΔH* values practically cover the total contribution to ΔG*, and accordingly, the entropic contribution is negligible.

Table 3: Thermodynamic activation parameters of the viscous flow of P84 (1 wt. %) in presence of additives

ADDITIVE	ΔG^* (kJ mol^{-1})	ΔH* (kJ mol^{-1})	ΔS* (J mol^{-1} K^{-1})
[Na_2SO_4] M			
0	3.70	3.84	0.46
0.1	3.68	3.77	0.29
0.5	-0.90	-0.89	0.01
[NaCl] M			
0.1	1.90	1.88	0.05
0.5	0.71	0.70	0.01
1.0	-1.90	-1.88	0.05
1.5	-2.38	-2.260	0.40
[$AlCl_3$] M			
0.1	0.37	0.45	0.28
0.5	-1.40	-1.38	0.05
1.0	-2.25	-2.22	0.07
1.5	-4.29	-4.25	0.12
[P84] wt. %			
0.1	1.60	1.58	0.05
0.5	1.55	1.53	0.04
1.5	1.50	1.49	0.04
2.0	1.48	1.47	0.05

Clouding Behaviour of Pluronic P84 Solutions

One characteristic feature of non-ionic surfactants solutions is their instant separation upon heating into two phases. The temperature at which this phase separation occurs is known as the cloud point (CP). CP is the manifestation of solvation/desolvation phenomena in a non-ionic surfactant solution. The desolvation of hydrophilic group of surfactant leads to the formation of clouding. The cloud point phenomenon in non-ionic polyoxyethylenated surfactants is believed to be due to aggregation [23]. The hydration of polyoxyethylene groups opposes this aggregation of micelles. As the temperature is increased, the head groups

become dehydrated; the size of the surfactant aggregates increases as the CP is approached. The CP is very sensitive to presence of additives even at low concentrations.

Block copolymers show amphiphilic properties in aqueous solutions due to different polarities of the blocks. The amphiphilic behaviour of these polymers is highly temperature-dependent. As the temperature is increased, the polymers become gradually hydrophobic, until finally CP is reached and phase separation occurs. The conformation of the polymer chains changes with increasing temperature to a high energy form. The polarity of chains thereby is influenced, along with the amphiphilic behaviour of the polymer [32]. It is believed to be as a result of enhanced intermolecular association driven by hydrophobic interaction between the surfactant tail groups and/or decreased hydration of the PEO chain.
The cloud points reported were measured with 1 wt. % P84 surfactant solution. Figure 10 shows variation the cloud point for P84 solution as a function of the concentration of inorganic salts. As illustrated in the figure, P84 surfactant exhibits a cloud point depression in the presence Na_2SO_4 and NaCl, whereas an increase is observed for P84+$AlCl_3$ system. The phase separation temperature of the copolymer-water system is dependent on the addition of salts, both the concentration and type being important

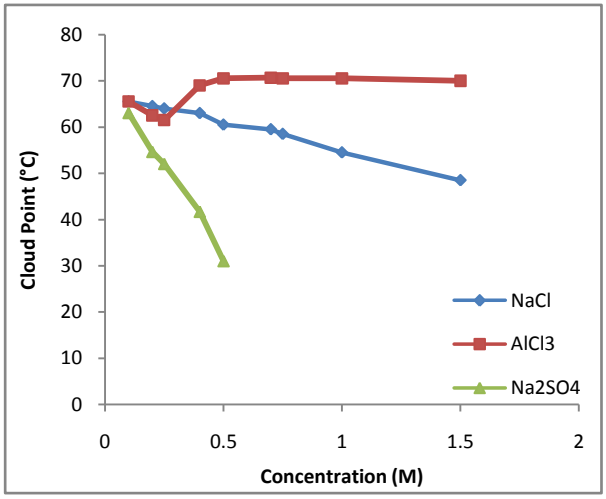

Figure 10: Cloud point of P84 (1 wt. %) versus concentration of electrolytes (Na_2SO_4▲, NaCl♦, $AlCl_3$■)

Electrolytes that raise the cloud point extend the temperature range in which the surfactant is soluble in water (salting in) while electrolytes that lower the cloud point reduce the solubility range (salting out). At high salt concentration, cloud point decreases due to high ionic strength leading to "salting out" of the polyelectrolyte-type polyoxyethylene [7]. This "salting out" effect is generally attributed to the dehydration of the ethylene oxide chains, thereby resulting in the disruption of the hydrogen bonding forces responsible for maintaining water solubility. The electrolytes studied decreased the cloud point of P84 solution. Na_2SO_4 is a more effective cloud point lowering agent at much lower concentration than monovalent cation (Na^+) whereas, tri-valent cation (Al^{3+}) is effective only at low concentration (up to 0.25 M) above which the CP rises. SO_4^{2-} ions enhance the structure of water, promoting association among water molecules and/or compete with the surfactant for water of hydration, salt it out and reduce the cloud point. Na^+ ions suppress the cloud point by dehydration. Tri-valent cation (Al^{3+}) "salts in" the polyoxyethylated surfactant by complexation with its ether groups. The polyoxyethylene moiety of the amphiphiles acts as a polydentate ligand. Weak cation binding imparts a slightly cationic character to the non-ionic

surfactants micelles, which accounts for the salting in [33]. PEG at the 0.1-2 wt. % concentration range did not significantly affect the cloud point of the copolymer. In addition to commonly known interacting forces between small molecules, one expects the excluded volume effect to come into play in the interaction between PEG and P84 surfactant. The excluded volume effect is derived from steric exclusions between molecules, i.e., two molecules cannot occupy the same space at the same time. One would therefore expect the steric exclusion effect to favor the phase separation of non-ionic surfactant and lower the cloud point.

CONCLUSION

Physico-chemical properties of anionic and non-ionic aqueous surfactant solutions in presence of additives are reported. In presence of additives, the formation of micelles is more spontaneous and increases by increasing the additive concentration. Thermodynamically, it is more favorable for SDS to form micelles in presence of inorganic salts than in PEG and P84. The intrinsic viscosity of P84 far much decreases with increase in both the temperature and the concentration of the inorganic salt. Low values of free energies of activation (ΔG^*) of Pluronic P84 in absence and presence of additives, indicate the existence of spherical micelles in all the systems studied. Presence of inorganic salt additives affects the CP of P84 surfactant solution, and the effect of either raising or lowering depends on whether the salt is "salting in" or "salting out" electrolyte. The results demonstrate that solution properties of P84 and SDS surfactant systems can be modulated in presence of additives, a significant characteristic regarding product formulation design for achievement of enhanced performance properties.

ACKNOWLEDGEMENT

The authors acknowledge The University of Eldoret, Department of Chemistry and Biochemistry, for the support they offered in their laboratory facilities.

REFFERENCES

1. Abdallah Gherbi. (2008) "Non-ionic Florocarbons Surfactants Phase Diagrams and X-ray Diffraction Study" *European Journal of Scientific Research,* 24: 523-537.
2. Kipkemboi, P.; Ali, K.; Lindman, B.; Viveka, A. (2003) "Phase Behaviour and Structure of Amphiphilic Molecules Poly(ethylene oxide)-Poly(propylene oxide) tri-block Copolymers, $[(EO)_4(PO)_{59}(EO)_4$ and $(EO)_{17}(PO)_{59}(EO)_{17}]$ in Ternary Mixtures in Water and Xylene" *Canadian. J. Chem.*, 81: 897-908.
3. Patel, K.; Bharatiya, B.; Kadam, Y.; Bahadur, P. (2010) "Micellization and Clouding Behaviour of Block Copolymer in Aqueous Solution"*J. Surfactants and Detergents,* 13: 89.
4. De Lisi, R.; Milioto, S.; Nicola, M. (2009) "Thermodynamics of Surfactants, Block Copolymers and their Mixtures in Water: The Role of the Isothermal Calorimetry" *International Journal of Molecular Science*, 10(7).
5. Kanyi, C. W.; Kipkemboi, P.K. (2005) "Micellar Properties of One and Two Headed Surfactant Systems: Sodium DedocylSulphate, Disodium 1, 2-Dedocyl Disulphate and Disodium 1, 12-Dedocyl Disulphate" *Journal of the Kenya Chemical Society,* 2 (2): p 31-35.
6. Sadeghi, R; Hosseini, R. (2009) "Thermodynamic Properties of Surfactant: Sodium n-heptylSulphonate in Water and in Aqueous Solutions of Poly(ethylene glycol) at Different Concentrations" *Colloids and Surfaces A: Physico-chem. Eng. Aspects,* 348: 177-185.

7. Holmberg, K.; Jonsson, B.; Kronberge, B.; Lindman, B. (2003) "Surfactants and Polymers in Aqueous Solution"*2nd ed., Willey Interscience,* p 1-66, 197-199.
8. Cambou, M.A.; Juarez, J.; Topete, A.; Mistry, D.; Attwood, D.; Barbosa, S.; Taboada, P.; Mosquera, V. J. (2011)Micellization of tri-block Copolymer of ethylene Oxide and 1, 12-Butylene Oxide: Effect of B-block Length" *Elsevier, Colloid Interface Sci.*, 361(1): 154-158.
9. Joshi, T.; Jitendra, M.; Pratap, B. (2005) "Micellization and Interaction of Anionic and Non-ionic Mixed Surfactant Systems in Water" *Elsevier, Colloids and surfaces A: Physico-chem. Eng. Aspects*, 260: 209-215.
10. Sulthana, S.B.; Rao, P.V.C.; Bhat, S.G.T.; Nakano, T.Y.; Sughihara, G.; Rakshit, A.K. (2000) "Solution Properties of Non-ionic Surfactants and their Mixtures: Polyoxyethylene (10) Alkyl Ether [C_nE_{10}] and Mega-10" *Langmuir,American Chem. Society,* 16: 980-987.
11. Song, H.; Guo, C.; M.A.J.; Xiang, J.; Luu, H-Z. (2009) "Micellization Interaction and Microenvironment in Mixed Solution of Pluronic and Surfynol 104 with Nuclear Magnetic Resonance" *The Chinese Journal of Process Eng*., 9 (No.4).
12. Kam C.T. and Evan W. (2006) "Insights on polymer surfactant complex structures during the binding of surfactants to polymers as measured by equilibrium and structural techniques" *The Royal Society of Chemistry, Reviews,* 35: 693–709
13. Bastrzyk A.; Polowczyk I.; Szelag E. and Sadowski Z. (2012)"Adsorption and Co-adsorption of PEO-PPO-PEO Block Copolymers and Surfactants and Their Influence on Zeta Potential of Magnesite and Dolomite" *Physicochemical Problems of Mineral Processing* 48(1), 2012, 281-293
14. Rakesh S.; Rajaraman M. and Chivukula N.M. (2012) "Clouding and Aggregation Behavior of PPO-PEO-PPO Triblock Copolymer (Pluronic®25R4) in Surfactant Additives Environment" *Tenside Surfactants Detergents*: 49 (2):136-144.
15. Jayita B.; Gunjan V.; Aswal V.K. and Hassan P.A. (2008) "Small Angle Neutron Scattering Study of Doxorubicin-Surfactant Complexes Encapsulated in Block Copolymer Micelles" *PRAMANA- Journal of Physics*, 71(5): 991-995
16. Rosen, M.J. (2004) "Surfactants and Interfacial Phenomena" *3rd Edition, Willey Interscience,* New York, p 95- 139.
17. Mehta, S.K.; Bhasin, K.K.; Renu, C.; Shilpee, D.(2005) "Effect of Temperature on Critical Concentration and Thermodynamic Behavour of Dodecyldimethylammonium Bromide and Dodecyldimethylammonium Chloride in Aqueous Media " *Elsevier, Colloids and surfaces A: Physico-chem. Eng. Aspects*, 2255: 153-157.
18. D'Aprano, A.; Sesta, B., Proietti, N.; Mauro, V. (1997)"Conductivity of Lithium Perflourononanoate in Water-Poly(vinyl pyrrolidone) Solutions" *Journal of solution Chem.*, 26: 649-662.
19. Cambou, M.A.; Juarez, J.; Topete, A.; Mistry, D.; Attwood, D.; Barbosa, S.; Taboada, P.; Mosquera, V. J. (2011) "Micellization of tri-block Copolymer of ethylene Oxide and 1, 12-Butylene Oxide: Effect of B-block Length" *Elsevier, Colloid Interface Sci.*, 361(1): 154-158.
20. Benito, G.M.A.; Monge, C.; Saz, J.M.; Marina, M.L. (1997) "Spectrophotometric and Conductimetric Determination of Critical Micellar Concentration of Sodium DedocylSulphate and Cetyltrimethylammonium Bromide Micellar Systems Modified by Alcohols and Salts" *Colloids and Surfaces A: Physico-chem. Eng. Aspects*, 125: 221-224.
21. Sarkar, B., Lam, S.; Alexandridis, P. (2010) "Micellization of Alkyl-propoxy-ethoxylate Surfactant in water-Polar Organic Solvent Mixtures" *Langmuir,* 26(13): 10532-40.

22. Alexandridis, P.; Vassiliki, A; Hatton, A.T. (1995) "Pluronic -P105 PEO-PPO-PEO Block Copolymer in Aqueous Urea Solutions: Micelle Formation Structure and Micro-environment"*Langmuir, American Chem. Society,* 11: 2442-2450.
23. Sharma, S.K.; Rakshit, A.K.(2004) "Investigation of Properties of Decaoxyethylene n-dedocyl Ether, $E_{12}O_{10}$, in Aqueous Sugar Rich Region" *J. Surfactants and Detergents,* 7: 305-315.
24. Dubey, N. (2008) "A Conductometric Study of Interaction between Sodium Dodecyl Sulphate and Propanol, 1-Butanol 1-Pentanol and 1-Hexanol at Different Temperatures" *J. Surface Sci. Technology*, 24: 139-148.
25. Chen, Li-Jen; Lin, S.Y.; Haung C.H.; Chen, E.M. (1998) "Temperature Dependence of Critical Micelle Concentration of Polyoxethynated Nonionic Surfactants" *Elsevier, Colloids and surfaces A: Physico-chem. Eng. Aspects*, 135: 175-181.
26. Yapar, E.A.; Inal, Ö. (2012) "Poly(ethylene Oxide)-Poly(propylene Oxide)-Based Copolymers for Transdermal Drug Delivery: An Overview" *Langmuir, Tropical J. Pharm. Research,*11(5): 855-866.
27. Alexandridis, P.; Allan, H.T. (1995) "Poly(ethylene oxide)-Poly(propylene oxide)-Poly(ethylene oxide) Block Copolymer Surfactants in Aqueous Solutions and at Interfaces: Thermodynamics, Structure, Dynamics, and Modeling" *Elsevier, Colloids and surfaces A:Physico-chem. Eng. Aspects, Review*, 96: I 46.
28. Irina-Elama, L.; Maria, B.; Simona, M. (2009) "Intrinsic Viscosity of Aqueous Polyvinyl Alcohol Solution" *Institute of Micromolecular Chem., Review*, 54: 981-986.
29. Kumar, S.; Bansal, D.; Kabir, U.D. (1999) "Micellar Growth in Presence of Aromatic Hydrocarbons: Influence of the Nature of the Salt" *Langmuir, J. American Chem. Society,* 15: 4960-4965.
30. Jain, N. J.; Aswal, V. K.; Goyal, P.S.; Bahadur, P. (2000) "Salt Induced Micellization and Micelle Structures of' PEO-PPO-PEO Block Copolymers in Aqueous Solution" *Colloids and Surfaces A: Physico-Chem. Eng. Aspects*, 173(1-3): p 85-94.
31. Sepulveda, L.; Gamboa, C. (1987) "Effect of Temperature on Viscosity of Cationic Micellar Solutions in the Presence of Added Salts" *Colloids and Interfacial Science,* 118(1): 87-90.
32. Kipkemboi, P.K.; Kiprono, P.C.; Ndalut, P.K. (2009) "Preparation of Mesoporous Silica with Amphiphilic Poly(oxyethylene)/Poly(oxybutylene) di-block, and Poly(oxyethylene)/poly(oxypropylene) tri-block Copolymers as Templates" *Indian Journal of Chem.*, 84 A: 498-503.
33. Marcela, M.A.; Messina, P.V.; Schulz, P. C. (2005) "The Interaction of Electrolytes with Non-ionic Surfactant Micelles*" Colloidal and polymer science, springer-verlag***.**

Investigations on wastewater treatment techniques in selected smallholder tea factories in Kenya

[1]Gitu, L[*]., [2] Chege, V. N. and [3]Ndegwa, G.
[1*.] Department of Chemistry, JKUAT
[2.] Institute of energy and environmental technology, JKUAT
[3] Department of Land Resources, JKUAT
[*] Corresponding author, Email: gitumleo@gmail.com

ABSTRACT

In Kenya there are fifty seven smallholder tea factories with annual production capacity of 180,000 tones of black tea per annum. The average water consumption per factory per day is approximately 30,000 cubic meters which translates to approximately 750,000 cubic meters per month. Large volumes of wastewater are therefore generated as effluent from these facilities. This effluent is usually collected in open lagoons and trenches to allow natural degradation of the pollutants to take place. Grab samples (from selected sites east and west of Rift) were collected at the inlet, middle and the last retention points from the lagoons, trenches and from a small wastewater treatment system. The electrical conductivities of the wastewater ranged between 660 ± 18.2 µs/cm and 1220 ± 26.2 µs/cm at the entry point, 663 ± 16.4 to 1234 ± 23.9 µs/cm at the mid point and 548 ± 16.8 to 1603 ± 30.2 µs/cm at the last point. These levels were below the 2000 µs/cm allowed by NEMA (K) for discharge into the environment. Biochemical Oxygen Demand (BOD), Chemical Oxygen Demand (COD), Total Suspended Solids (TSS) and colour concentrations were higher in the trenches than in the lagoons. At the retention points, trenches recorded the highest values of BOD_5, COD, TSS and colour intensities which were 1700 ± 26.7 mgO_2/L, 13500 ± 37.4 mgO_2/L, 6200 ± 36.7 mg/L and 3250 mgPt/L respectively. These were slightly higher than the values recorded for the lagoons at the same sampling point which were 1150 ± 17.5 mgO_2/L, 1500 ± 28.4 mgO_2/L, 900 ± 36.3 mg/L and 3150 ± 22.5 mgPt/L respectively. In all the sampling points, BOD_5, COD, TSS and Colour did not meet the requirements for discharge into the environment which are 30 mgO_2/L, 50 mgO_2/L, 30 mgO_2/L and 15mgPt/L respectively. The wastewater in these facilities had both positive and negative social and environmental impacts. Bacterial action in this wastewater with insufficient dissolved oxygen caused a strong and unpleasant odour which polluted the air around these facilities. It is recommended that measures be put in place to improve the final effluent quality to the level acceptable for discharge into the environment which may be done by installing appropriate wastewater treatment plants. Water conservation measures should also be put in place to minimize water usage. Comprehensive integrated water and wastewater planning and a wise investment in wastewater management would generate significant returns, as addressing wastewater is a key step in sustaining ecosystems.

Key words: waste water, lagoons, trenches, COD, BOD_5, TSS, color, treatment, tea factories.

Introduction

Agriculture is the single largest user of freshwater on a global basis. Water is an important requirement in many industrial processes such as heating, cooling production, cleaning and rinsing. Overall, some 5 - 20 percent of total water usage goes to industry (WWAP, 2009), with subsequent generation of substantial proportion of total wastewater. If unregulated, industrial wastewater has the potential to be highly toxic source of pollution. The vast array of complex organic compounds and heavy metals used in modern industrial process if

released into the environment can cause both human health and environmental disasters. In addition, has been reported to be a major cause of degradation of surface and groundwater resources through erosion and chemical runoff, there is then cause for concern about the global implications on water quality (FAO, 2000).

Wastewater is a combination of one or more of: domestic effluent consisting of black-water (excreta, urine and feacal sludge) and grey-water (kitchen and bathing water), water from commercial establishment and institutions including hospitals; industrial effluent, storm water and other urban run off; agricultural, horticultural, and aquaculture effluents either dissolved or as suspended matter (Raschid-Sally and Jayakody, 2008). Characteristics and composition of wastewater streams depend on the types of process from which it emerges (Tchobanoglous, *et al*; 2003), hence treatment strategies also vary (Falkenmark, 1998).

Re-use of wastewater has been successful for irrigation of a wide range of crops and an increase in crop yields from 10-30% has been reported (E L- Haary, 1998). In addition, re-use of treated waste land for irrigation and industrial purposes can be used as a strategy to release freshwater for domestic use, and to improve the quality of river waters used for abstraction of drinking water (by reducing disposal of effluent into rivers). Wastewater is used extensively for irrigation in certain countries. For instance, approximately, 67%, 25% and 24% of the total effluent in Israel, India and South Africa respectively are re-used for irrigation through direct planning, though unplanned re-use is considerably greater (E L-Haary, 1998).

There are a variety of wastewater treatments which encompass a number of steps which filters, clarify and clean the wastewater from start to finish (Karen, 1996). Industrial wastewater treatment covers the mechanisms and processes used to treat waters that have been contaminated in some way by anthropogenic industrial or commercial activities prior to its release into the environment or its re-use. There are several methods/techniques that are used to treat industrial wastewater. Some of these techniques include solids, oils and grease removal, biodegradable pollutants and organism removal.

Methodology

Study sites

The study sites were seven selected smallholder tea factories from both east and west of the Rift Valley Region in Kenya. The selection criterion was based on the method of treatment namely; lagoons (Gathuthi, Ngere, Nyankoba), trenches (Kagwe, Gachege, Kapkatet) and wastewater treatment plant (Ragati).

Sampling

During sampling the bottles were rinsed with wastewater three times and then filled from each of the designated sampling points. Grab (simple random) samples were collected from the inlet, center and last discharge points. Simple random sampling method was employed. The sampling was done at three different points; that is at the entry point, at the middle and at the last retention point of the wastewater facilities.

Chemical and microbial analysis

The samples for bacteriological analysis were taken in sterile bottles, stored in a cool box and transported to the laboratory. Samples for physico-chemical analysis were collected in clean plastic bottles. Electrical conductivity and pH samples were collected in clean plastic bottle

and analyzed on site. Samples for BOD, COD and TSS, TDS, Colour, Oil and grease were collected in clean plastic bottles and stored in cool box and transported to the laboratory.
pH and electrical conductivity were determined by Multitester sensor module WMS -24-01 (DKK-TOA CORPORATION, Japan). BOD_5 was determined as the difference between the oxygen concentration of an appropriately diluted sample before and after incubation for 5 days at 20 ± 1 ^{0}C. BOD was obtained by the equation 1 (APHA, 2005).

Molarity of FAS (Ferrous Ammonium Sulphate) = $\frac{Volume\ \ of\ 0.0167\ MK2Cr2O7\ solution\ \ titrated\ \ mL\ x\ 0.1000}{Volume\ \ of\ FAS\ used\ in\ titration\ \ (mL)}$

$$\text{COD, mg } O_2\text{/ L} = \frac{(A-B)xMx800}{sample\ \ volume\ ,\ \ mL} \quad \text{.....(1)}$$

where A = mL FAS used for blank
B = mL FAS used for sample
M = molarity of FAS
800 = milliequivalent of O_2 x 100l/L

Closed reflux, titrimetric method was used. The sample was refluxed with potassium dichromate and sulfuric acid in presence of silver sulfate which was a catalyst. The quantity of potassium dichromate used was directly proportional to the oxidizable organic matter in the wastewater sample. COD was obtained by the equation 2 (APHA, 2005).

$$BOD_5\text{, mg } O_2\text{/L} = \frac{D1-D2}{P} \text{.....(2)}$$

where D1 = DO of diluted sample immediately after preparation, mg/L
D2 = DO of diluted sample after 5 days incubation at 20 ± 1 ^{o}C, mg/L
P – Decimal volumetric fraction of sample used

A homogeneous sample was filtered through a standard glass fiber filter (0.45µm) into a weighed crucible, and the filtrate was dried at 180^{0}C to a constant weight. The increase in weight of crucible represented the TDS as equation 3 (APHA, 2005).

$$\text{TDS, mg/L} = \frac{Difference\ \ in\ weig\ ht\ x\ 1000}{Sample\ \ volume\ ,\ \ mL} \quad \text{.....(3)}$$

A mixture of each sample, petroleum ether, and concentrated HCl was homogenized and later filtered into a pre-weighed conical flask. The organic layer was dried using a steam bath. The increase in weight of the conical flask represented the oils and grease in the sample as in equation 4 (APHA, 2005). The sample was transferred into a special lovibond comparator test tube.

$$\text{Oils and grease content} = \frac{(A-B)x1000}{Volume\ \ of\ the\ sample\ ,\ \ mL} \quad \text{.....(4)}$$

Using an appropriate colour disc (long range), the colour match of the sample and the distilled water in a lovibond comparator was observed. The values at which the colour matched with the distilled water were taken and recorded (APHA, 2005). The presence of

feacal coli forms was determined in three stages that include presumptive test, confirmed test and completed test (APHA, 2005).

Results and discussion

Determination of pH

The pH values of the influent (at the entry point) ranged between 7.98 ± 0.98 at Gathuthi to 7.54 ± 1.0 at Nyankoba (Table 1). The wastewater at this point is mixed with freshly released effluent (2 - 3 days), which has contributed to the high pH values at this point. The wastewater at this point may also have high concentrations of the cleaning detergents. The mid-point showed a reduction on the pH mean values ranging between 6.86 ± 0.98 at Kagwe to 6.7 ± 0.98 at Ragati. At this point, the oxidation process of the waste tea leaves is taking place and this may contribute to the low pH values. The last retention point had the lowest pH ranging between 6.87 ± 0.98 at Gachege to 6.5 ± 0.98 at Gathuthi. This may be as a result of high accumulation of products preceding acidogenesis reaction by breaking down of the detergents and other pollutants in the wastewater. There was no notable difference in mean concentrations at each of the sampling point for the three wastewater management techniques used. In all the sampling points the mean values of the pH were within the recommended rage of 6.5-8.5 for disposal of the wastewater in to the environment (Water quality regulations Kenya, 2006.)

Table 1: Means and Standard Deviations of pH Values for the Three Sampling Points

	Trenches			**Lagoons**			
Sampling Point	**Kapkatet**	**Gachege**	**Kagwe**	**Nyankoba**	**Gathuthi**	**Ngere**	**Ragati**
Entry point	7.93±0.97	7.86±0.96	7.54±1.0	7.78±0.97	7.98±0.98	7.72±0.98	7.68±0.97
Mid Point	6.72±0.05	6.75±0.96	6.82±0.96	6.86±0.98	6.78±0.98	6.76±0.97	6.7±0.98
Final Point	6.73±0.96	6.87±0.98	6.54±1.01	6.68±0.97	6.5±0.98	6.85±0.98	6.63±0.98
Max All. Limit	**6.5-8.5**	**6.5-8.5**	**6.5-8.5**	**6.5-8.5**	**6.5-8.5**	**6.5-8.5**	**6.5-8.5**

Electrical Conductivity (EC)

There was a gradual increase in conductivity mean values of samples the entry point to the last retention point where the last retention point recorded the highest mean values. Samples from the trenches recorded slightly higher mean conductivity values than the samples from the lagoons where Kagwe recorded the highest mean value of 1603 ± 30.2 at the retention point for the trenches and 995 ± 22.6 at Nyankoba for the lagoons. The lowest values were recorded at Ragati's final effluent at 548 ± 16.8. The high levels of conductivity may be attributed to high concentrations of the detergents and also presence of non point pollutants from the storm runoff which may have a variety of salt contents. There was no significant difference in values of EC between the two methods of difference at 95% confidence level. The concentrations in all the sampling points were lower than the recommended Kenyan standards of 2000 µs/cm (water quality regulation Kenya, 2006). Figure 3 show the trend of ECw values in all the sampling points.

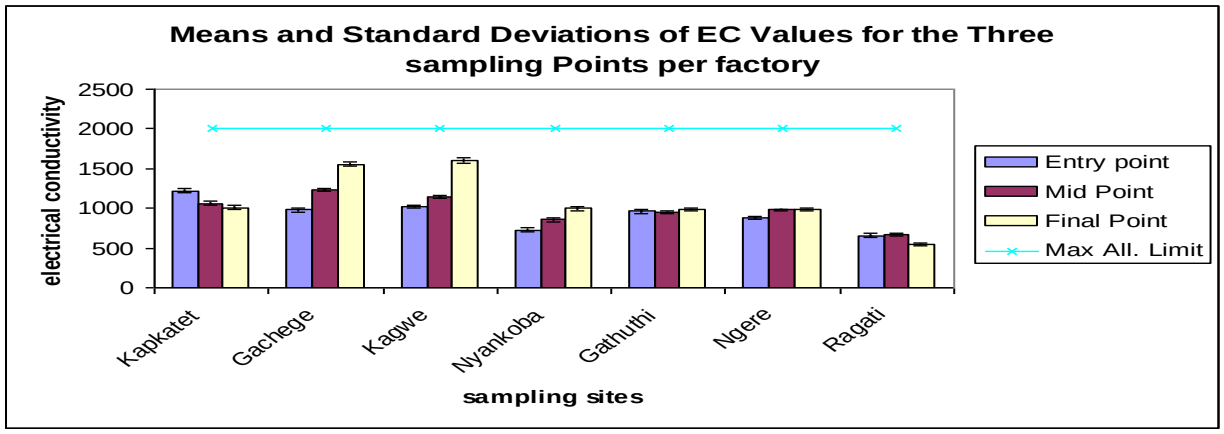

* Kapkatet, Gachege, Kagwe - Trenches
** Nyankoba, Gathuthi, Ngere - Lagoons

Figure 1: Mean and standard deviation of Electrical Conductivity

Biochemical Oxygen Demand (BOD_5)

There was a gradual increase in BOD_5 mean concentrations from the entry point to the last retention points. The factories that use trenches recorded slightly higher levels of BOD_5 compared to the factories using lagoons in all the sampling points. At the entry point, the highest concentrations of 550 ± 21.8 were recorded at Gachege and 500 ± 28.4 at Nyankoba representing trenches and lagoons respectively. At mid stage, the levels of BOD_5 were higher than the entry point with the highest concentrations recorded at Gachege and Nyankoba. At Gachege the mean concentration was 950 ± 18.9 while at Nyankoba the concentration was 600 ± 18.2. The last retention points recorded the highest mean concentrations in all the sampling point. At this point the concentrations at the trenches were slightly higher than that of the lagoons. The highest concentration of 1700 ± 26.7 was recorded at Kapkatet for the trenches and 1150 ± 17.5 at Nyankoba for the lagoons. The variations in the BOD_5 levels between the two methods could be attributed to the high organic loading. The trenches had high loads of organic materials compared to the lagoons where the coarse materials were removed from the wastewater before discharging in to the system. There was also frequent disludging of the lagoons. Ragati recorded the lowest BOD_5 concentration of 130 ± 29.4 at last point due to partial treatment of the wastewater. Figure 4 shows the trend of the BOD5 recorded in all the sampling points.

High levels of BOD_5 in all sampling points could also be attributed to the temperatures changes. The temperatures above 20 ^oC are conducive for bacterial action on organic matter (Gambrill *et al.*, 1986) and this could be the cause of the high levels of BOD_5 recorded at all the sampling points. There was no significant difference in levels of BOD_5 between the two methods of difference at 95% confidence level. The water quality regulations Kenya (2006) recommend the wastewater of BOD_5 level of 30 $mg/O_2/L$ to be discharged to the environment.

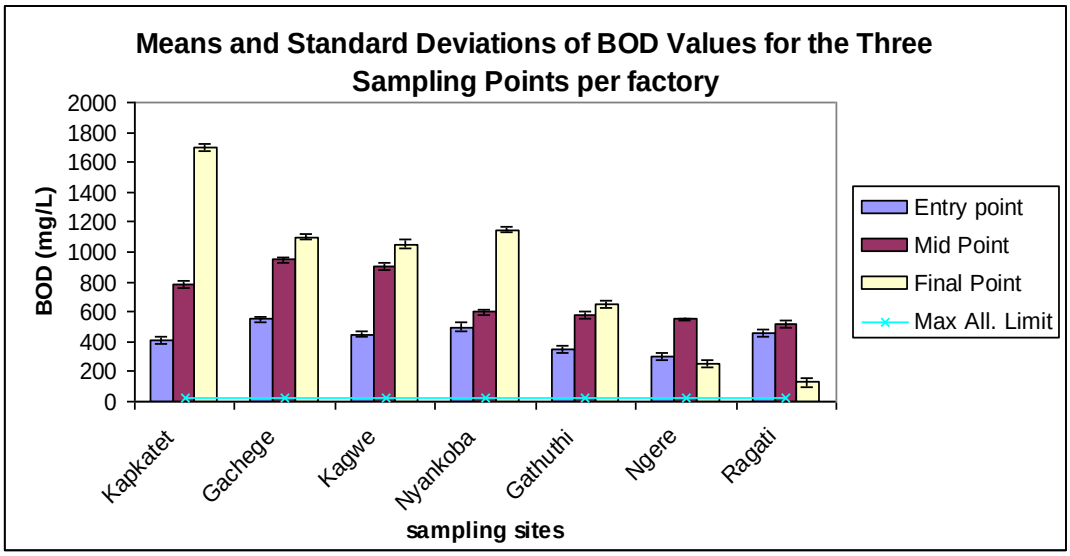

* Kapkatet, Gachege, Kagwe - Trenches
** Nyankoba, Gathuthi, Ngere - Lagoons

Figure 2: Means and Standard Deviations of BOD5

Chemical Oxygen Demand (COD)

There was a progressive increase in mean COD concentrations from the entry point to the last retention points. The entry point recorded the lowest mean concentrations while the last retention point recorded the highest mean concentrations. Trenches recorded slightly higher levels of COD than the lagoons. At the entry point, the highest mean concentration was recorded at Kagwe and Nyankoba for the trenches and lagoons respectively. Mean concentration at Kagwe was 1580 ± 26.3 while at Nyankoba was 560 ± 30.5. At the mid point the highest concentrations were again recorded at Kagwe and Nyankoba. Kagwe recorded mean concentration of 7000 ± 36.8 while Nyankoba recorded 1640 ± 37.8. In all the sampling points, Kagwe recorded the highest mean concentration which may be attributed to high levels of organic and inorganic compounds from petroleum products in the effluent. The high levels of COD in all the sampling points could also be attributed to accumulation of non-point pollutants from the surface run off and high accumulation of the biodegradable soaps and detergents used for cleaning. There was no significant difference in COD levels between the two methods of difference at 95% confidence level. The COD concentrations in all the sampling points were higher than the recommended Kenyan standards of 50 mg0_2/L (water quality regulation Kenya, 2006).

Table 2: The means and standard deviations of the COD at the three sampling points

	Trenches			**Lagoons**			
Sampling Point	**Kapkatet**	**Gachege**	**Kagwe**	**Nyankoba**	**Gathuthi**	**Ngere**	**Ragati**
Entry point	920±37.7	880±46.3	1580±26.3	560±30.5	450±28.3	250±32.7	540±33.7
Mid Point	1340±36.4	2140±38.5	7000±36.8	1640±37.8	720±32.4	600±33.9	580±36.8
Retention Point	3000±38.5	3000±59.3	13500±37.4	1500±28.4	1050±42.2	1050±32.9	520±38.1
Max All. Limit	**50**	**50**	**50**	**50**	**50**	**50**	**50**

Total Suspended Solids (TSS)

There was a progressive increase in TSS mean concentrations from the entry point to the last retention point for the trenches whereas there was a significant reduction in TSS concentrations at the last retention point for the lagoons. At the entry point, Kagwe recorded the highest mean concentration of 3260 ± 46.1 while Nyankoba which uses lagoons recorded the highest concentration of 1050 ± 39.6. At the mid point again Kagwe and Nyankoba recorded the highest concentrations of 4450 ± 40.5 and 1100 ± 33.2 respectively. The variations in the mean concentrations between the different methods of wastewater management used by the tea factories may be attributed mainly to the partial screening of the effluent before entering into the lagoons and the frequent disludging of the lagoons. The last retention point recorded the highest TSS mean concentration for the trenches. Kagwe recorded the highest at 6200 ± 36.7 while as lagoons had the lowest concentration at this point. Nyankoba recorded 900 ± 36.3 and the lowest concentration was at Ragati at 110 ± 20.7. Wastewater at Ragati is partially treated. The high concentrations at the trenches may also be attributed to the accumulation of sludge for a long period of time, the pollution from the vegetation around the wastewater facilities and other non point pollutants. There was no significant difference in TSS levels between the two methods of difference at 95% confidence level. The mean concentrations of the wastewater in these facilities exceed the recommended Kenyan standard of 30 mg/L for the wastewater disposal in to the environment (Water quality regulations Kenya, 2006).

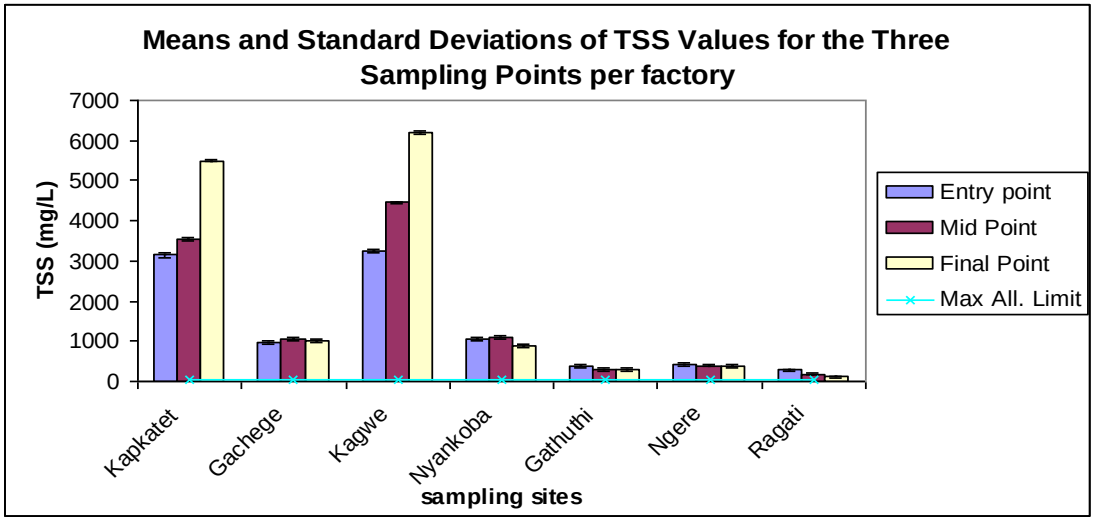

* Kapkatet, Gachege, Kagwe - Trenches

** Nyankoba, Gathuthi, Ngere - Lagoons

Figure 3: Means and Standard Deviations of TSS

Total Dissolved Solids (TDS)

Figure 9 shows the trend and the variations of the TSS levels in all the sampling points where the trenches recorded significantly higher levels than the lagoons and the treatment plant.

The mean TDS concentrations recorded showed a slight increase from the entry point to the last retention point. The samples from the trenches recorded slightly higher values than those from the lagoons. At the entry point, Gachege samples recorded the highest mean concentrations of 880 ± 15.6 for the trenches while Nyankoba had the highest concentrations of 490 ± 20.3 at this point. At the mid point Gachege recorded mean concentration of 950 ± 17.3 which was the highest for the trenches and Nyankoba recorded 694 ± 16.5 the highest recorded for the lagoons at this point. Ragati had the lowest mean values of 250 ± 22.3 at this point due to partial treatment of the effluent. The last retention point recorded the highest

mean concentrations in all the sampling points with Gachege recording 965 ± 17.5 and Nyankoba recording the highest for the lagoons at 670 ± 15.5. Ragati had the lowest mean concentration of 130 ± 15.2 which was the lowest recorded in all the sampling points. This was mainly due to the treatment of the effluent which reduced the mean values in all the sampling points. High values recorded may be attributed to the high levels of dissolved pollutants due to high accumulation of sludge material in the wastewater for a long period of time for both the trenches and the lagoons. There was no significant difference in TDS levels between the two methods of difference at 95% confidence level. The concentrations in all the sampling points were lower than the recommended Kenyan standards of 1200 mg/L (Water quality regulations Kenya, 2006).

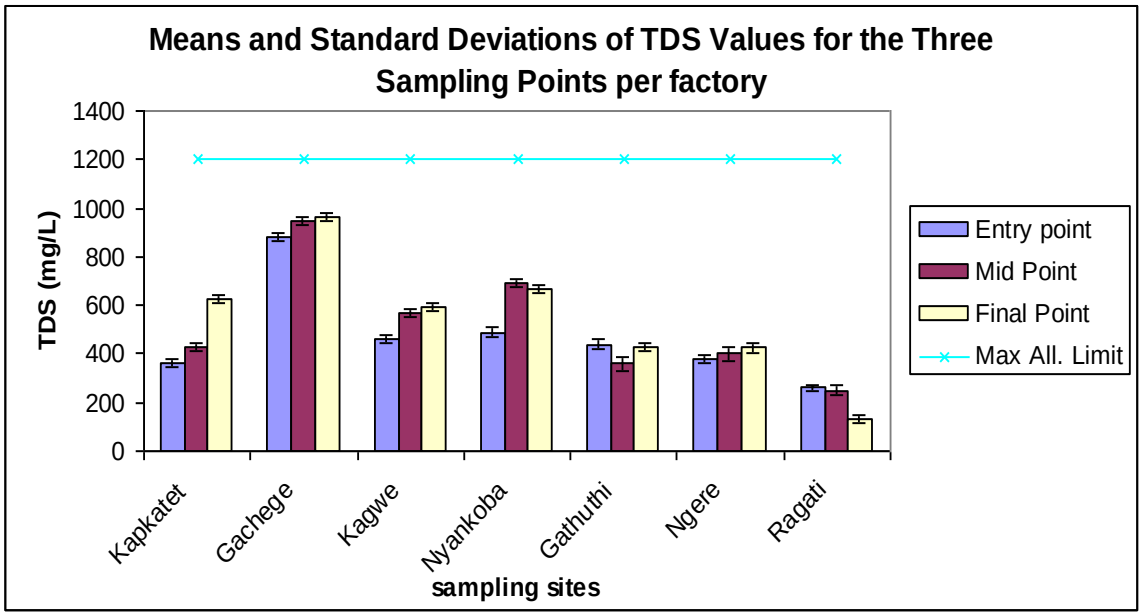

* Kapkatet, Gachege, Kagwe - Trenches
** Nyankoba, Gathuthi, Ngere - Lagoons

Figure 4: Means and Standard deviations of TDS

Oils and Grease

Low levels of oils and grease were detected at selected sampling points. At the entry point, Gathuthi and Ragati sites were not detected while the other samples had low levels. Kagwe recorded the highest levels of 1.52 ± 0.3 followed by Ngere at 0.32 ± 0.02. There was no notable difference in mean concentrations between the three methods used. The mid point samples showed a significant increase in oil and grease levels with Gathuthi recording 0.2 ± 0.02. The presence of oils and grease at Gathuthi samples was an indicator of pollutants accumulation in the lagoons. The last retention points showed some oils and grease accumulation with Kagwe recording the highest value of 7.8 ± 0.2. Ngere and Ragati samples were not detected. High levels recorded at Kagwe and the other sampling points may be attributed to the non point petroleum pollutants. There was no significant difference in oils and grease levels between the two methods of difference at 95% confidence level. The Kenya's standard of wastewater for disposal to the environment does not permit any trace of oil and grease to be released into the environment (Water quality regulations Kenya, 2006).

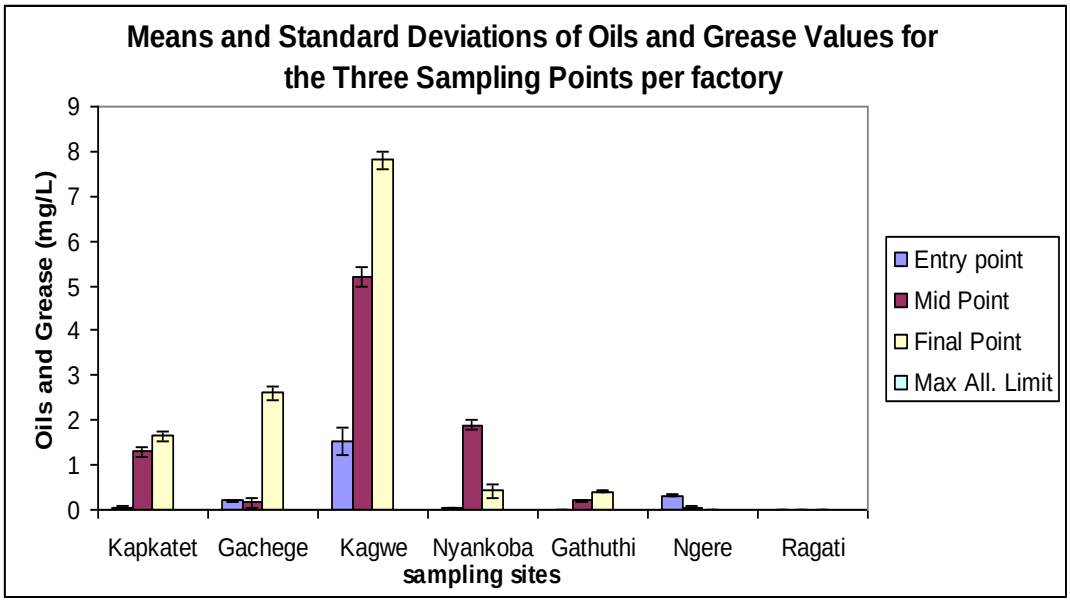

* Kapkatet, Gachege, Kagwe - Trenches
** Nyankoba, Gathuthi, Ngere - Lagoons

Figure 5: Means and Standard Deviations of Oils and Grease

Colour

The entry points had low colour intensities which intensified at the mid and retention points of the trenches and lagoons. The colour was more intense for the trenches and less intense in the samples from the lagoons. This may be due to the suspended matter in the wastewater and colour pigments formed during black tea processes when discharged into the wastewater stream may also be responsible for the intense colour in the effluent. This is also attributed to the varying contents of theaflavins (redish-orange pigments in tea) responsible for colour (Robert, 1982). The concentrations in all the sampling points were higher than the recommended Kenyan standards of 15 MgPt/L (Water quality regulations Kenya, 2006).

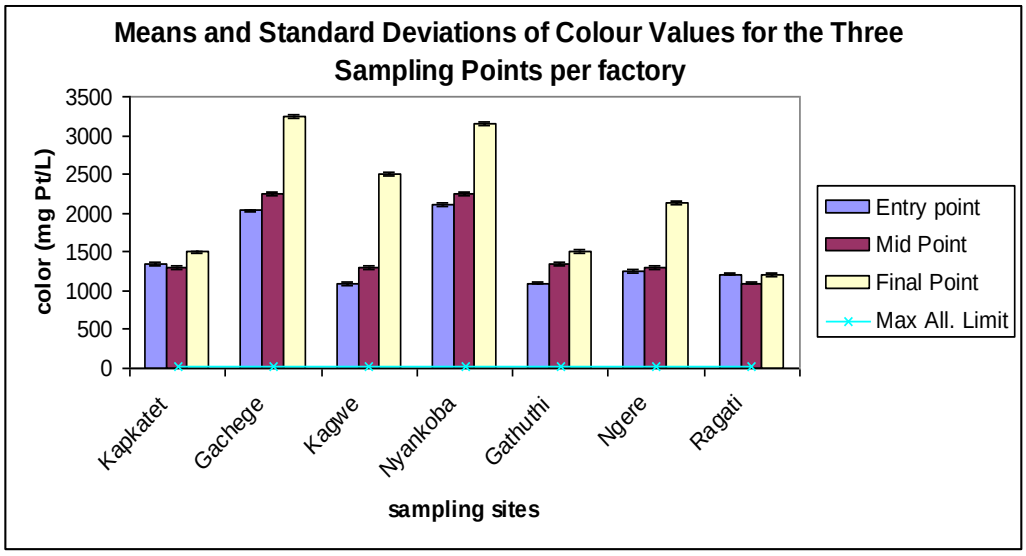

* Kapkatet, Gachege, Kagwe - Trenches
** Nyankoba, Gathuthi, Ngere - Lagoons

Figure 6: Means and Standard Deviations of Colour

Total coliforms

All the sampling sites except Ragati's final effluent were positive indicating the presence of coliforms. The positive tests in all the sampling points were an indicator of feacal contamination. This may be attributed to the non point pollutants from the storm run off.

Conclusions and recommendations

The overall efficiency of the management techniques used by the factories is given on the basis of the analytical and social findings. The analytical findings show the quality of the wastewater while the social finding showed the impacts of the wastewater generated by the factories and the management methods in place. Higher concentrations were obtained in most of the parameters analyzed – and in particular the effluents at the last retention points which were above the recommended levels for disposal to the environment. This generally indicates that the treatment/management techniques used by selected factories are not effective in pollutant removal/reduction. Concentrations of most of the parameters analyzed were higher for the trenches than those recorded for the lagoons. The concentrations of BOD_5 was high in all stages with the highest concentration recorded at the last retention points in six sites except in Ragati where the concentrations were lower but higher than the recommended levels of 30mg/l. The TSS concentrations discharged from the final effluent were between 110 and 120.89 mg/L against expected 30 mg/L. Though the wastewater treatment system was in place at Ragati, most of the parameters analyzed for the final effluent were higher than the expected. The efficiency of the system was low due to operational problems or the maintenance of the system. The presence of coliform bacteria in wastewater was an indicator of feacal contamination an indicator of presence of non point pollutants. The bacterial action in the wastewater with insufficient dissolved oxygen could be the main cause of the odour from the water retention points.

All the tea factories should adapt the concept of sustainability in all levels of operations. This may include sustainable agriculture and Good Manufacturing practices. Investing in wastewater management will generate significant returns as addressing wastewater is a key step in securing sustainability of the natural resources. .

Acknowledgements

The authors would like to appreciate with thanks KTDA staff for their cooperation in this research.

References

APHA (2005). Standard Methods for the Examination of Water and Wastewater. American Public Health Association.

FAO – Corporate Document Repository, (2000). Control of Water Pollution from Agriculture; pp 742-777.

EL-Haary, (1998). Performance Assessment of a Wastewater Treatment Plant Producing Effluent for Irrigation in Egypt; pp 306-310.

Falkenmark. M. (1989). The Massive Water Scarcity now Threatening Africa. pp 18,112 - 118.

Karen, M. (1996). Wastewater Treatment Principles and Regulations. MSc Thesis. Ohio State University.

Raschid- Sally and P. Jayakody (2008). Drivers and Characteristics of Wastewater Agriculture in Developing Countries; pp 35.

Roberts, E.A.H (1982). Economics Importance of Flavonoid Substances; Tea Fermentation in the Chemistry of Flavonoid Compounds; pp 468-512.

Tchobanoglous, M; Mannarino, FL; and Stensel, H. D. (2003). Wastewater Engineering Treatment/Disposal and Reuse *The Science of Total Environment,* 249–261.

Water Quality Regulations, Kenya (2006). Environmental Management and Coordination (Water Quality) Regulations. Kenya gazette Supplement No 68. (Legislative supplement No 36). Legal notice no 120.

WWAP.(2009). The United Nations World Water Development Report; Water in a changing world.

The Product Distribution and Molecular Modeling of Ethyl Benzene and Toluene

Joshua K. Kibet*[1], Anthony B. Mathenge[1], Lusweti Kituyi[2], and Timothy Okumu[2]
[1]*Department of Chemistry, Egerton University P.O Box 536, Egerton*
[2]*Department of Chemistry and Biochemistry, University of Eldoret, P.O Box 1125, Eldoret*
*Corresponding author: jkibet2@yahoo.com Tel. +254 720 352 437

Abstract
The thermal degradation of complex plant materials such as tobacco gives rise to a variety of toxic organic substances known to affect the clinical health of tobacco consumers. In this paper we explore the theoretical characteristics of common toxic molecular products; toluene and ethyl benzene from the pyrolysis of Sportsman cigarettes between 373 and 1223 K under conditions that simulate actual cigarette smoking. Accordingly, this work was conducted at 1 atmosphere in increments of 50 K. Gaussian 03 computational suite of programs was used to perform thermochemical calculations of toluene and ethyl benzene. Toluenyl and ethyl benzyl radical stabilization energies were also calculated. HyperChem computational package with Quantitative Structural Activity Relationship (QSAR) technique was used to calculate the relative toxicities of ethyl benzene and toluene, and their corresponding radicals. The toxicity values were 1.75 and 1.77 for toluene and ethyl benzene respectively while those for the corresponding radicals were 2.15 (toluenyl) and 2.17 (ethyl benzyl) based on octanol-water partition coefficient. To complement computational calculations, the experimental Gas Chromatography-Mass Spectrometry (GC-MS) data on the evolution of toluene and ethyl benzene between 200 and 700 ˚C has been presented to determine the smoking temperatures at which toluene and ethyl benzene are produced in high yields. Accordingly, the concentration of toluene and ethyl benzene was found to peak between 400 and 600 ˚C. This is consistent with thermochemical data which predicted that in the same temperature range, the formation of ethyl benzyl and toluenyl radicals were generally favoured. The clinical impacts of molecular toluene and molecular ethyl benzene, and their respective free radicals have also been discussed.

Key words: *density functional theory, molecular orbitals, pyrolysis, tobacco, toxicity*

Introduction

Research on biological and environmental health impacts of cigarette smoking has attracted a lot of attention in recent years [1-3]. The formation and emission of potentially toxic by-products from tobacco at various combustion temperatures are a major health concern due to associated health diseases such as heart attack, stroke and cardiovascular death, mental illnesses, and lung cancer [3]. There is considerable evidence that inhaled toxicants such as cigarette smoke can cause both irreversible changes to the genetic material (DNA mutations) and putatively reversible variations to the epigenetic landscape (changes in the DNA methylation and chromatin alteration state) [4, 5]. The diseases that are believed to involve genetic and epigenetic perturbations include lung cancer, chronic obstructive pulmonary disease (COPD), and cardiovascular disease (CVD), all of which are strongly linked epidemiologically to cigarette smoking [4]. Lung cancer development involves various genomic aberrations, such as point mutations, deletions, and gene amplifications [4]. Direct DNA damage has been linked to cardiovascular disease; the increase of micronuclei, which is indicative of DNA damage, correlates with the severity of atherosclerosis [4, 5]. Additionally, Reproductive function and fertility are thought to be compromised by behaviors such as cigarette smoking [5].

Toxicological risks of tobacco smoke

The toxicity of a cigarette smoke is believed to be a function of the concentrations of individual toxicants present in smoke [6]. Benzene and its derivatives which may include toluene and ethyl benzene are metabolized, primarily in the liver, to a series of phenolic and ring-opened products and their conjugates [7]. Nonetheless, the toxicology of toluene and ethyl benzene is scarce in literature. Several scientific and epidemiological evidences have explicitly established that cigarette smoking is a risk factor for various degenerative diseases like cancer of the lungs and other organs and cardiovascular disease [8]. Even in smokers without any obvious clinical symptoms, the overall life expectancy is reduced, ranging up to 10 years fewer than non-smokers [8]. Benzene is a well-investigated chemical, with some acute and chronic exposures being directly associated with observed hematologic effects in humans and animals and subsequently acute myelogenous leukemia (AML) [3]. It is known to have a depressive effect on the bone marrow following chronic exposure, occasionally leading to complete failure of the blood-forming elements [3]. The major environmental source of benzene exposure for most persons around the world is active and passive cigarette smoking [3]. Ethyl benzene and toluene (derivatives of benzene) are not only expected to be more reactive but more potent than benzene itself. In this regard, their investigation is necessary. This paper has investigated the formation of toluene and ethyl benzene from and experimental perspective as well from a theoretical point of view. The experiment to determine the emission of toluene and ethyl benzene over the whole temperature range was conducted using the state-of-the art Gas-chromatography hyphenated to mass selective spectrometer detector (MSD). The level of theory employed to explore the quantum behaviour of these toxicants was the density functional theory (DFT) with Gaussian computational platform.

The tobacco cigarette

Sportsman cigarettes are a class of cigarette brands sold to smokers in Kenya. It should be noted however, that 'Sportsman' is just a marketing name but the fundamental component is tobacco. Most modern cigarettes are engineered to have filter tip ventilation with the aim of diluting the mainstream cigarette smoke [9]. Sportsman cigarette does not meet this threshold and therefore may be one the most toxic cigarettes in the market. The principle behind ventilation is to reduce tobacco toxicants, although this has not yielded significant results [1]. Tobacco biomass is of great interest because of its use in the form of cigarettes which generate various smoke compounds during pyrolysis reactions [10-13]. Tobacco is a complex biomass material consisting of over 2500 chemical constituents, among them biopolymers, non-polymeric and inorganic compound [14]. Tobacco in a smoldering cigarette can reach up to 950 ˚C [15]. It is thought that much of the biomass decomposition has occurred by this temperature with the exception of lignin that may decompose above 950 ˚C [16].

The concept of tobacco development, composition, and toxicity is a very rich area of study [17]. In recent years a lot of effort has been devoted to the evaluation of by-products of tobacco burning and the potency of cigarette smoking [17]. However, the shortfalls in describing the toxic compound formation mechanism during tobacco burning and challenges of developing model compounds which can burn under conditions that simulate actual cigarette smoking with respect to heating rate, temperature distribution, variation in oxygen concentration, and residence time, impede this undertaking [18]. Although many efforts have been engaged towards understanding the pyrolytic behaviour of tobacco, many complex and uncertain reaction processes are yet to be understood. Evidently, the pyrolysis of tobacco has much in common with the pyrolysis of other forms of biomass [19]. Pyrolysis experiments offers the possibility of unraveling mechanistic information about the complex processes

involved in the thermal decomposition of tobacco [10,11]. Pyrolysis is a process by which a biomass material such as tobacco is thermally degraded in absence of oxygen or air [20]. The concept of biomass pyrolysis is extremely complex because of the formation of a myriad reaction intermediates and reaction products [20].

Accordingly, the use of computational models plays a critical role in the study of environmental pollutants. The relationship between environmental emissions and human toxicological impacts therefore is an area that requires undivided attention because the consequences of potent emissions have serious health implications. During the sequence from lighting a cigarette to inhaling a puff of smoke into the respiratory system, various overlapping chemical and physiological phenomena occur [9]. This work is in two parts; the experimental results and the theoretical results.

Experimental section

Materials and experimental protocol

Sportsman cigarettes were purchased directly from vendors and used without further treatment. The cigarette was burned and the smoke was allowed to pass through a transfer line by flowing nitrogen (pyrolysis gas). The pyrolysate was collected in 1 mL methanol in crimp top vials for 5 minutes. The sample was then analyzed using a Gas Chromatography hyphenated to a Mass selective detector (MSD). 1 µL of sample was injected into a GC column (HP-5MS, 30 m x 250 µm x 0.5 µm). The temperature of the injection port was set at 150 ˚C. Temperature programming was applied at a heating rate of 15˚C for 10 minutes, holding for 1 minute at 200˚ C, followed by a heating rate of 25 ˚C for 4 minutes, and holding for 5 minutes at 300 ˚C. The target of this experiment was to monitor the evolution of toluene and ethyl benzene. Electron Impact ionization energy of 70 eV was used. The compounds were identified using National Institute of Science and Technology software (NIST, USA). This was further confirmed by comparing the peaks and retention times of the components with those of the actual compounds (Standards). The experimental pyrolysis temperature was varied from 200 ˚C to 700 ˚C in increments of 100 ˚C.

Computational methodology

All calculations have been performed with the *Gaussian 03* computational program [21]. *ab initio* calculations including correlation effects have been made by using the DFT level of theory with 6-31++G(d,p) basis set. Enthalpy changes were computed between the enthalpies of formation of the reactant (neutral compound) and its corresponding free radical. QSAR in HyperChem computational package was used to estimate the toxicity indices of both molecular by-products and radicals [22]. The relative toxicities of the compounds in this study were investigated using the QSAR platform in the HyperChem computational suite [22]. The logarithim of the octanol-water partition coefficient is a key parameter in determining the relative toxicity of combsustion by-products and their respective free radicals [23]. It determines the lipophilicity and hydrophobicity of a pollutant. Lipophilicity correlates with many biological activities such as mutagenicity and carcinogenicity [23, 24]. QSAR modeling determines the preliminary assessment of the impact on environmental health by a primary pollutant and the set of transformation products that may be persistent and toxic to not only the human health but also the environment [25]

To compute the energy change for formation of nicotine from its radical, the following thermochemical equation was used [26].

$$\Delta rH^0 = \sum \left(\varepsilon_0 - H_{corr}\right)_{products} - \sum \left(\varepsilon_0 - H_{corr}\right)_{reac\,tan\,ts}$$

Equation 1

where ΔrH^0 is change in enthalpy of the reaction

H_{corr} is correction to the thermal enthalpy

ε_0 is the sum of electronic and thermal enthalpies

Results and Discussion

Figure 1 shows the experimental results for ethyl benzene and toluene from the pyrolysis of sportsman cigarettes. It is evident that ethyl benzene and toluene are released in approximately equal amounts during cigarette burning. Nevertheless, ethyl benzene appears to be evolved in larger quantities in comparison to toluene. The two compounds (ethyl benzene and toluene) reach a maximum release at a peak temperature of 500 ˚C before decreasing exponentially to relative concentration of $\approx 6.0\, x\, 10^6$ GC area counts at 700 ˚C. These data shows that the fatal temperatures for smokers is between 400 and 600 ˚C although at higher temperatures, it is believed that cancerous polycyclic aromatic hydrocarbons (PAHs) such as benzo(a)pyrene are formed notwithstanding their low concentrations [27].

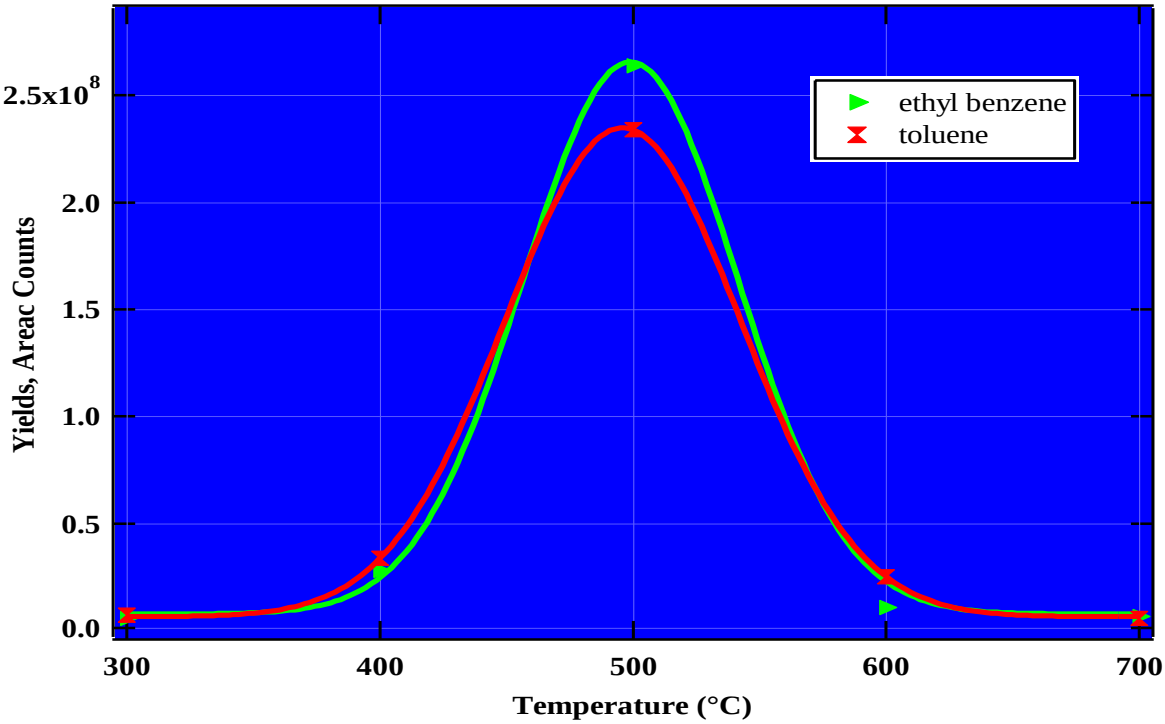

Fig.1. The Yields (GC-Area Counts) of ethyl benzene and toluene from the pyrolysis of Sportsman cigarettes

It is nonetheless remarkable that at temperatures below 300 ˚C, ethyl benzene and toluene are formed in low amounts. This observation is important in investigating the possibility of developing cigarettes that can be smoked at lower temperatures and consequently avoid inhaling high concentrations of hazardous combustion by-products. During the natural smolder period between the puffs, temperatures of almost 800 ˚C occur in the center of the burning cone [1]. During a puff the temperature increases to 910–920 ˚C at the burning zone periphery, about 0.2–1.0 mm in front of the paper burn line [1]. Consequently, this study is conducted at high temperatures with a view to simulate actual cigarette smoking. It should nevertheless, be noted that experiments at temperatures above 1100 K are hazardous and in most cases, it may result in the melt down of the reactor. In such cases therefore, it would be crucial to probe data at extremely high temperatures using computational procedures.

Free radicals and thermochemical properties

About 10^{16} alkyl- and alkoxy radicals are present in the gas-phase of one cigarette, or 5×10^{14} radicals per puff [1]. It is well known that these types of radicals have lifetimes in the order of fractions of a second. However, it has been observed that cigarette smoke radicals seem to have longer lifetimes of up to 5 min [1, 6] although the exact nature of these radicals is yet to be understood [6]. The primary focus in this study was to determine the enthalpy changes between pyrolysis products (toluene and benzene) and their corresponding free radicals. This information is critical in understanding the ease of formation of toluenyl and ethyl benzyl radicals from their parent molecular compounds. Scheme I shows how toluenyl and ethyl benzyl free radicals are formed from toluene and ethyl benzene respectively.

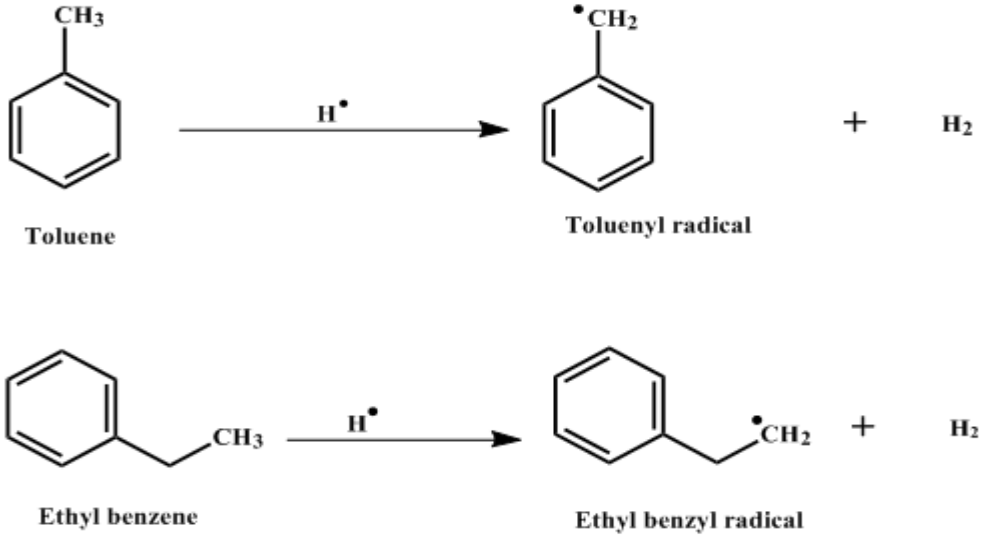

Scheme 1. Transformation of molecular toluene and ethyl benzene to corresponding free radicals

The thermochemical behaviour of toluene and ethyl benzene was calculated between 373 and 1223 K (usually the smoking range of tobacco). Table 1 gives the enthalpy of toluene and ethyl benzene and their respective free radicals while Fig. 3 gives the variation in enthalpy change with between molecular toluene and toluenyl radical (Fig. 3A), and ethyl benzene and ethyl benzyl radical (Fig. 3B).

Fig. 2. Enthalpy changes as a function of temperature for formation of free radicals from their parent compounds (A: toluene-toluenyl radical and B: ethyl benzene-ethyl benzyl radical)

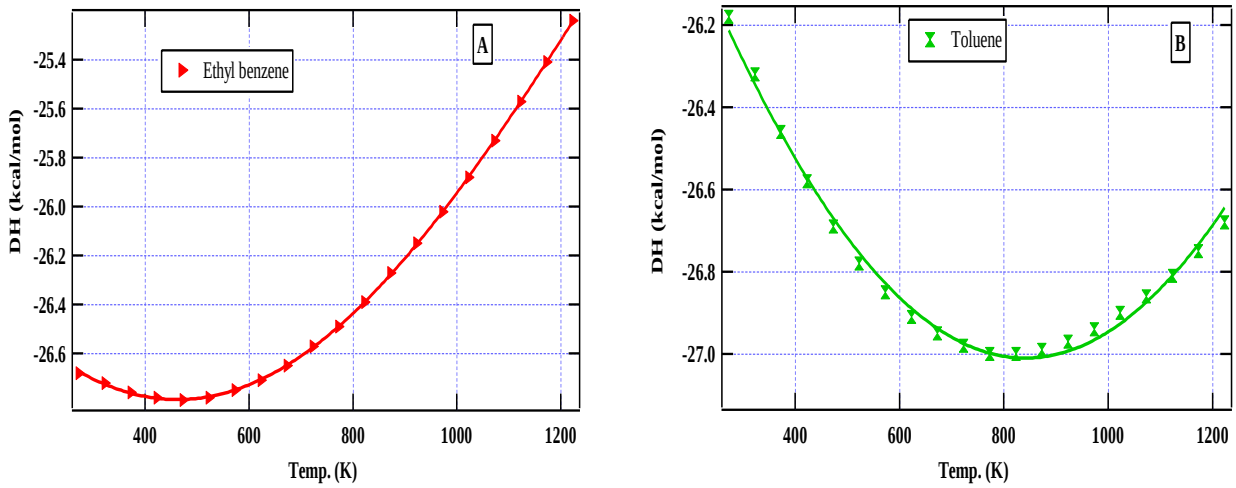

Whereas, the enthalpies of molecular products (toluene and ethyl benzene) and their corresponding free radicals appear not to change by much with temperature (Table 1, *vide infra*), the enthalpies of formation of free radicals from their corresponding parent products are significant (Fig. 2). It is clear from the graph (Fig. 2A) that the exothermicity for the formation of toluenyl radical from toluene decreases with temperature. On the other hand, the formation of ethyl benzyl radical from ethyl benzene exhibits an increase in exothermicity with increase in temperature up to about 800 K when the reaction approaches endothermicity as the temperature is increased (Fig. 2B). Nevertheless, the enthalpy changes for the formation of free radicals from the two compounds under study (toluene and ethyl benzene) lie within a comparable range (-25 – -27 kcal/mol) indicating that both radicals may have similar activities in biological systems as predicted by the QSAR data in Table 2, *vide infra*. The more stable a compound or a radical is, the more it persists in the environment and this may cause extensive biological assault and serious environmental impacts.

Table. 1: Enthalpies for toluene, benzene, and their corresponding reaction products

Sum of thermal and electronic enthalpies calculated using DFT analytical gradient with 6311++G(d,p) basis set (Hartree/Particle)				
Temp. (K)	**Ethyl benzene**	**Ethyl benzene radical**	**Toluene**	**Toluenyl radical**
373	-310.64	-309.98	-271.37	-270.71
423	-310.64	-309.98	-271.36	-270.71
473	-310.63	-309.98	-271.36	-270.70
523	-310.63	-309.97	-271.36	-270.70
573	-310.63	-309.97	-271.35	-270.70
623	-310.62	-309.96	-271.35	-270.69
673	-310.62	-309.96	-271.35	-270.69
723	-310.61	-309.95	-271.34	-270.69
773	-310.61	-309.95	-271.34	-270.68
823	-310.60	-309.94	-271.33	-270.68
873	-310.60	-309.94	-271.33	-270.67
923	-310.59	-309.93	-271.33	-270.67
973	-310.58	-309.93	-271.32	-270.67
1023	-310.58	-309.92	-271.32	-270.66
1073	-310.57	-309.92	-271.31	-270.66
1123	-310.57	-309.91	-271.31	-270.65
1173	-310.56	-309.90	-271.30	-270.65
1223	-310.55	-309.90	-271.29	-270.64

Toxicity values

It is evident from Table 2 below that the toluenyl and the ethyl benzyl radicals are respectively about 141 and 148 more soluble in octanol than in water and therefore highly hydrophobic. The formation of free radicals (toluenyl and ethyl benzyl) appears to be favoured at high temperatures as predicted in Fig. 2. These radicals consequently attack biological systems because of their reactive nature leading to heightened oxidative stress and extensive cellular injury [23]. The molecular products, toluene and ethyl benzene are less hydrophobic than their corresponding free radicals judging from the toxicity data presented in Table 2. This suggests that they are more soluble in water than their corresponding free radicals. Low toxicity index does not imply that a compound is less toxic but may react with non-polar biological constituents such as lipids ultimately causing cancer and gene mutation.

Hydrophobic by-products of tobacco are not easily excreted by the kidney and thus cross-cell barriers resulting deteriorating health by tobacco consumers. Molecular toluene and ethyl benzene are therefore hazardous to cigarette smokers.

Table 2: QSAR toxicity indices for propanol, phenol, and their corresponding free radicals

Compound/Radical	P	Log P
Toluene	56.23	1.75
Toluenyl radical	58.88	1.77
Ethyl benzene	141.25	2.15
Ethyl benzyl radical	147.91	2.17

Molecular geometries

Geometrical parameters such as bond lengths and bond angles have a great influence on the strength of the bonds involved and consequently the potential energy surface. The stronger the molecular bond of a compound, the higher the vibrational frequency. Fig. 3 presents the optimized structures investigated in this work.

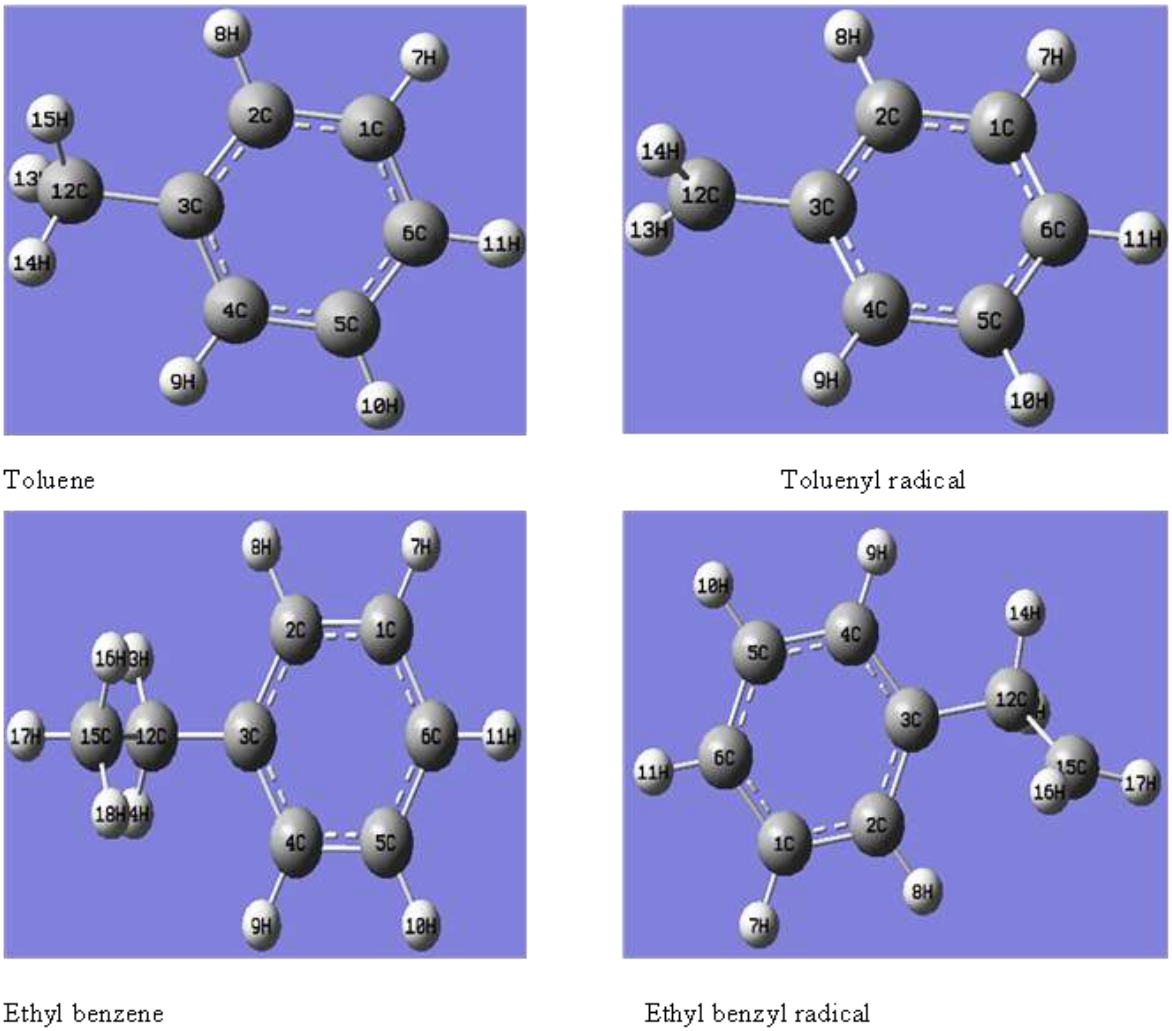

Fig.3. Optimized structures of toluene, ethyl benzene and their corresponding free radicals

Electronic properties and molecular orbitals

The theory of linear combination of atomic orbitals (LCAO) treats bonding as the overlap between the highest occupied molecular orbital (HOMO) and the lowest unoccupied molecular orbital (LUMO) [28, 29]. It is well-known that the gap between the highest

occupied molecular orbital (HOMO) and the lowest unoccupied molecular orbital (LUMO), is directly related to the electronic stability of the chemical species [28]. Fig. 4 reports the molecular orbital diagrams of molecular toluene and molecular ethyl toluene (The cross-sectional representation of toluene and ethyl benzene are also given for comparison).

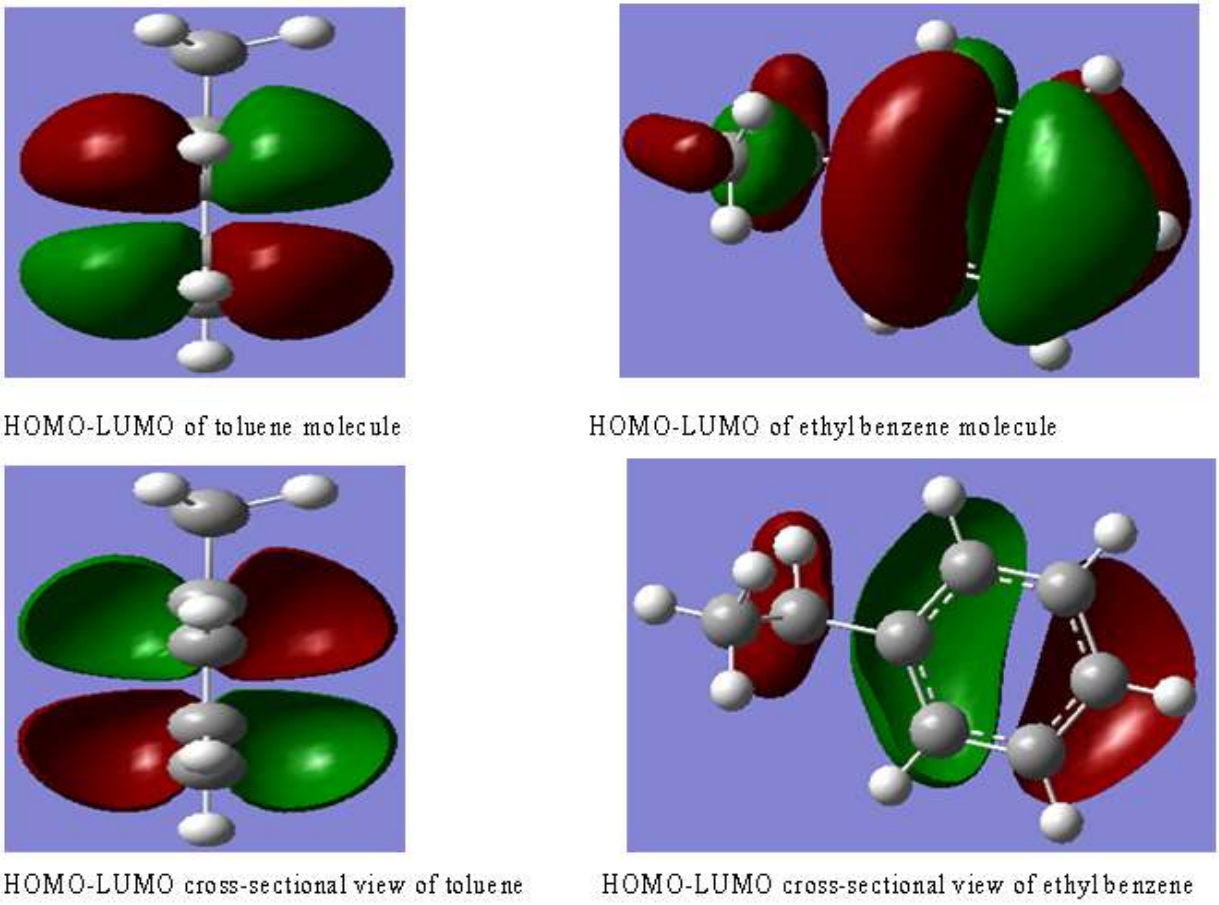

Fig. 4. Molecular orbital diagrams for toluene and ethyl benzene

Conclusion

Based on toxicological indices presented in this work molecular toluene and molecular ethyl benzene may be very toxic but their corresponding free radicals may be even more toxic because of their electron deficient character. This makes toluenyl and ethyl benzyl radicals more reactive and their presence in tobacco smoke are clinical candidates for a myriad of diseases bedeviling smokers (aging, cancer, stroke, and emphysema). We established in this study that most of the toluene and ethyl benzene consumed by smokers is evolved between 400 and 600 ˚C. This is a region that may need to be avoided in the quest for cigarettes that can be smoked at a lower temperature. Smoking cigarettes at a lower temperature would therefore be beneficial. Nonetheless, the safest way to avoid inhaling potentially hazardous toxicants from tobacco burning is to quit smoking altogether. The thermochemical behaviour of toluene and ethyl benzene from a quantum mechanical point of view indicate that the formation of free radicals; toluenyl and ethyl benzyl is generally exothermic. Remarkably, there is considerable relationship between the temperatures at which maximum production of toluene and ethyl benzene occur and the temperatures at which the formation of their corresponding free radicals are easily formed. The data presented in this study is the first to be conducted on sportsman cigarettes and provides a base-line for studies on other types of cigarettes.

Acknowledgement
The authors wish to thank the Department of Chemistry at Egerton University for providing the necessary computational resources and the mass spectrometry data used in this work. Many thanks are accorded to Dr. Limo of the Department of Physics at the University of Eldoret for making critical inputs towards the success of this manuscript.

References

1. Borgerdinga, M. and K. Klus, *Analysis of complex mixtures – Cigarette smoke.* Experimental and Toxicologic Pathology, 2005. **57**: p. 43–73.
2. Liu, C., et al., *The use of a novel tobacco treatment process to reduce toxicant yields in cigarette smoke.* Food and Chemical Toxicology, 2011. **49**(9): p. 1904-1917.
3. Galbraith, D., S.A. Gross, and D. Paustenbach, *Benzene and human health: A historical review and appraisal of associations with various diseases.* Informa Healthcare; Critical Reviews in Toxicology, 2010. **40**(S2): p. 1-46.
4. Talikka, M., et al., *Genomic impact of cigarette smoke, with application to three smoking-related diseases.* Informa Healthcare USA, Inc, 2012. **42**(10): p. 877–889.
5. Sadeu, J.C., et al., *Alcohol, drugs, caffeine, tobacco, and environmental contaminant exposure: Reproductive health consequences and clinical implications.* Informa healthcare; Critical Reviews in Toxicology, 2010. **40**(7): p. 633–652.
6. Blakley R. L, H.D.D., Smith C. J., *Lack of correlation between cigarette mainstream smoke particulate phase radicals and hydroquinone yield.* Food Chem Toxicology, 2001(39-40): p. 1-6.
7. Snyder, R., G. Witz, and B.D. Goldstein, *The toxicology of benzene.* Environmental Health Perspectives, 1993. **100**: p. 293-306.
8. Ghosh, A., et al., *Cigarette smoke induces p-benzoquinone-albumin adduct in blood serum: Implications on structure and ligand binding properties.* Toxicology, 2012. **292**(2-3): p. 78-89.
9. Thielen, A., H. Klus, and L. Muller, *Tobacco smoke: Unraveling a controversial subject.* Experimental and Toxicologic Pathology, 2008. **60**(2-3): p. 141-156.
10. Kibet, J.K., L. Khachatryan, and B. Dellinger, *Molecular products from the pyrolysis and oxidative pyrolysis of tyrosine.* Chemosphere, 2013. **91**(7): p. 1026-1034.
11. Busch, C., et al., *Pyrolysis and combustion of tobacco in a cigarette smoking simulator under air and nitrogen atmosphere.* Analytical and Bioanalytical Chemistry, 2012. **403**(2): p. 419-430.
12. Mitschke, S., et al., *Application of time-of-flight mass spectrometry with laser-based photoionization methods for time-resolved on-line analysis of mainstream cigarette smoke.* Analytical Chemistry, 2005. **77**(8): p. 2288-2296.
13. Baker, R.R., *Sugars, carbonyls and smoke.* Food and Chemical Toxicology, 2007. **45**(9): p. 1783-1786.
14. Kelly Cho, J.C.F., Heping Zhang, Laura L. Miller, and Jeffrey R. Gruen, *Prenatal Exposure to Nicotine and Impaired Reading Performance.* The Journal of Pediatrics, 2013. **162**: p. 713-718.
15. Czegeny, Z., et al., *Formation of selected toxicants from tobacco under different pyrolysis conditions.* Journal of Analytical and Applied Pyrolysis, 2009. **85**(1-2): p. 47-53.
16. Baker, R.R. and L.J. Bishop, *The pyrolysis of tobacco ingredients.* Journal of Analytical and Applied Pyrolysis, 2004. **71**(1): p. 223-311.
17. Zhou, S., et al., *The pyrolysis of cigarette paper under the conditions that simulate cigarette smouldering and puffing.* Journal of Thermal Analysis and Calorimetry, 2011. **104**(3): p. 1097-1106.

18. Schlotzhauer, W.S., et al., *Pyrolytic studies on the contribution of tobacco leaf constituents to the formation of smoke catechols.* Journal of Agricultural and Food Chemistry, 1982. **30**(2): p. 372-374.
19. Sharma, R.K., et al., *On the role of peptides in the pyrolysis of amino acids.* Journal of Analytical and Applied Pyrolysis, 2004. **72**(1): p. 153-163.
20. Babu, B.V., *Biomass pyrolysis: a state-of-the-art review.* Biofuels Bioproducts & Biorefining-Biofpr, 2008. **2**(5): p. 393-414.
21. Zhang, Z., L. Lina, and L. Wang, *Atmospheric oxidation mechanism of naphthalene initiated by OH radical. A theoretical study.* Phys. Chem. Chem. Phys, 2010. **14**: p. 2645–2650.
22. HyperChem®, *HyperChem Release 7.* HyperChem, 2002. **7**: p. 1-2170.
23. Smith, C.J. and C. Hansch, *The relative toxicity of compounds in mainstream cigarette smoke condensate.* Food and Chemical Toxicology, 2000. **38**(7): p. 637-646.
24. Young, C.D., *Compuational Chemistry: A Practical Guide for Applying Techniques to Real-World Problems.* John Wiley & Sons, Inc., 2001: p. 1-398.
25. Carlsen, L., B.N. Kenessov, and S.Y. Batyrbekova, *A QSAR/QSTR Study on the Environmental Health Impact by the Rocket Fuel 1,1-Dimethyl Hydrazine and its Transformation Products.* Environmental Health Insights, 2008. **1**: p. 11-20.
26. Ochtorski, J.W., *Thermochemistry in Gaussian.* Gaussian, Inc, 2000.
27. Wang, S.F., et al., *Gas chromatographic-mass spectrometric determination of polycyclic aromatic hydrocarbons formed during the pyrolysis of phenylalanine.* Journal of Chromatography A, 2004. **1025**(2): p. 255-261.
28. Osorio, E., et al., *Theoretical design of stable small aluminium-magnesium binary clusters.* Physical Chemistry Chemical Physics, 2013. **15**(6): p. 2222-2229.
29. chemwiki_ucdavis.edu, *MO-theory.* university of california Davis.

Levels of chromium in peel, seeds, red flesh and white flesh of Varieties of Watermelons grown in Kenya

Esther W. Nthiga[1], Ruth Wanjau[2], Jane I. Murungi[1]
Department of chemistry in the school of pure and applied sciences, Kenyatta University, Kenya, P.O BOX 43822-00100, Nairobi
Corresponding author: E –mail: nthigaew@gmail.com Tel: 0721822163

ABSTRACT
Watermelons belong to the family cucurbitaceous, they are fruits like cantaloupe, pumpkin and similar to plants that grow on vines on the ground. There are over 1,200 varieties of watermelons in the world, several of these varieties have been recommended for Kenya range of climate, however only three varieties are commercially grown in Kenya namely; the Charleston Grey, Crimson sweet and Sugar baby. Watermelon has four distinct parts; the seeds, the pink flesh, the white flesh and the peel. Watermelon has high content of water of about 93%. It is a rich source of essential minerals such as Ca, Mg, K, Na and smaller amounts of Cu, Fe, Zn, Se and Cr among others. The levels of nutrients in different parts of the watermelons may be different. Different people consume different parts and varieties of watermelon and thus depending on the part/variety of watermelon consumed these people may get different nutrients and levels of the same. However, levels of nutrients in various parts/varieties of watermelon have not been documented. Chromium (III) has been known to be a micronutrient for mammals for more than four decades. Studies have shown a potential role of Chromium in regulating blood sugar. Studies have shown that lack of chromium appears to be involved in the development of maturity onset diabetes; it also plays a role in the management of heart diseases by regulating fat and cholesterol synthesis in the liver. This study quantitatively determined the level of chromium in seeds, white fleshy, peel and the red flesh parts of three varieties of watermelons; Charleston grey watermelons, crimson sweet and Sugar baby watermelons. Samples were purchased from Mwea market and Githurai markets in Kenya. Samples were treated to a wet digestion method and concentration of Chromium in the samples was determined using Varian Atomic Absorption Spectrophotometer. Significant high mean levels (p =0.002) of 44.67±1.10 µg/g Cr were recorded in seeds compared to other parts of watermelons samples. Charleston grey watermelons samples recorded significantly high amount of Cr of 28.89±3.33 µg/g. All the parts of watermelon samples analyzed were found to contain chromium with the seeds of Sugar baby variety recording the highest amounts. It is advisable to consume all the parts of watermelons.

Key words: *Charleston grey, Sugarbaby, Crimson Sweet, seeds, fleshy white and red*

1.0 Introduction

Consumption of fruits and vegetables plays a vital role in providing a diversified and nutritious diet (WHO, 2005). Daily intake of fresh fruits and vegetables in adequate quantities is recommended to reduce risk of coronary heart diseases, stroke and high blood pressure (WHO/FAO, 2003). Chromium plays a role in the management of heart diseases by regulating fat and cholesterol synthesis in the liver (WHO, 1999)

Fruits and vegetables are rich sources of chromium which regulates blood sugar, thereby reducing insulin needs in diabetic patients (Bahkru, 2006). Watermelon *(Citrullus lunatus)* belongs to cucurbitaceous family. It is related to cantaloupe, squash and pumpkin and other plants that grow on vines on the ground. The flesh may be red, pink, orange, yellow or white; the seeds can be brown, white green, or yellow and a few varieties are actually seedless (Murray *et al*., 2005). Watermelon is a good source of pure water- about 93%, it is a thirst quencher that may also quench the inflammation that contributes to conditions like asthma, atherosclerosis, diabetes, colon cancer and arthritis and an excellent diuretic. Because it has high water content and low calorie content it delivers more nutrients per calorie which is an outstanding health benefits (Murray *et al*., 2005). Watermelons can be eaten as a whole without discarding any part (waste). For example, the rind/peel is either pickled or stir fried, stewed to make it a delicious serving and its seeds are also found useful as a snack (Mayo, 2007), the pickles are used to prepare cakes.(NRC, 2008), the de-skinned and de-fruited white fleshy part is cooked with Olive oil, garlic, chili peppers and sugar (Collins, *et al.,* 2005). The objective of this study was to determine the levels of chromium in the peel, white flesh, red flesh and seeds of Charleston grey, Crimson sweet and Sugarbaby watermelons.

1.2 Role of chromium (III) in the body

Chromium (III) is essential for plants and animal growth. Most plants contain chromium in levels less than 1 ppm while in others it ranges from 4 ppm to 6 ppm (Underwood, 1977). It is widely distributed in human tissue in extremely low and variable concentration. Chromium total body content is less than 6 mg (Underwood, 1977). While human plasma contains 0.01 to 0.1 µg chromium per day (Mindell and Mundis, 2004). Chromium of the plasma is bound to transferring component of β-globulin fraction of the plasma protein. Biological activity of chromium is demonstrated by the trivalent state. In foods, chromium exists both in poorly absorbed inorganic form and biologically active complex. Hexavalent chromium is better absorbed than the latter (Mindell and Mundis, 2004).

Chromium regulates blood sugar, thereby reducing medication and insulin needs in diabetic patients (Bahkru, 2006). It also works with insulin in metabolism of sugar, thus normalizing blood sugar levels. Maintenance of blood sugar levels stems from the fact that the active agent (glucose tolerance factor) consists of chromium chemically bound with nicotinic acid which is a member of vitamin B complex. If a person has mild diabetes, chromium may save him/her from getting full-fledged disease and can help improve glucose tolerance. Diabetes responds to chromium supplementation thus occurrence of diabetes may be due to lack of chromium in the body (Mindel and Mundis, 2004). Lack of chromium also appears to be involved in the development of maturity onset diabetes, since it has been found that levels of the mineral in tissues drop with age. Chromium also helps the body keep fat in small particles since when fat globules get too large causing narrowing and hardening of arterial walls (Al Durtsch, 1999).

Chromium also plays a role in the management of heart diseases by regulating fat and cholesterol synthesis in the liver (WHO, 1999).

The LDL (low density lipoprotein) cholesterol in diabetes is more susceptible to oxidation and thus more likely to become toxic. The oxidized LDL cholesterol is more likely to clog arteries thus diabetics are 2 to 3 times at high risk of development heart diseases (Bakhru, 2006). The dangerous oxidized LDL cholesterol is caused by high levels of Sugar in the blood. However, as sugar is metabolized it releases oxygen free radicals that tend to make cholesterol toxic. Chromium activates vitamin C which is beneficial to human health since it increases resistance to infections and prevents cancer. It also aids in iron absorption and reduces oxidative stress and HIV viral load (WHO, 1999).

The Recommended Daily Allowances (RDA) value of chromium is 50 to 200 µg (Bakhru, 2006). The estimated safe and adequate daily dietary intake of chromium is 50 to 200 µg for adult and adolescents (NRC, 1989). In the United States adult women consume about 23 µg to 29 µg of Cr per day from food while men consume an average of 39 µg to 54 µg per day and infants obtain about 0.2 µg from breast milk (NRC, 1989). No tolerable upper intake level for this mineral has been established (Stoecker, 1987). A recent study on analysis of a bitter cucumber *(momordica charantia*) grown in south Nigeria showed that it contains 162.00 mg/Kg of Cr (Ayoola *et al*., 2010). A study in Kenya has shown that watermelon seeds contain 6.20 µg/g of chromium while pumpkin seeds contain 5.26 µg/g of chromium (Muchemi, 2006).

3.0 MATERIALS AND METHODS

3.1 Sampling procedure and Pre-treatment

Purposive strategy was used to select the sampling sites. The sampling sites were Mwea and Githurai markets; the main criterion for selection of sampling sites was the availability of the three varieties of watermelons. Sampling for the each variety was done for six times at intervals of two months for a period of twelve months. This was done to avoid biasness due to seasonal variations. Each time three watermelons of the same variety were bought from three different vendors. The selection of vendors was subject to availability of the variety of watermelon being bought. The watermelons were selected randomly from the vendor. This was repeated for six times in each sampling site (market).

The obtained watermelon samples were packed in plastic bags and transported to laboratory. The three watermelons of the same variety sampled were cleaned using distilled water, four parts were extracted namely the peel/rind, fleshy red part, fleshy white part and seeds and dried at 105 °C in a gravity oven until there was no further change in weight. Each of the dry parts from the three watermelons was homogenized by grinding to form one sample; a total of four samples (four parts). The ground samples were stored in well labeled plastic bags awaiting digestion and analysis. This was repeated each time sampling was done.

3.2 Chemicals and Reagents

All reagents used in this study were of analytical grade. Concentrated nitric acid, sulfuric acid, hydrogen peroxide, potassium nitrate and hydrochloric acid were sourced from Thomas Baker Chemicals Ltd Mumbai India whereas sodium borate ($Na_2B_4O_7.10H_2O$), Chromium (Cr)

commercially prepared standards were purchased from Fluka Chemie GmbH Aldrich chemical company, Inc. USA.

3.3 Equipments and AAS operating conditions

The equipments used in this study include the analytical balance (Model AAA, Adam Co Ltd.) from Britain, water distillation machine (Model WSB/4) from England and Varian Atomic Absorption Spectrophotometer (Model AA-10) from Australia. The operating conditions for the AAS were as follows Operating parameters: Wavelength (nm): 357.9, Slit width (nm): 0.2, Flame type: Air- acetylene, Oxidant flow rate (l/min): 1.5, Sensitivity (ppm): 0.055, Detection limit (ppm): 0.005, Lamp current (mA): 5, Optimum working range (ppm): 2.0-8.0

3.4 Cleaning of Apparatus

All plastic ware and glass ware apparatus were washed with liquid detergent and hot water then rinsed severally with tap water followed by soaking overnight in 10 % analytical grade nitric acid. Apparatus were rinsed with distilled water. The glass ware were dried in an oven at 105 °C and the plastic bottles in open racks and stored in lockable drawers.

3.5 Preparation of standards

Working standards were freshly prepared from stock solutions each time an analysis was carried out. Calibration graphs were established from a plot of absorbance readings of standards against their concentration were used to determine the concentration of Cr.

3.6 Digestion of watermelon samples

A 0.500 g of each sample was weighed accurately using electronic balance (model AAA, Adam Co ltd). A 9 ml mixture of HNO_3 and H_2SO_4 in the ratio 2:1 were first added to the 0.500 g of sample in Kjeldahl flask and then gently heated on hot mantle until the dense brown fumes began to appear. Hydrogen peroxide was added drop wise to clear the brown fumes. Digestion was allowed to continue until the solution was clear and white fumes observed. The digested sample was cooled and filtered using filter paper (whatman No 42) into 100 ml clean dry volumetric flask and then diluted to the mark with distilled water. They were then transferred into separate plastic bottles, labeled and appropriately stored under refrigeration until analysis.

3.7 Digestion of the blank samples and calculation of detection limit

In order to account for the background effects from the acids and to correct for changes resulting from digestion procedures, six blank samples were digested following the same procedures as the samples and each of the blank samples were determined for Cr by atomic absorption spectrophotometer. The absorbance's were recorded. Their means and standard deviations were calculated and limit of detection was calculated using the Equation as described by Christian (2005).

$$\text{Limit of detection} = \frac{3\text{xStandard deviation of blank readings}}{\text{Absorbance of standard} - \text{Mean absorbance of six blanks}}$$

3.8 Instrument and Method Optimization

Instrument optimization involves the analytical sequence to demonstrate that the instrument is working properly during the analysis of the elements. In this study the instrument was calibrated by analysing calibration solutions that produced responses of 0.000 absorbance and standards of

known concentration for Cr. Regression analysis was done where the slope (m), and intercept (c) of linear equations ($y = mx + c$) that best fits data from calibrations were determined and the correlation coefficients(r). If x and y have a strong positive correlation r is close to 1 (Gareth, 2011). Where errors in preparations of calibration standard solutions, deviations from linearity and contamination were observed new solutions were prepared correctly and the calibration was repeated.

To determine the accuracy of the analytical procedure a recovery test was conducted. The recovery test was investigated by spiking a suitable known amount of the analyte into a test portion of the sample having a known concentration of the analyte and analyzing the spiked test portion along with the original sample. The precision of the method was expressed as a percent relative standard deviation (% RSD) of the triplicate analyses. In cases where the test solutions did not agree with the recommended range of 90-110 % recovery and ± 5 % relative differences (Hight, 1998) the test solutions were prepared again and re-calibration of instrument done to analyze the test solutions.

For this research, in order to demonstrate the validity of whole analytical procedure, the recovery test was done as follows: A 10 ml aliquot of 5 µg/ml Cr was spiked into a conical flask containing 0.5 g of dried watermelon samples. Then same digestion procedure was followed for non-spiked and spiked watermelon samples side by side. Each sample was analyzed for their respective spiked metals by atomic absorption spectrophotometer. The concentration of un-spiked sample was subtracted from the concentration of the spiked sample to determine the amount recovered. The recovered amount was divided by the concentration of the known standard added (spiked) and multiplied by 100 and expressed as a percentage recovery.

3.9 Determination and calculations of concentration of chromium

Determination of chromium was done in replicates using computerized Varian Atomic Absorption Spectrometer model AA-10. The samples were analyzed in replicates under the same conditions as standards and blanks. For precision, standards were measured before and after the sample solution. The calibration of the instrument using standards and blank was frequently done between samples to ensure stability of the base line. The concentration of essential elements in the samples was worked out from the obtained AAS analytical results (read out) using the Equation;

$$Actual\ Concentration(\mu g / g) = \frac{Concentration(\mu g / ml) x Volume\ digested(ml)}{Weight\ of\ \ dried\ \ sample(g)}$$

The concentration of Cr in the samples was worked out by calculating the mean and standard deviation (standard errors) (SE) values of the replicate measurements.

3.10 Data analysis

Mean values obtained for Chromium studied in the four parts of watermelons and the three varieties of watermelon samples were compared by One-Way ANOVA at 95% level using SPSS (version 18.0). The assumption was that there were no significant differences among them when the statistical comparison gives $p < 0.05$. Whenever a significance difference exists, the means were compared at $p = 0.05$ significance level which accounts for errors since a sample was used to represent a population (Sawyer *et al.,* 2004).

4.0 RESULTS AND DISCUSSION

4.1Method validation

4.1.1 Regression Analysis and Detection limit

Regression analysis was used to evaluate the linearity of AAS using the established calibration curves. The absorbance readings and concentration of ideal standards were used to calculate the correlation coefficients (r). The detection limits were calculated as the concentration that give signals equal to three times the standard deviations of the six blanks as described in section 3.7. The calibration curves were established by a plot of absorbance readings (y-axis) against the corresponding concentration (x-axis) of standards with optimized instrumental conditions. The detection limits, the correlation coefficients, the equations of the calibration curves and the range of standards used to establish them in are represented in Table 1.

Table 1: Detection limits, correlation coefficients and equations of the calibration curves for the determination of chromium in watermelon samples by AAS

Method Detection limit(µg/ml)	Concentration range of standards (µg/ml)	Correlation coefficient of calibration curve	Equations for calibration Curve
0.003	0.0-70.0	0.9998	Y=0.019x+0.001

In Table 1; x-concentration, Y- absorbance

From Table 1 the correlation coefficient of the calibration curve was 0.9998, which shows that there was a very good correlation (relationship) between concentration and absorbance (Gareth, 2011). The method detection limits for all the metals were < 0.1 µg/ml which indicate that the method is applicable for the determination of metals at trace levels. The performance of AAS spectrophotometer was therefore good and reliable to warrant its use in the analysis of the element in the watermelon samples.

4.1.2 Recovery test

The recovery test for watermelon samples was performed in triplicates. The recovery test results are indicated in Table 2.

Table 4.2: Recovery test results for the metal (percentage)

Concentration (µg/ml)			Mean % Recovery	(%)RSD
Un-spiked sample Mean±SE	Standard added to the sample	Spiked sample Mean±SE		
0.15±0.01	5.00	5.13±0.02	99.87	0.62

Results in Table 2 indicate that the percentage recovery was 99.87 % this was within the acceptable range for percentage recovery of 90-110 % and RSD (0.04−0.62 %) which is within the acceptable range for all metals ±5 % (Hight, 1998). This confirms that the method is of good precision and accuracy and therefore the results presented are valid.

4.2 Mean levels of chromium in parts of watermelons

The mean levels of chromium in the parts each variety of watermelon from each sampling sites determined and compared at α =0.05 level as recorded in Table 3.

Table 3: Mean levels and range (µg/g) of chromium in parts watermelons

Varieties of watermelons /sampling sites		Concentration (µg/g)-Mean ±SE				P- value
		Peel/rind	White flesh	Red flesh	Seeds	
Charleston Grey	Githurai	12.89±1.15^{a}	16.89±2.41^{a}	16.13±6.05^{a}	19.78±0.76^{a}	0.549
	Mwea	21.11±4.14^{ab}	40.11±2.63^{c}	36.78±9.86^{ab}	17.56±2.70^{a}	0.024
Crimson Sweet	Githurai	18.00±0.91^{c}	3.47±0.25^{a}	9.22±1.51^{b}	25.33±1.42^{d}	0.001
	Mwea	16.00±0.46^{c}	5.56±0.37^{a}	12.00±0.96^{b}	23.34±1.45^{d}	0.001
Sugarbaby	Githurai	17.56±2.54^{a}	25.00±4.86^{ab}	29.44±1.97^{b}	44.67±1.10^{c}	0.001
	Mwea	15.56±1.10^{a}	27.33±4.22^{bc}	22.00±1.72^{ab}	34.17±3.39^{c}	0.002

In Table 3 mean values with the same small letters within the same row are not significantly different at α =0.05.

Results in Table 3 indicates that samples of Charleston Grey bought from Githurai market, chromium mean levels recorded by the peel, white flesh, red flesh and the seeds did not differ while those bought from Mwea market recorded highest chromium mean levels in white flesh as compared to other parts. Consuming any of the four parts statistically it means that one gets the same nutritional values of chromium. In Crimson Sweet watermelons the seeds recorded the highest mean levels as compared to other parts. Only about 3 g of the dried seeds would provide the RDA of 50 to 200 µg (Bakhru, 2006). The Sugar baby watermelons the seeds recorded the highest amount of chromium and from the data only 2 g of the seeds would be required to meet the recommended RDA. Regardless of the type and source of the water melon approximately 100 g of a piece of watermelon would provide the minimum RDA if all the parts were to be consumed.

4.3 Mean levels of chromium in varieties of watermelons

Mean levels of chromium obtained in parts of each variety were averaged and the values obtained in the two markets were used to compare the three varieties as shown in Table 4.

Table 4: Mean levels (µg/g) of chromium in varieties of watermelons

Varieties of watermelons/ Sampling sites	Concentration (µg/g)			p-value
	Charleston Grey (SugarF1)	Crimson Sweet (Zebra)	Sugarbaby	
Githurai market -Mean±SE	16.42±1.63[a]	14.46±0.84[a]	29.17±2.49[b]	0.001
Mwea market -Mean±SE	28.89±3.33[b]	14.23±1.41[a]	24.76±1.96[b]	0.001

In Table 4 mean values with the same small letters within the same row are not significantly different at α =0.05.

Results in Table 4 indicate that the Sugarbaby watermelons samples obtained in Githurai market recorded the highest chromium mean levels as compared to Charleston Grey and Crimson Sweet watermelons samples (p = 0.001). In watermelon samples obtained from Mwea market, Charleston Grey recorded chromium mean levels which were the highest as compared to those recorded by Crimson Sweet (p = 0.001) but did not differ significantly with mean levels recorded by Sugarbaby, this means that consuming any of them would provide the similar amounts of chromium.

The variations in chromium mean levels in the varieties of watermelons can be attributed to such factors as the genetic makeup of the watermelons, the sites, amounts of chromium, pH and the physical conditions of the soils the watermelons were grown in (Pallardy and Theodore, 2008). Mean levels of chromium reported in this study were higher than those reported in watermelons and pumpkin seeds (Muchemi, 2006) but were lower than those reported in bitter cucumber (Ayoola *et al*., 2010). However, they were comparable to those reported in broccoli of 22 µg/g (Anderson *et al*., 1992).

5.0 CONCLUSION AND RECCOMENDATIONS

All the parts of watermelon samples analyzed were found to contain chromium with the seeds of Sugar baby variety recording the highest amounts. It is advisable to consume all the parts of watermelons.

5.0 Acknowledgement

The authors wish to thank the department of chemistry Kenyatta university for supplying chemicals and providing laboratory bench and apparatus used in this study and department of geology and mines, ministry of environment and natural resources for providing analytical equipments used in this study.

6.0 References

(NRC) National research council. (2008). Lost Crops of Africa: fruits. Board on Science and Technology for International Development. National academics press. Pp 167.

(WHO) World health organization. (1999). Trace elements in human nutrition and health, Geneva. Pp 72-103.

(WHO) World health organization. (2005). Preventing chronic diseases a vital investment. WHO Press. Pp 36-50.

(WHO/FAO) World health organization /Food Agricultural Organization. (2003). Expert consultation on diet, nutrition and the prevention of chronic diseases. Geneva, Switzerland. WHO *Technical Report;* **916**:4-10, 129.

Al Durtsch, D. (1999). Chromium deficiency diseases and good nutrition: Nutrition Basic Home. Walton Feed. Pp 1-2.

Anderson, R.A. Byden, N.A. and Polansky, M.M. (1992). Dietary chromium intake in freely chosen diets, institutional diets and individual foods. *Biological Trace Elements Research*; 32:17-121.

Ayoola, P.B.; Adeyeye, A. and Onawumi, O.O. (2010). Trace Elements and Major Minerals *Evaluation of Spondias mombin, Vernonia amygdalina* and *Momordica charantia* Leaves. *Pakistan Journal of Nutrition; **9:** 755-758.*

Bakhru, H. (2006). Healing through natural fruits. Jaico press, Mumbai. Pp 34-39.

Christian, G. D. (2005). Analytical chemistry. 6th edition. John Willy & Sons Pte. Ltd, Asia. Pp 111-112.

Collins, J.K., Davis A.R., Perkins-Veazie, P.M and Adams, E. (2005). Sensory evaluation of low sugar watermelon by consumers. *Horticultural Science*; **40**: 883.

Gareth, T. (2011). Medical chemistry: An introduction. 2nd edition. John Willy and Sons ltd. England. Pp. 646

Hight, S. C. (1998). Flame Atomic Absorption Spectrometric Determination of Lead and Cadmium Extracted from Ceramic Foodware. Food and Drug Administration, Division of Field Science, Rockville, MD. *Food and Drug Administration. Laboratory Information Bulletin;* **no.4126**

Mayo Foundation for Medical Education and Research. (2007). Antioxidants-Preventing Disease, Naturally. Mayo Clinic. com. Accessed June 10, 2010.

Mindell, E. and Mundis, H. (2004). Vitamin Bible; Updated information on nutraceuticals, herbs, alternative therapies and anti-aging supplements. Warner book group, New York. Pp 13-17 and 56-71.

Muchemi, N.G. (2006). Determination of some immune boosting trace elements in selected food grains, herbal spices and seeds. Thesis. Keny.atta University. Nairobi. Pp 76-77.

Murray, M.T.; Pizzorno, J. and Pizzorno, L. (2005). The condensed encyclopedia of healing food. ATRIA books, New York. Pp 960.

Pallardy, G.S and Thiodore, T.K. (2008). Physiology of woody plants. 3rd edition. Elsevier. Oxford. UK. Pp 261

Sawyer, W. Heineman and Beebe, A. (2004). Chemistry experiment for instrumental methods. Wiley, New York. Pp 43-51

Underwood, E.J. (1977). Trace elements in human and animal nutrition. Academic press, New York. Pp 149-165.

Stoecker, B.J. (2001). Chromium in Present Knowledge in Nutrition, 8th Edition. ILSI Press, Washington DC. Pp 366-372.

Underwood, E.J. (1977). Trace elements in human and animal nutrition. Academic press, New York. Pp 149-165.

EXPLORING THE NUTRACEUTICAL VALUES OF RESIDUES OF MANGIFERA INDICA L. GROWN IN EMBU COUNTY, KENYA

Njiru, M.K*[1], Odundo, J.O[1], Wanjau, R.N[1] and Nawiri, M.P[1]
*Corresponding author: njirumike31@gmail.com
Kenyatta University, Chemistry Dept. P.O Box 43844-00100 Nairobi

ABSTRACT
The mesocarp (edible part) of Mangifera indica L. (mango) fruit is known for its contribution towards addressing nutritional challenges, most of which are prevalent in the developing countries. Based on the Recommended Daily Allowance (RDA) levels by National Research Council (NRC) USA, mangoes would provide sufficient amounts of essential minerals, sodium (Na), potassium (K), magnesium (Mg), calcium (Ca), Zinc (Zn), copper (Cu), iron (Fe) and manganese (Mn). The mango residues (non edible parts), namely the epicarp (peels), endocarp (shell) and the seed kernels account for 40-50 % of the fruit and result to over 150,000 tonnes of dumping thus posing an environmental concern. A knowledge gap on the potential nutritional contribution and benefits of these residues in the aim of reducing environmental pollution is therefore called for. Mineral content (Na, K, Mg, Ca, Zn, Cu, Fe, Mn) in residues of ngowe, apple and van dyke varieties of mangoes grown in Mbeere South, Embu County, Kenya were explored. Mature mangoes were randomly sampled for analysis of minerals which was performed using Atomic Absorption and Emission Spectrometry. Among the residues studied, the endocarp was found to contain both the minimum and maximum level of minerals, thus 0.38 mg/100g Cu and 1689.5 mg/100g Ca in the ngowe and van dyke varieties respectively. With regard to the RDA recommended levels of minerals, these findings indicate that mango residues are a rich source of essential minerals. This potential can be explored for other benefits such as for use in animal feeds/supplements thus preventing environmental pollution. This would provide a dual advantage, leading to an eco-friendly waste management and income generation.

Key words: *Mangifera indica* L., essential minerals, mango residues, environmental pollution.

1.1 INTRODUCTION

Mangifera indica L. (mango) belong to the genus *mangifera* of the family *Anacardiaceae.* The worldwide production of this fruit is estimated to be over 40 million tons (FAO, 2011). In Kenya, about 30,000 ha are under cultivation of both the local and exotic varieties with an output of nearly 450,000 metric tonnes. It is grown in the Eastern (particularly Mbeere South in Embu County), Central, Nyanza, Western and Coastal regions of the country, with the Eastern region producing the highest yields (MOA, 2007). Over 75 % of the local mango varieties produced include ngowe, dodo, batawi and boribo while exotic varieties include kent, tommy, atkins, apple, van dyke and sensation (Griesbach, 2003; Gathambiri *et al*., 2006; MOA, 2007; Msabeni *et al.,* 2010).

A number of inorganic elements are essential for normal growth and reproduction in animals. The edible part (mesocarp/flesh) of *Mangifera indica* L. (mangoes) is reported to be of nutritional benefits being rich not only in amino acids, carbohydrates, fatty acids, organic acids, proteins and vitamins but also in minerals including Zn, Na, K, Mg, Cu, Fe, Mn and Ca (USDA, 2001; Gouado *et al.,* 2007). Other than for the edible part, mangoes have a thick epicarp/exocarp

(peel), a woody endocarp (pit) and seed (together referred to as residues in this study) which account for approximately 40-50 % of the fruit weight. Consumption of the mesocarp leads to over 150,000 tonnes as waste from the non-edible parts dumped into the environmental (Berardini *et al*., 2005; Sruamsiri and Silman, 2009; Heuze′ *et al*., 2012). The variation in the levels of minerals in varieties in parts of plants has been attributed to differences in soil composition, varietal differences in parent trees and the ability to take up minerals by the plants (Zurera *et al.,* 1989; Sharma *et al.,* 2006; Sharma *et al.,* 2009; Saeed *et al.,* 2010) . However, mango peels and seeds combined with rice straws and *Leucaena* leaves have been reported to be good in aiding cattle digestion and as well, they have been fed successfully to snails, poultry and sheep **(**Sruamsiri and Silman, 2009; Omole *et al*., 2004**)**. The National Research Council (NRC) USA documents Recommended Daily Allowance (RDA) for animals (NRC, 2005). In this study, the mineral profile (Zn, Na, K, Mg, Cu, Fe, Mn and Ca) in residues (peels, endocarp and seeds) of varieties of mangoes grown in Mbeere south, Embu County in Kenya was therefore investigated.

2.0 MATERIALS AND METHODS

The reagents used in this study; concentrated nitric (V) acid (HNO_3), sulphuric (VI) acid (H_2SO_4), hydrogen peroxide (H_2O_2) and hydrochloric acid (HCl) were of analytical grade and were sourced from Thomas Baker Chemicals Ltd, Mumbai, India. All the other reagents including pure zinc granules (Zn), sodium (Na), potassium (K), magnesium (Mg), copper (Cu), iron (Fe), manganese (Mn) and calcium (Ca) metals were of analar grade and sourced from Fluka Chemicals Company, USA.

2.2 Sampling, pre-treatment and digestion

Mango fruits were sampled from Kiritiri division of Mbeere South in Embu County, Kenya, based on the availability of three mango varieties from six farms. A total of sixteen mangoes of each variety were randomly sampled twice in each farm (radius 5 km) within a period of four weeks and transported to Kenyatta University laboratories. The fruits were repeatedly washed with distilled water, and the peels, endocarps and seeds separated from the mesocarps then chopped into small pieces. The resultant pieces were, oven dried at 105°C to constant weight (moisture content <10%) and ground prior to digestion.

The digestion process was achieved by adding 0.5 g of the dried and ground sample into 9.0 ml of the digestion mixture (HNO_3:H_2SO_4; 2:1) in a Kjeldahl flask. The mixture was heated gently on a hot mantle until dense brown fumes began to appear which were immediately cleared by adding hydrogen peroxide drop-wise. The heating process proceeded and the complexion of the reaction was indicated by the appearance of a clear solution with production of white fumes. The solution was filtered into a conical flask and transferred into a 100 ml volumetric flask and diluted to the mark using deionized water. All the tests were done in triplicates.

2.3 Measurements and data analysis

Calibration curves were drawn from a computerized variant atomic absorption and emission Spectroscopy (model AA-10) using standard solutions of Zn, Na, K, Mg, Cu, Fe, Mn and Ca prior to sample measurements. The operating conditions for the AAS and AES were set as per the instructors' manual.

Data was analyzed with SPSS 18.0 for windows. The mean and standard deviation of means were calculated and one-way analysis of variance (ANOVA) was used for statistical differences with Duncan's multiple range tests used to separate means ($p = 0.05$). The means were compared with the recommended levels for cattle and chicken.

3. RESULTS AND DISCUSSIONS

The mean levels of the minerals in the residues of Ngowe, Apple and Van dyke mangoes are presented in table 1.

All the residues of the mangoes under study were found to contain some level of the minerals Zn, Na, K, Mg, Cu, Fe, Mn and Ca. The general trend observed in decreasing concentration was Ca>K>Mg>Na>Fe>Mn>Zn>Cu which could be attributed to the mineral abundance in soils (Zurera *et al.,* 1989). The concentration range of the minerals in the three residues was varied between with the mango varieties although the general trend of Cu being recorded as the lowest amount of mineral and Ca being the highest was maintained. In seeds, a minimum amount of 0.48±0.05 mg/100g Cu was recorded in the apple variety and a maximum of 1492.05±43.75 mg/100g Ca was recorded in ngowe. In the endocarps, the ngowe variety was found to contain the minimum level of 0.38±0.02 mg/100g Cu while a maximum level of 1689.5±9.15 mg/100g Ca was observed in van dyke. Similarly, as noted to contain the lowest Cu levels in the endocarp, the peels of ngowe variety were also found to contain the minimum amount of 0.38±0.03 mg/100g Cu. The highest content of mineral in the peels was recorded in the apple mango variety with a value of 1482±2.05 mg/100g.

Ngowe and van dyke varieties generally had significantly higher levels of the minerals ($p<0.05$) and this could be attributed to differences in uptake of the minerals from soils as observed in a study on heavy metal uptake from greenhouse border soils for edible vegetables (Zurera *et al.,* 1989) . The peel and the seed had significantly high levels of the minerals in comparison to the endocarp ($p<0.05$).The differences in the levels of the minerals in both the residues and in varieties can be explained to be due differences in soil composition, varietal differences in parent trees and the ability to take up minerals by the plants (Sharma *et al.,* 2006; Sharma *et al.,* 2009; Saeed *et al.,* 2010).This is however not diminishing to the value of the endocarp, since the levels of Na, K, Ca and Mg in the endocarp were found to be above the RDA for livestock and poultry and those of Fe and Mn were within the RDA range in cattle, sheep and poultry (NRC, 2005). In general, the levels of minerals were within the range reported by previous studies and as such, these findings also support that the residues be explored for use as animal feeds since the benefits of inorganic elements for animals cannot be overstated and as well this will avoid the current dumping practice (Sruamsiri and Silman, 2009; Omole *et al*., 2004). This move will prevent environmental pollution to lead to an eco-friendly waste management and as well can be income generating.

Table 1: Mean levels of minerals in residues of Ngowe, Apple and Van dyke mangoes[1]

Element	Mango varieties	Residue concentration in mg /100g; n=12)			p-value
		Peel	Endocarp	Seed	
Na	Ngowe	192.00±6.00^{b}	149.00±1.00^{a}	160.70±4.30 ^{a}	<0.05
	Apple	291.55±0.45^{b}	188.50±0.50^{a}	189.85±0.15^{a}	
	Van dyke	216.45±0.45^{b}	174.85±0.15^{a}	236.75±5.05^{c}	
K	Ngowe	935.90±0.10^{c}	785.70±2.30^{a}	866.10±1.90^{b}	
	Apple	777.60±1.60^{c}	458.30±0.70^{a}	645.45±0.45^{b}	
	Van dyke	669.10±0.10^{b}	456.60±1.00^{a}	970.10±5.90^{c}	
Mg	Ngowe	280.00±6.00	273.50±0.50	261.90±4.80	>0.05
	Apple	242.60±0.60^{b}	160.35±6.65^{a}	233.60±7.60^{a}	<0.05
	Van dyke	183.60±3.60^{a}	238.00±4.00^{b}	259.10±4.20^{c}	
Zn	Ngowe	3.08±0.02^{c}	1.98±0.02^{b}	0.90±0.03^{a}	
	Apple	1.12±0.02^{b}	1.22±0.02^{b}	0.87±0.07^{a}	
	Van dyke	1.90±0.03^{c}	1.07±0.00^{b}	0.70±0.03^{a}	
Cu	Ngowe	0.38±0.02^{a}	0.75±0.02^{b}	0.72±0.02 ^{b}	
	Apple	1.50±0.17^{b}	1.25±0.02^{b}	0.48±0.05^{a}	
	Van dyke	0.42±0.02^{a}	0.52±0.02^{b}	0.65±0.02^{c}	
Fe	Ngowe	11.15±0.02^{b}	9.70±0.23^{a}	16.35±0.02^{c}	
	Apple	4.95±0.02^{a}	6.33±0.03^{b}	33.32±0.02^{c}	
	Van dyke	23.55±0.22^{b}	13.65±0.12^{a}	30.56±0.56^{c}	
Mn	Ngowe	4.85±0.12^{c}	2.93±0.03^{b}	1.13±0.03^{a}	
	Apple	3.65±0.02^{c}	1.65±0.02^{b}	1.53±0.03^{a}	
	Vandyke	4.60±0.07^{c}	1.52±0.02^{a}	2.15±0.02^{b}	
Ca	Ngowe	845.80±0.90^{a}	1413.70±0.0^{c}	978.30±5.00^{b}	
	Apple	1081.60±8.30^{c}	887.90±1.20^{a}	974.95±0.05^{b}	
	Van dyke	910.45±0.35^{a}	1689.15±9.15^{c}	976.70±0.70^{b}	

[1]Means followed by the same small letter(s) within the same row are not significantly different (snk, α=0.05)

CONCLUSION

These findings show that the peels, endocarp and seeds of ngowe, apple and van dyke mango varieties have sufficient minerals. As such, these residues can be considered for animal feed preparations and in turn reduce the burden that results due to their dumping into the environment to serve as a better waste management strategy.

ACKNOWLEDGEMENT

We are grateful to Kenyatta University for laboratory space, Geology and Mines Kenya for the AAS and AES machines.

REFERENCES

Berardini, N., Knodler, M., Schieber, A. and Carle, R. (2005). Utilization of mango peels as a source of pectin and polyphenolics. *Innovative Food Science & Emerging Technologies* 6: 442-452.

Food and Agriculture organization (FAO). (2011). http://faostat. Fao.org/default. aspx.

Gathambiri, C.W., Gitonga, J.G., Kamau, M., Njuguna, J.K., Kiiru, S.N., Muchui, M.N.,

Gatambia, E.K. and Muchira, D.K. (2006). Assessment of potential and limitation of postharvest value addition of mango fruits in Eastern province: A case study in Mbeere and Embu districts.

Gouado, I., Schweigert, F.J., Ejoh, R.A., Tchouanguep, M.F. and Camp, J.V. (2007). Systemic levels of carotenoids from mangoes and papaya consumed in three forms (juice, fresh and dry slice). *European Journal of Clinical Nutrition* **61**: 1180-1188.

Griesbach, J. (2003). Mango growing in Kenya. World agro forestry centre (ICRAF), Nairobi, Kenya. Pgp 111.

Heuzé, V., Tran, G., Bastianelli, D., Archimède, H. and Lebas, F. (2012). *Mango Mangifera indica fruit and by-products*. Feedipedia.org. A programme by INRA, CIRAD, AFZ and FAO

http://www.feedipedia.org/node/516.

Ministry of Agriculture Kenya. (MOA). (2007). Annual report.

Msabeni, A., Muchai, D., Masinde, G., Matoke, S. and Gathaara, V. (2010). Sweetening the mango: Strengthening the value chain. *Working Document Series* **136:** 1-74.

National Research Council (NRC). (2005). Mineral tolerance of animals. Second revised edition. Pg 1-469.

Omole, J.A., Ayodeji, O.I. and Raji, M.A. (2004). "The potential of peels of mango, plantain, cocoyam and pawpaw as diets for growing snails (*Archachatina marginata)*". *Livestock Research For for Rural Development* **16:**102.

Saeed, A., Safina, N., Tuseef, S.M., Seema, M., Muhammad, N. and Anwaar, A. (2010). Physico-chemical attributes and heavy metal content of mangoes (*Mangifera. Indica* L.) cultivated in different regions of Pakistan. *Pakistan Journal of Botany* **42**: 2691-2702.

Sharma, R.K., Agrawal, M. and Marshall, F.M. (2006). Heavy metals contamination in vegetables grown in waste water irrigated areas of Varanasi, India. *Bulletin of Environmental Contamination and Toxicology* **77**: 311-318.

Sharma, R.K., Agrawal M. and. Marshall, F.M. (2009). Heavy metals in vegetables collected from production and market sites of a tropical urban area of India. *Food and Chemical Toxicology* **47**: 583-591.

Sruamsiri, S. and Silman, P. (2009). Nutritive value and nutrient digestibility of ensilaged mango by products. *Maejo International Journal of Science and Technology* **3**: 371-378.

United States Department of Agriculture. (USDA). (2001). Mango fruit national nutrient database for standard reference, release 14.

Zurera, G., Moreno, R., Salmeron, J. and Pozo, R. (1989). Heavy metal uptake from greenhouse border soils for edible vegetables. *Journal of the Science Food and Agriculture* **49**: 307-314.

Phytochemical and antimicrobial studies of Teclea nobilis Del. used in traditional medicine in Kenya

Evans M. Onyancha[1], Paul K. Tarus[2*], Alex K. Machocho[1] and Sumesh C. Chhabra[1]

[1]Department of Chemistry, Kenyatta University, P.O. Box 43844, 00100 GPO, Nairobi, Kenya.
[2]Department of Chemistry and Biochemistry, University of Eldoret, P.O. Box 1125 - 30100, Eldoret, Kenya.

Abstract

*The organic extracts from the leaves of Teclea nobilis were subjected to fractionation and seven compounds were isolated by use of chromatographic techniques. The five isolated alkaloids were kokusaginine (**1**), 4,8-dimethoxy-7-(3-methylbut-2-enyloxy)furo[2,3-b]quinoline (**2**), skimmianine (**3**), dictamine (**4**) and flindersiamine (**5**). The common triterpenoid, lupeol (**6**), and the plant sterol, β-sitosterol (**7**) were also isolated. The compounds showed antibacterial activity ranging from mild to moderate activity with inhibition zones ranging from 7 to 11 mm. The structure determination of these compounds was done by use of ^{1}H, ^{13}C and 2 D NMR techniques and literature comparison. The alkaloids (**1**-**5**) obtained were tested for their antimicrobial activity against Gram-positive and negative bacteria. Agar diffusion assay was used for the determination of the sensitivity of test organisms to the samples. The results of the diffusion test showed that only kokusaginine was active on all the tested micro-organisms, whilst the inhibition effect of the crude extract and that of 4,8-dimethoxy-7-(3-methylbut-2-enyloxy)furo[2,3-b]quinoline and dictamine was observed on 87.5% of the tested microbial species. The overall results provide promising basis for the use of the crude extract as well as the isolated alkaloids in the treatment of specific microbial infections.*

Key words: *Teclea nobilis, Furoquinoline alkaloids, antibacterial activity and Artemia salina.*

*Address correspondence to this author at Department of Chemistry and Biochemistry, University of Eldoret, P.O. Box 1125 - 30100, Eldoret, Kenya; Tel: +254725000150, E-mail: paultarus@uoeld.ac.ke

10. Introduction

The genus *Teclea*, 'Olgelai' (Maasai), 'Ekodek' (Turkana) and 'Odar' (Luo) is widely distributed in wet highland forests, particularly in the Lake Victoria basin. It prefers sites in highland forests between the altitudes of 1700 and 2700 meters. Both the leaves and roots are used in local medicine. The roots are used to treat colds and chest problems. The wood is moderately hard, tough, and pale and is used for walking sticks, tool handles, bowls, clubs, spear shafts, poles, and hoe pins[1].

Ethno medical survey reveals widespread and diverse medical usage of this species. Some species have shown antibacterial, antimalarial, antipyretic, anti-inflammatory and analgesic activity at various levels of concentration[2]. Phytochemical analysis on *T. trichocarpa* has yielded a number of bioactive phytochemicals which include skimmianine, melicopidine, arborinine, tecleanthine and many others. The last three are acridone alkaloids while the first one is a quinoline alkaloid all of which exhibit bioactivity against bacteria and the malaria causing plasmodia[3].

An investigation on phytochemical composition of *T. nobilis* has yielded a number of furoquinoline alkaloids such as tecleabine, tecleoxine, melicopidine, methylnkolbsine as well as lupeol among others[4]. *Teclea verdoorniana*, a plant predominant in dry rocky areas of the tropics, especially in North and West Africa areas, has been shown to contain a number of terpenoids and quinoline alkaloids just like other members of this genus. Some of these phytochemicals include flindersiamine, kokusaginine, tecleaverdoornine and the terpenoid, lupeol[5].

Other *Teclea* species have more or less the same phytochemicals although some have yielded some unique compounds. *T. grandifolia,* for example, in addition to the phytochemicals mentioned earlier, showed the presence of evoxanthine, an alkaloid, as well as a triterpene called tecleanin. *Teclea oubanguensis,* a species predominantly found in Cameroon, has shown a number of quinoline alkaloids and triterpenoids through its phytochemical investigation, most of which have been highlighted above[6].

2.0 Methodology

The NMR spectra obtained from Varian Gemini 200 and 300 MHz. ^{1}H NMR spectra in $CDCl_3$ and CD_3OD depending on solubility. Chemical shifts (δ) were recorded in ppm relative to tetramethyl silane (TMS). Coupling constants, *J*, recorded in hertz (Hz). ^{13}C NMR spectra run at 50 MHz. TLC plates, Polygram® sil G/UV_{254} and Alugram® sil G/UV_{254} (Machery-Nagel GmbH and Co Frankfurt, Germany) were used. VLC, Kiesegel silica gel 60G (Merck, Germany) was used. CC was packed with Kiesegel silica gel 240G and Sephadex LH20 (Merck, Germany). Melting points of the pure compounds determined on a Gallenkamp apparatus (Sanyo, West Sussex-U.K) and were uncorrected. Long and short wavelength UV (365 nm and 254 nm) used

for visualizing spots on TLC (Spectronics Corporation Westbury, U.K). Visualization also done by spraying TLC plates with *p*-anisaldehyde or Dragendorff's reagent for alkaloids.

2.1 Plant material

The *Teclea nobilis* is an important medicinal plant the the Keiyo ethnic group and aerial parts (leaves) were collected from Siroch, Keiyo Sub county, Elgeyo-Marakwet County, 40 kilometers North East of Eldoret town. Voucher specimen (No. EMO/2/05/10) was deposited at the Kenyatta University herbarium on identification confirmed at East Africa herbarium museum. The air dried leaves ground into a fine powder using a motor grinding laboratory mill (Christy and Norris Ltd., Chelmsford, England).

2.2 Extraction and isolation of compounds

Dry powdered leaves of *T. nobilis* weighing 2.35 kg were soaked in the four solvents, in order of increasing polarity starting from hexane, DCM, EtOAc and MeOH with occasional swirling. After two days they were filtered and concentrated under vacuum by use of a rotary evaporator below 45°C. This was done three times for each extracting solvent and the resulting crude extracts were combined for each solvent. Combined concentrated crude extracts were sealed, labeled and stored in pre-weighed sample bottles at -20°C in a deep freezer.

The green paste of DCM extract (58.32 g) was subjected to VLC, CC, TLC and re-crystallization in pure acetone to yield kokusaginine (**1**), 4,8-dimethoxy-7-(3-methylbut-2-enyloxy)furo[2,3-*b*]quinoline (**2**), skimmianine (**3**), dictamine (**4**), flindersiamine (**5**), lupeol (**6)**, and *β*-sitosterol (**7**).

Characterization of these compounds was done using NMR (proton and carbon), COSY, HMQC, HMBC and DEPT spectra. Comparison with literature spectral values was also used.

Kokusaginine (**1**)**:** Yellow amorphous solid, Mass; 54.7 mg, Melting point; 167-169^{o}C. ^{1}H-NMR (300 MHz) data; δ 4.11 (*s*, 3H), 4.12 (*s*, 3H), 4.50 (*s*, 3H), 7.11 (*d*, 2.7 Hz, 1H), 7.42 (*s*, 1H), 7.53 (*s*, 1H) and 7.64 (*d*, 2.7 Hz, 1H). ^{13}C-NMR (75 MHz) data; δ 142.6 (C-2), 106.5 (C-3), 101.0 (C-3a), 163.4 (C-4), 113.1 (C-4a), 101.9 (C-5), 152.9 (C-6), 155.8 (C-7), 104.8 (C-8), 142.7 (C-8a), 148.1 (C-9a), 58.9 (CH_3O-4), 56.3 (CH_3O-6) and 56.3 (CH_3O-7).

4,8-Dimethoxy-7-(3-methyl-but-2-enyloxy)-furo [2, 3-*b*] quinoline (**2**): Yellow crystals, Mass; 38.3 mg, Melting point; 167-168^{o}C. ^{1}H-NMR (300 MHz) data; δ 1.76 (*s*, 3H), 1.76 (*s*, 3H), 4.11 (*s*, 3H), 4.51 (*s*, 3H), 4.94 (*d*, 7.2 Hz, 2H), 7.12 (*t*, 7.2 Hz, 1H), 7.32 (*d*, 2.7 Hz, 1H), 7.66 (*s*, 1H), 7.67 (*s*, 1H) and 8.11 (*d*, 2.7 Hz, 1H). ^{13}C-NMR (75 MHz) data; δ 152.9 (C-2), 105.0 (C-3), 102.2 (C-3a), 164.5 (C-4), 115.1 (C-4a), 112.2 (C-5), 118.4 (C-6), 142.3 (C-7), 141.1 (C-8), 143.2 (C-8a), 157.4 (C-9a), 70.8 (C-2′), 121.5 (C-3′), 138.0 (C-4′), 26.2 (C-5′), 18.4 (C-6′), 59.3 (CH_3O-4) and 57.1 (CH_3O-6).

Skimmianine (**3**): Light yellow crystals, Mass; 13.1 mg. Melting point; 175-177^{o}C. The ^{1}H-NMR (300 MHz) data; δ 4.13 (*s*, 3H), 4.21 (*s*, 3H), 4.52 (*s*, 3H), 7.14 (*d*, 1.2 Hz, 1H), 7.33 (*d*,

9.3 Hz, 1H), 7.68 (*d*, 1.2 Hz, 1H) and 8.10 (*d*, 9.3 Hz, 1H). ^{13}C-NMR (75 MHz) data; δ 152.5 (C-2), 105.0 (C-3), 102.3 (C-3a), 164.7 (C-4), 115.2 (C-4a), 112.2 (C-5), 118.5 (C-6), 142.2 (C-7), 141.8 (C-8), 143.3 (C-8a), 157.5 (C-9a), 59.3 (CH_3O-4), 57.1(CH_3O-7) and 62.0 (CH_3O-8).

Dictamine (**4**): Yellowish crystalline solids. Mass; 8.2 mg. ^{1}H-NMR (300 MHz) data; δ 4.45 (*s*, 3H), 7.08 (*d*, 2.8 Hz, 1H), 7.43 (*dt*, 1.5 Hz, 8.0 Hz, 1H), 7.62 (*d*, 2.8 Hz, 1H), 7.67 (*dd*, 1.5 Hz, 8.0 Hz, 1H), 7.99 (*dd*, 1.5 Hz, 8.0 Hz, 1H) and 8.27 (*dd*, 1.5 Hz, 8.0 Hz, 1H). ^{13}C-NMR (75 MHz) data; δ 143.6 (C-2), 103.4 (C-3), 101.3 (C-3a), 156.8 (C-4), 118.7 (C-4a), 104.7 (C5), 122.3 (C-6), 127.8 (C-7), 123.7 (C-8), 129.6 (C-8a), 145.6 (C-9a) and δ 59.0 (CH_3O-4).

Flindersiamine (**5**): Yellowish powder. Mass; 18.7 mg. Melting point; 214-216°C. ^{1}H-NMR (300 MHz) data; δ 4.24 (*s*, 3H), 4.39 (*s*, 3H), 6.04 (*s*, 2H), 7.01 (*d*, 2.4 Hz, 1H), 7.25 (*s*, 1H) and 7.57 (*d*, 2.4 Hz, 1H). ^{13}C-NMR (75 MHz) data; δ 143.0 (C-2), 104.3 (C-3), 114.9 (C-3a), 156.1(C-4), 103.0 (C-4a), 92.4 (C-5), 138.0 (C-6), 137.7 (C-7), 135.9 (C-8), 146.8 (C-8a), 162.6 (C-9a), 60.6 (CH_3O-4), 59.0 (CH_3O-8) and 101.5 (OCH_2O).

Lupeol (**6**): A resinous white powder. Mass; 21.3 mg. Melting point; 208-215°C. ^{1}H-NMR (300 MHz) data: δ 0.18 (*s*, 3H), 0.80 (*d*, 1H), 0.86 (*s*, 3H), 0.87 (*s*, 3H), 0.88 (*s*, 3H), 0.94 (*s*, 3H), 1.08 (*m*, 1H), 1.09 (*m*, 1H), 1.09 (*m*, 1H), 1.17 (*m*, 1H), 1.20 (*s*, 3H), 1.21 (*m*, 2H), 1.22 (*m*, 1H), 1.22 (1H), 1.29 (1H), 1.34 (1H), 1.51 (1H), 1.59 (1H), 1.60 (2H), 2.05 (1H), 2.45 and 1.80 (*m*, 1H), 2.50 (*m*, 1H), 3.35 (1H), 4.80 and 4.68 (*m*, each 1H), ^{13}C-NMR (75 MHz) data; δ 40.3 (C-1), 27.8 (C-2), 79.3 (C-3), 39.2 (C-4), 55.6 (C-5), 18.7 (C-6), 34.6 (C-7), 41.1 (C-8), 50.7 (C-9), 37.5 (C-10), 21.3 (C-11), 28.3 (C-12), 38.4 (C-13), 43.2 (C-14), 30.1 (C-15), 35.9 (C-16), 43.3 (C-17), 48.6 (C-18), 48.3 (C-19), 151.4 (C-20), 30.2 (C-21), 39.0 (C-22), 28.6 (C-23), 16.5 (C-24), 15.7 (C-25), 14.9 (C-26), 16.3 (C-27), 18.3 (C-28), 110.0 (C-29) and δ 19.6 (C-30).

***β*-Sitosterol** (**7**): White solid. Mass; 36.2 mg. Melting point; 131-133^{o}C. ^{1}H NMR (300 MHz) data; δ 0. 68 (*d*, 6.7 Hz, 3H), 0.73 (*d*, 6.5 Hz, 3H), 0.75 (*t*, 7.4 Hz, 3H), 1.10 (*s*, 3H), 3H), 1.25 (*d*, 6.5 Hz, 1.57 (*s*, 3H), 3.53 (*m*, 1H), 5.35 (*m*, 1H). ^{13}C-NMR (75 MHz) data; δ 36.9 (C-1), 30.1 (C-2), 72.2 (C-3), 42.6 (C-4), 141.2 (C-5), 121.4 (C-6), 32.3 (C-7), 34.3 (C-8), 50.5 (C-9), 36.6 (C-10), 21.5 (C-11), 40.2 (C-12), 42.7 (C-13), 57.2 (C-14), 24.7 (C-15), 28.7 (C-16), 56.4 (C-17), 12.3 (C-18), 19.2 (C-19), 36.6 (C-20), 18.2 (C-21), 34.3 (C-22), 42.7 (C-23), 46.2 (C-24), 29.5 (C-25), 19.4 (C-26), 20.2 (C-27), 23.4 (C-28) and 12.4 (C-29).

2.3 Brine shrimps lethality test

Brine schrimps (*Artemia salina*) were used for cytotoxicity tests. They were hatched and the drugs prepared as per Solis *et al* [9]. Lethal dose fifty (LD_{50}) values in µg/ml of the extracts were then calculated using probit analysis.

2.4 Antibacterial activity tests

A total of five bacteria affecting human beings were used. These were *Staphylococcus aureus* (ATCC 35844), *Streptococcus pneumoniae* (ATCC 33400), *Bacillus subtilis* (ATCC 6051), *Salmonella typhi* (ATCC 19430) and *Escherichia coli* (ATCC 11775). The human pathogens were obtained from Plants and Microbial Sciences Department of Kenyatta University. The standard antibiotics, Ampicillin and Gentamycin obtained from Sigma Aldrich, Germany were used as reference drugs for the human pathogenic bacteria. A concentration of 100 mg/ml of each of the crude extracts in DMSO was used. The filter paper disc assay method as described by Chhabra and Uiso (1991)[10] was employed. The procedure was carried out in a laminar flow hood (Labcare Systems Ltd., London, England) to prevent contamination.

3.0 Results and discussion

Dry powdered leaves of *Teclea nobilis* weighed 2.35 kg and the masses of various extracts were as shown in Table 1. The MeOH extract had highest yield (10.95%) while EtOAc had the least (1.57%).

Table 1: Yields and percentage yield of *Teclea nobilis* extracts

Extract	**Hexane**	**DCM**	**EtOAc**	**MeOH**
Yield (grams)	64.14	58.32	36.87	257.32
% Yield	2.73	2.48	1.57	10.95

These extracts were subjected to brine shrimp lethality and antibacterial tests before fractionation commenced. The biological assay results are as table 2 and 3. The mean LD_{50} values of extracts found to be below 240 µg/ml against *Artemia salina* was taken to be cytotoxic. The DCM extract was the most active (165 µg/ml) while EtOAc was the least active (557 µg/ml). This shows that most *T. nobilis* extracts are not toxic except for the DCM extract.

Table 2: The mean LD_{50} values for *T. nobilis* extracts against *Artemia salina*

Extract	**Hexane**	**DCM**	**EtOAc**	**MeOH**
LD50 (µg/ml)	235	165	557	268

The fact that there was some activity towards the Gram-negative bacteria by some extracts like MeOH and DCM is a good indicator since the Gram-negative bacteria are known to be difficult to be inhibited by many antibiotics[7]. These results vindicate the bioactivity of the four extracts. Hence, the need for a systematic phytochemical analysis of the plant was evident. The TCL profiles of the crude extracts revealed the presence of several UV active compounds that were of interest such as alkaloids and plant sterols.

Table 3: The inhibition zones (in mm) of the four crude extracts of the air dried leaf extracts of *T. Nobilis*

Test organisms	*S. aureus*	*S. pneumoniae*	*B. subtilis*	*S. typhi*	*E. coli*
Extract					
Hexane	9	8	7	6	6
DCM	10	9	6	7	7
EtOAc	7	6	6	6	6
MeOH	7	8	8	7	7
Control	6	6	6	6	6
Ampicillin	14	15	13	14	12
Gentamycin	13	13	15	17	16

Characterization of these compounds was done using NMR (proton and carbon), COSY, HMQC, HMBC and DEPT spectra. Comparison with literature spectral values was also used. These compounds were found to belong to a range of structural classes of alkaloids and sterols. Kokusaginine, 4,6-Dimethoxy-7-(3-methyl-but-2-enyloxy)-furo[2,3-*b*]quinoline, skimmianine, dictamine and flindersiamine all exhibit a furoquinoline skeleton spectra with modifications on the groups attached at various positions on the ring. Kokusaginine, skimmianine and dictamine differ by the number and position of methoxy groups attached to the ring. 4,6-Dimethoxy-7-(3-methyl-but-2-enyloxy)-furo[2,3-*b*]quinoline shows signals that can be associated with an isoprene unit at carbon 7. The ^{1}H and ^{13}C NMR spectral data of these compounds compared well with literature values.

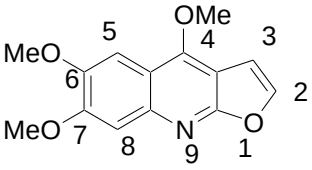

(1)

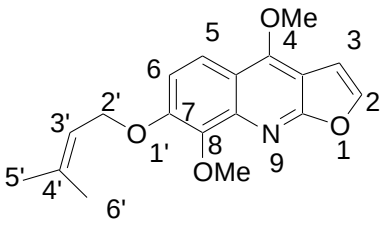

(2)

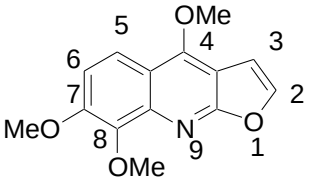

(3)

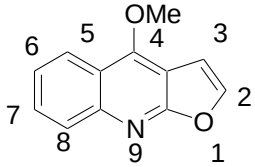

(4)

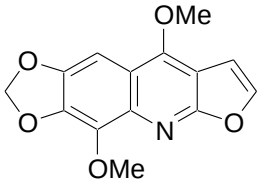

(5)

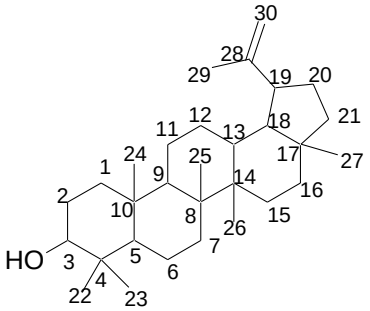

(6)

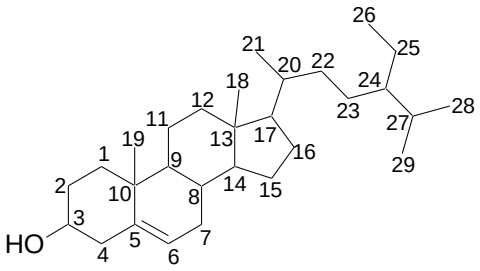

(7)

Figure 1: Structures of the seven compounds isolated from the organic extracts of *T. nobilis*

Flindersiamine shows signals of a methylenedioxy group at position 6 and 7 on the ring. Lupeol showed the unique seven singlet signals, each integrating to three protons at δ 0.99, 1.00, 1.13, 1.26, 1. 27, 1.29 and 1.82, strongly suggested pentacyclic lupeol-type triterpenoids and the ^{13}C NMR data of lupeol correlated very well with literature values[8]. β-Sitosterol has notable peaks at three sections, the peak at the low field at δ 141.2 was assignable to the bridge quaternary carbon atom. The signal at δ 121.4 was for olefinic carbon atom that was protonated. There was also a notable peak at δ 72.2, which was assigned to carbon 3 due to the hydroxyl group. The remaining band comprising of the upper end of the spectrum, from δ 57.2 to 12.3, is mainly made up of a number of the ring and methyl carbons and are characteristic of plant sterols.

The seven compounds showed moderate to low activity (7-11 mm). The inhibition zone was measured as in the crude extracts using the same pathogens. The results were as tabulated in table 4.

Table 4: The inhibition zones (in mm) of the isolated compounds

Bacteria	***S. aureus***	***S. pneumonia***	***B. subtilis***	***S. typhi***	***E. coli***
Compounds					
1	11	9	8	6	6
2	10	10	9	6	6
3	10	9	9	6	6
4	11	10	6	6	8
5	10	9	8	6	7
6	8	8	6	7	6
7	9	10	7	6	7
Negative Control	6	6	6	6	6

Compound (**1)** and (**4)** were the most active towards *S. aureus* bacteria with an inhibition of 11 mm. The bacteria *S. pneumonia*, was more susceptible to compounds (**2)**, (**4)** and (**7)** than the other four compounds. The least susceptible bacteria to all the seven compounds was *S. typhi* with an exhibition diameter of 6 mm. There was activity exhibited earlier towards Gram-negative bacteria by the DCM crude extract which is not evident with any of the compounds isolated. This can most likely be attributed to, among other factors, the synergic effect which would have boosted the activity of the compounds in the crude state, which is not present after isolation of the pure compounds.

4.0 Conclusion

This study has shown that *Teclea nobilis* leaves contain furoquinoline alkaloids, a triterpenoid, and a plant sterol. The isolated compounds individually showed low activity against the bacterial test organisms, the low activity of the isolated compounds of *T. nobilis* could be due to loss of synergism. There is therefore still a basis for traditional use of the *T. nobilis* against pathogenic organisms like bacteria. Some of these compounds may find use as templates for the synthesis of derivatives of these compounds with changes in functional groups might give promising anti-microbial activities.

Acknowledgements
We would wish to extend our sincere thanks to Mr. Elias Maina, Chief Technician, Chemistry Department, Kenyatta University, for his cooperation and availing the apparatus and reagents throughout the bench work period. Thanks also go to Lake Victoria Research Initiative (VicRes), for partially sponsoring this research. We are greatly indebted to Dr. Martin Onani of University of Western Cape, Cape Town, South Africa for assisting us to run the NMR spectra for the isolated compounds. We also appreciate the input from Dr. Hamisi Malebo, especially on techniques of isolation of alkaloids.

References

1. Beentje, H. (1994). Kenya trees, shrubs and lianas. National museum of Kenya. Nairobi, Kenya. pp 78-89.

2. Muthaura, C.N., Rukunga, G.M., Chhabra, S.C., Mungai, G.M. and Njagi, E.N.M. (2007). Traditional phytotherapy of some remedies used in treatment of malaria in Meru district of Kenya *South African Journal of Botany* **73**, 402-411.

3. Muriithi, M.W., Abraham, W.R., Addae-Kyereme, J., Scowen, I., Croft, S.L., Gitu, P.M., Kendrick, H., Njagi, E.N.M. and Wright, C.W. (2002). Isolation and *in vitro* antiplasmodial activities of alkaloids from *Teclea trichocarpa*: *in vivo* antimalarial activity and X-ray crystal structure of normelicopicine. *Journal of Natural Products* **65**, 956-959.

4. Adnan J. Al-Rehailya, Mohammad S. Ahmada, Ilias Muhammad Assad, A. Al-Thukairc and Herman P. Perzanowskic (2003). Furoquinoline alkaloids from *Teclea nobilis. Phytochemistry* 64, 1405–1411.

5. Ayafor, J.F. and Okogun, J.I. (1982). Nkolbisine, a new furoquinoline alkaloid and 7-deacetylazadirone from *Teclea verdoorniana*. *Journal of Natural Products* **45**, 182-185.

6. Ayafor, J.F., Sondengam, B.L., Bilon, A.N. and Connolly, J.D. (1986). Limonoids of *Teclea ouabanguiensis*. *Journal of Natural Products* **49**, 583-587.

7. Solis, P.N., Wright, C.W., Anderson, M.M., Gutopa, M.P. and Philipson, J.D. (1992). A microwell cytotoxicity assay using *Artemia salina* (Brine shrimp). *Plant Medica* **59**, 250-252.

8. Chhabra, S.C. and Uiso, F.C. (1991). Antibacterial activity of some Tanzanian plants used in traditional medicine. *Fitoterapia* **62**, 499–501.

9. Tait-Kamradt, A., Davies, T., Appelbaum, P.C., Depardieu, F., Courvalin, P., Petitpas, J., Wondrack, L., Walker, A., Jacobs, M.R. and Sutcliffe, J. (2009). Two New Mechanisms of Macrolide Resistance in Clinical Strains of *Streptococcus pneumoniae* from Eastern Europe and North America. *Journal of Antimicrob Agents* **44**, 337-340

10. Satomi, F., Naomichi T., Tsuyoshi, I., Masateru, O., Alaa, M.N., Toshihiro, N., Hiroyuki, S., Shima, D. and Hideo, Y**.** (2002). Two Novel Long-chain alkanoic acid esters of lupeol from *Alecrim-Propolis*. *Chemical and Pharmaceutical Bulletin* **50**, 439-440.

Levels of Selected Heavy Metals in Aloe vera Branded herbal Soaps sold in the Kenya Market

Onyambu Z.M[1]., Nawiri, M.P*[1]., Kareru, P[2] and Wanjau, R.N[1]
[1]Department of Chemistry, Kenyatta University, P.0. B0X 43844-00100 Nairobi, Kenya.
[2]Department of Chemistry, JKUAT, P.O Box 6200-00100 Nairobi, Kenya
*Corresponding author. Email: nawiri.mildred@ku.ac.ke

Abstract
There are persistent human health concerns of interaction with heavy metals which may arise through various means. The high increase of production and use of herbal cosmetics (soaps, oils, lotions) trigger a need to evaluate their heavy metal content. Levels of Hg, Pb, Cd, Zn, Mn and Cr were determined in five brands of soaps in the Kenyan market that are made from a herbal cosmetic, Aloe vera. The analytical methods employed were Atomic Absorption Spectroscopy and Cold Vapour Atomic Absorption Spectroscopy. The mean levels (µg/g) reported ranged as follows: Hg (0.09-0.21), Pb (0.14-0.83), Cd (0.01-0.15), Zn (0.02-0.07), Mn (0.01-0.06) and Cr (0.03-0.05). Hg, Pb, Zn and Mn were detected in all brands of soap. It is evident that the Aloe vera cosmetic soaps exposes users to levels of heavy metals pointing out to fears of long term adverse effects of the same.

Keywords: Aloe vera, cosmetics, soaps, heavy metals

INTRODUCTION

There is a widespread use of cosmetics for routine care of skin, hair, nails and teeth[1]. A wide range of cosmetic products exist including creams, emulsions, lotions, gels, oils, face masks, tinted bases, make up powders, toilet soaps, perfumes, shower and bath preparations, deodorants and antiperspirants, depilatories, hair care products and shaving products[2]. Depending on the ingredients with which they are made from, cosmetics can either be herbal (those of natural origin and are made of ingredients that are gentler and less likely to be harmful) or synthetic (those which are conventional and made of ingredients likely to be harmful)[3]. Among the most commonly used skin cosmetics are those made of ingredients such as formaldehyde and formaldehyde releasing ingredients, hydroquinone, parabens and phthalates which could be harmful to human body[4].Herbal cosmetics such as *Aloe vera*, neem and olive oil are more preferred because they are mild, biodegradable and have low toxicity profile[5].

Aloe vera (*Aloe barbadensis* Miller) is commonly used due to its medicinal nature. It plays an important role on the skin that would result into preventing penetration of UV-light, and is key in wound healing and skin repair. *Aloe vera* cosmetics are available in the market (not excluding Kenya) in the form of lotions, creams, soaps and shampoos[6,7]. Worth noting is that *Aloe vera* plant absorbs heavy metals from the soil and can be a cause of recall of cosmetics and other product when the presence of heavy metals are toxic to human[8]. Heavy metals toxicity can result to damaged or reduced mental and central nervous function, lower energy levels and damage to blood composition, lungs, liver, kidneys and other vital organs[9]. Repeated long term contact with some of these heavy metals or their compounds may cause cancer, contact dermatitis and skin

irritations which are caused by Cr, Ni and Co[9, 10]. Their exposure however, continues and is even increasing particularly in less developed countries[11].

Heavy metals can be absorbed into the organism through the skin and can be detected in sweat, blood and urine within periods of between six hours to 45 days of skin application[10, 12]. Moist skin particularly promotes absorption of water soluble toxic elements and their compounds into the body[10]. As such, continuous use of cosmetics may result in an increase in the heavy metal levels beyond acceptable limits as set by WHO[1, 13]. Due to the harmful effects of heavy metals to man, the possibility of their presence in herbal cosmetics warrant investigation[1]. We report the evaluation of heavy metals in soaps sold in the Kenyan market that are made from *Aloe vera*.

MATERIALS AND METHODS

Equipment and chemicals

A Buck scientific Absoprtion spectrophotometer (model VGP-210) was used to measure the analytes. All chemicals, reagents and solvents used were of analytical grade and included cadmium, lead, zinc and manganese metals and standards of mercury and chromium were purchased from Fluka Chemie GmbH Chemical Company, inc. USA. Hydrochloric acid, concentrated nitric acid, hydrogen peroxide, concentrated hydrochloric acid, sulphuric acid, stannous chloride, silica gel, potassium permanganate and potassium chromate (K_2CrO_4) were sourced from Thomas Baker Chemicals Ltd Mumbai, India.

Sample collection

Five different brands (coded SP1, SP2, SP3, SP4 and SP5). of *Aloe vera* soaps (two batches of each brand) were sampled from major supermarkets in Nairobi County. A total of thirty samples were obtained.

Determination of heavy metals

Sample and blank digestions were done under standard procedure as per[14]. Briefly 0.5 grams of the soap sample (omitted for blank) was measured into a pre-weighed Telfon Vials and 10 ml of digest acid comprising 70% nitric acid and 30% sulphuric acid was added. It was capped tightly and placed in an oven at 60^o C for 12 hours. 30 ml of deionised water was added when the digested sample had cooled. The sample was then filtered with the help of whatman number 1 filter paper. The clear solution was used for metal quantification

Measurement of levels of heavy metals was done using Flame Atomic Absorption Spectroscopy FAAS for Pb, Cd, Zn, Mn and Cr while Cold Vapour Atomic Absorption Spectroscopy CV-AAS was employed for Hg with settings as provided by the manufacturer's manual. The digested samples were aspirated in triplicates with regular intercepts of standards to maintain a check on the instrument stability. The analysis proceeded only when the results were within 10% of earlier readings.

RESULTS AND DISCUSSION

The findings are reported in **table 1.0.**

Mercury was detected in all the *Aloe vera* soaps with mean levels ranging from 0.09±0.01 to 0.21±0.01 µg/g. The levels were found to differ significantly ($P<0.05$) between the brands for soaps in batch 2. Although Hg has been reported as a common ingredient in the manufacture of cosmetics to act as a skin lightener, the labels were not indicative of this[12, 15]. However, the levels were all below the maximum WHO recommended limit of 1µg/g [16]. Lead was found to be present in all the *Aloe vera* soaps analyzed. The mean levels ranged from 0.14±0.07 µg/g to 0.83±0.01 µg/g. The levels differed significantly between the brands in batch 2 ($P<0.05$). Lead has been found to be a common contaminant in various cosmetics[1]. The levels of lead in the soaps, however, were below 10 µg/g, the WHO maximum recommended limits[16].

Cadmium was detected in all soaps except SP1 batch 1 with mean levels ranging from 0.01±0.01 to 0.15±0.01 µg/g. The levels differed significantly between the brands ($P<0.05$). In cosmetics cadmium find usefulness due to its deep yellow to orange pigmentation. The levels were however below the maximum recommended limits of 10 µg/g[16.] Slightly higher levels ranging from 0.623 to 1.875µg/g were recorded earlier[15]. Low levels ranging from 0.10 to 0.46 µg/g were recorded by[17]. Zinc was detected in all the soaps analyzed and recorded mean levels ranging from 0.02±0.01 to 0.07±0.01 µg/g. Although speciation studies were not within the scope of this study, zinc oxide is used as an ingredient in cosmetics to serve both as a sunscreen and to whiten the skin[18]. The levels of zinc recorded in this study were however lower than those reported in literature where zinc has been detected to levels as high as 56.57 µg/g [15, 17].

Manganese was detected in all the soaps analyzed. The mean levels ranged from 0.01±0.01 µg/g to 0.06±0.01 µg/g. The levels differed significantly between the brands and also between batches in SP1, SP3 and SP5 ($P<0.05$). Chromium was detected in SP3 only with mean levels ranging from 0.03±0.01 to 0.05±0.01 µg/g. The low levels recorded in this study are comparable to the levels recorded in some studies (ranges 0.50- 2.70 µg/g)[19].

Conclusion

The results show evidence of the presence of heavy metals in *Aloe vera* cosmetic soaps. Although the levels were lower than those set by WHO and KEBS, these does not warrant safety for users of these products since continuous use of cosmetics would be detrimental to health. As well, another cause of concern arises where users apply a combination of different *Aloe vera* soaps. The findings show need of these otherwise minute levels of heavy metals

Acknowledgement: The authors thank the Research, Planning and Extension (RPE) Division of Jomo Kenyatta University of Agriculture and Technology (JKUAT) for funding this work and as well the Chemistry department, JKUAT for laboratory space.

Table 1.0: Mean levels (µg/g) of heavy metals in five different *Aloe vera* cosmetic soaps

		Mean levels (µg/g) in different brands (Mean±SE; n=9)					
parameter	Batch	SP1	SP2	SP3	SP4	SP5	p-value
Hg	1	0.09±0.01	0.17±0.02	0.40±0.28	0.15±0.01	0.21±0.01	0.500
	2	0.11±0.01^{a}	0.14±0.01^{b}	0.17±0.01^{c}	0.16±0.01^{c}	0.21±0.01^{d}	<0.001
Pb	1	0.42±0.16^{b}	0.12±0.06^{a}	0.71±0.01^{c}	0.16±0.06^{a}	0.77±0.01^{c}	<0.001
	2	0.14±0.07^{a}	0.33±0.07^{b}	0.74±0.01^{c}	0.66±0.10^{c}	0.83±0.01^{c}	<0.001
Cd	1	BLD	0.01±0.01^{a}	0.01±0.01^{a}	0.02±0.01^{a}	0.77±0.01^{c}	<0.001
	2	0.01±0.01^{a}	0.01±0.01^{a}	0.02±0.01^{a}	0.06±0.01^{b}	0.83±0.01^{c}	<0.001
Zn	1	0.05±0.01^{b}	0.14±0.01^{d}	0.03±0.01^{a}	0.02±0.01^{a}	0.07±0.01^{c}	<0.001
	2	0.02±0.01^{a}	0.06±0.01^{c}	0.05±0.01^{b}	0.02±0.01^{a}	0.02±0.01^{a}	<0.001
Mn	1	0.01±0.01^{a}	0.04±0.01^{bc}	0.04±0.01^{b}	0.03±0.01^{b}	0.06±0.01^{c}	<0.001
	2	0.05±0.01^{ab}	0.06±0.01^{b}	0.06±0.01^{b}	0.02±0.01^{a}	0.03±0.01^{ab}	0.010
Cr	1	BLD	BLD	0.03±0.01	BLD	BLD	-
	2	BLD	BLD	0.05±0.01	BLD	BLD	-

Mean values within the same row followed by the same letters are not significantly different (SNK, α=0.05); BLD- Below Limit of Detection

REFERENCES

1. Chauhan, A.S., Bhadauria, R., Singh, A.K., Lodhi, S.S., Chaturvedi, D. K. and Tomar, V.S. (2010). Determination of lead and cadmium in cosmetic products. *Journal of Chemical and Pharmaceutical Research*; 2: 92-97.
2. Anton, C., Weyland, J. W. and Nater, J. P. (2005). Unwanted effects of cosmetics and drugs used in dermatology. Elsevier-Netherlands. Pp. 422-423.
3. Baumann, l. (2009). Cosmetic dermatology. Mc Graw-Hill Companies, USA. Pp. 142.
4. Conors, M.S. and Altshuler, L. (2009). The Everything Guide to herbal remedies. Adams media, U.S.A. Pp. 193.
5. Chanchal, D., Pharm, M. and Swarnlata, M. (2008). Novel approaches in herbal cosmetics. *Journal of Cosmetic Dermatology*; 7: 89-95.
6. Basmatker G., Jais N. and Daud F. (2011). Aloe Vera: A Valuable multifunctional cosmetic ingredient. *International Journal Arom. Plants*; 1: 338-341.
7. Haque, Z., Rout, A., Jalil, A., Islam, B., Islam, M. and Ahsan, A. (2012). Studies on the production of musabbra from *Aloe vera*. *Journal of advanced scientific Research*; 3: 51-54.
8. Rai, S., Shirma, D. Kr., Arora, S.S.,Sharma, M. and Chopra, A. K. (2011). Concentrations of heavy metals in *Aloe vera* L. (*Aloe barbadensis* Miller) leaves collected from different geographical locations of India. *Annals of Biological Research*; 2:575-579.
9. Linnila, P. M. (2000). Zinc, lead and cadmium speciation in deeper water bodies. *Lakes and Reservoirs: Research and Management*; 5: 261-270.
10. Omolaoye, J.A., Uzairu, A. And Gimba C.E. (2010). Heavy metal assessment of some eye shadow products imported to Nigeria from China. Achives of Applied Science Research; 2: 76-84.
11. Jarup, L. (2003). Hazards of heavy metals. *Oxford Journals;* 68: Pp. 167 – 182.

12. Sin K.W. and Tsang H.F. (2003). Large scale mercury exposure due to a cream cosmetic: community wide case series. *Hong Kong Medical Journal*; 9: 329-334.
13. Sin K.W. and Tsang H.F. (2003). Large scale mercury exposure due to a cream cosmetic: community wide case series. *Hong Kong Medical Journal*; 9: 329-334.
14. Nnorom, I.C., Igwe, J.C. and Oji-Nnorom, C.G. (2005). Trace metal contents of facial (Make-up) cosmetics commonly used in Nigeria. *African Journal of Biotechnology*; 4: 1133-1138.
15. Oyelakin, O., Saidykhan, J., Secka, P., Adjivon, A. And Acquaye, H. B. (2010). Assessment of the level of mercury present in soaps by the use of Cold Vapour Atomic Fluorescence Spectrometric Analysis- A Gambian case study. *Ethiopian Journal of Environmental Studies and Measurement;*3 : 8-12.
16. WHO (1995). Environmental health criteria. *International programme on chemical safety*. Geneva. World Health organisation. Pp 165.
17. Gentscheva, G. D., Stafilov, T. And Ivanova, E. H. (2010). Determination of some essential and toxic elements in herbs from Bulgaria and Macedonia using Atomic Spectrometry. *Eurasian Journal of Analytical Chemistry;* 5:104-111.
18. Butler, H. and Poucher, W.A. (2000). Poucher's perfumes, cosmetics and soaps. Kluwer Academic Publishers, Dordrecht, Netherlands. Pp. 484.
19. Dayan, A. D. and Paine, A. J. (2001). Mechanisms of chromium toxicity, carcinogenicity and allergenicity: Review of the literature from 1985 to 2000. *Human and Experimental Toxicology* ; 20: 439–451.